

**THE INTRICATE ROLE OF CONNECTIVE TISSUE GROWTH
FACTOR (CTGF/CCN2) IN PRENATAL OSTEOREGENESIS:
A HERETOFORE OVERSIMPLIFIED DOGMA OF THE CCN
FIELD**

A Dissertation
Submitted to
the Temple University Graduate Board

In Partial Fulfillment
of the Requirements for the Degree of
Doctor of Philosophy

By
Alex Gregory Lambi
May, 2015

Dissertation Examining Committee
Steven N. Popoff, Ph.D. – Department of Anatomy and Cell Biology
Mary F. Barbe, Ph.D. – Department of Anatomy and Cell Biology
Victor Rizzo, Ph.D. – Department of Anatomy and Cell Biology
Dianne Soprano, Ph.D. – Department of Biochemistry
Joan T. Richtsmeier, Ph.D. – Department of Anthropology, Pennsylvania State
University

UMI Number: 3604678

All rights reserved

INFORMATION TO ALL USERS

The quality of this reproduction is dependent upon the quality of the copy submitted.

In the unlikely event that the author did not send a complete manuscript and there are missing pages, these will be noted. Also, if material had to be removed, a note will indicate the deletion.



UMI 3604678

Published by ProQuest LLC (2013). Copyright in the Dissertation held by the Author.

Microform Edition © ProQuest LLC.

All rights reserved. This work is protected against unauthorized copying under Title 17, United States Code



ProQuest LLC.
789 East Eisenhower Parkway
P.O. Box 1346
Ann Arbor, MI 48106 - 1346

ABSTRACT

Connective tissue growth factor (CTGF/CCN2) is axiomatically necessary for proper skeletal development and function. We need not look further than the studies that have been done to date utilizing mice genetically engineered to lack CTGF production. These CTGF null or knockout (KO) mice fail to form a normal murine skeleton and instead yield one littered with bony dysmorphisms, including incompetent craniofacial development, kinked limb bones, and misshapen ribs that are not conducive to proper respiratory function. As a result, the global lack of CTGF is incompatible with postnatal life. A closer look at several sites demonstrated defects in physiologic processes necessary for bone formation – angiogenesis, chondrogenesis, and osteogenesis. Therefore, the dogma in the CCN protein field to date has been that systemic ablation of CTGF production *in vivo* results in global defects in bone development.

We believe this dogma is an oversimplification of the role of CTGF on skeletal development. Our initial impetus leading us to this belief was the gross identification of the specific skeletal sites malformed in CTGF KO mice, in particular the bones of the limbs. While in the lower limb of CTGF KO mice the tibiae and fibulae are misshapen, the adjacent femora and digits are phenotypically normal. The same is true for the upper limb, in which the radii and ulnae are phenotypically abnormal while the humeri and digits are normal. Therefore, we believe that the role of CTGF in skeletogenesis is site-specific such that its loss affects local skeletal patterning and/or mechanobiological cues resulting in the unique phenotype seen in CTGF KO mice.

The research of this dissertation constitutes a comprehensive skeletal analysis of CTGF KO mice and in so doing we determined the extent and location of skeletal

abnormalities. We found skeletal site-specific changes in growth plate organization, bone microarchitecture and shape and gene expression levels in CTGF KO compared to wild-type (WT) mice. Growth plate malformations included reduced proliferation zone and increased hypertrophic zone lengths. Appendicular skeletal sites demonstrated decreased metaphyseal trabecular bone, while having increased mid-diaphyseal bone and osteogenic expression markers. Axial skeletal analysis showed decreased bone in caudal vertebral bodies, mandibles, and parietal bones in CTGF KO mice, with decreased expression of osteogenic markers. Analysis of skull phenotypes demonstrated global and regional differences in CTGF KO skull shape resulting from allometric (size-based) and non-allometric shape changes. Localized differences in skull morphology included increased skull width and decreased skull length.

We further continued the skeletal characterization of CTGF KO bones with an analysis of bone cell ultrastructure and matrix composition. These studies demonstrated that, while CTGF is not necessary for complete morphologic maturation of bone cells, global ablation results in ultrastructural features not commonly seen in WT bones. Our findings include drastically dilated rough endoplasmic reticulum (RER) in osteoblasts of the tibial diaphyseal region, comprising the phenotypic kink in CTGF KO mice and ultrastructural dysmorphologies of CTGF KO osteoclasts including multi-layered, membranous inclusions, decreased vacuolization and ruffled border extents, and disproportionately large clear zones. Lastly, FT-IR analysis demonstrated heterogeneity in CTGF KO bone composition. The results of this dissertation have revealed a more complex role for CTGF in osteogenesis and have identified potential mechanisms and future research directions to fully understand this intricate story.

ACKNOWLEDGEMENTS

“I am a part of all that I have met; yet all experience is an arch wherethrough gleams that untraveled world, whose margin fades for ever and for ever when I move.”

—Alfred, Lord Tennyson (1809-1892)

Ulysses (1842)

The research of this dissertation would not have been possible without the efforts of many others. Whether it was through shared resources, scholarly input, teaching techniques, or involvement in data collection, these contributions were invaluable. Therefore, I would like to acknowledge several individuals who deserve my utmost gratitude for their role in my doctoral pursuits.

I would first and foremost like to thank my advisor, Dr. Steven Popoff. From the first days of medical school when taking Gross Anatomy, it was clear that not only was he an established scientist, but also a great teacher. I was confident that under his tutelage I would learn how to be a competent, independent scientist as well as an academician. I would also like to thank Dr. Mary Barbe who acted as a co-advisor to me; always available for immediate input and providing direction in the project based on her breadth of knowledge across many fields. I am also grateful for the efforts of my other distinguished dissertation committee members, Drs. Victor Rizzo, Dianne Soprano, and Joan Richtsmeier. Dr. Soprano, along with Tracey Hinton, provided a well-structured and interactive M.D., Ph.D. program that fostered the success of its students. Dr. Richtsmeier, as well as Talia Pankratz, were instrumental in our analysis of the craniofacial phenotype seen in our mouse model. The results of this collaboration were very fruitful and I was

fortunate to have been able to learn so much from an established expert in craniofacial development. I would also like to thank Dr. Maureen Gannon for providing us our mouse model and being very engaged in the research of our lab. My thanks to Drs. Nancy Pleshko and Cushla McGoverin for their resources and time in using the FT-IR analysis. I am also grateful for the efforts of Ray Meade and others at the University of Pennsylvania Electron Microscopy Center.

I would also like to acknowledge other graduate students, faculty, and staff in the Department of Anatomy and Cell Biology. Christina Mundy provided countless hours of input into the manuscript and was a great lab mate to have. Dr. Robin Pixley and Roshanak Razmpour were helpful in processing samples for micro-CT and histologic examination, respectively. And our front office staff of Anita Li, Sydnora Simon, and John Waterman, was always very helpful in processing vital paperwork.

Lastly, my undying gratitude goes out to my family and close friends, the ones who lived through the inevitable emotional ups and downs of my graduate education. They were a source of support whenever it was needed, whether in the form of a bike ride, a chat, or a drink. Most of all, to my parents and sister, they are the reason for my work ethic, my pursuit of knowledge, and my desire to push myself to achieve success in any life endeavor. Fittingly, Tennyson's *Ulysses* concludes with this line: "To strive, to seek, to find, and not to yield."

Vivitur ingenio, caetera mortis erunt.

Genius lives on, all else is mortal.

—Andreas Vesalius (1514-1564)

De humani corporis fabrica libri septem (1543)

TABLE OF CONTENTS

ABSTRACT	ii
ACKNOWLEDGEMENTS.....	iv
LIST OF FIGURES	ix
LIST OF TABLES	xi
CHAPTER 1: REVIEW OF THE LITERATURE	1
THE SKELETAL SYSTEM AND ITS ROLES	1
BONE CELLS.....	2
<i>Osteoblasts</i>	2
<i>Osteocytes</i>	3
<i>Osteoclasts</i>	3
PRENATAL BONE DEVELOPMENT (OSTEOGENESIS)	5
<i>Mesenchymal Cell Condensations</i>	5
<i>Ossification Processes</i>	5
<i>Congenital Defects involving Individual Ossification Processes</i>	9
<i>The Growth Plate and its Regulation</i>	9
CRANIOFACIAL BONE DEVELOPMENT	10
<i>The Calvaria (Desmocranum)</i>	11
<i>The Cranial Base (Chondrocranium)</i>	11
<i>The Facial Skeleton (Viscerocranum)</i>	12
POSTNATAL BONE GROWTH, REMODELING, AND HEALING	15
<i>Newborn Bone Development</i>	15
<i>Ossification Centers and Long Bone Expansion</i>	15
<i>Bone Remodeling</i>	16
<i>Bone Healing and Fracture Repair</i>	16
CTGF AND THE CCN FAMILY OF PROTEINS	17
<i>CTGF's Modular Structure and Function</i>	17
<i>Matricellular Interactions of CTGF</i>	19
THE ROLE OF CTGF IN SKELETAL DEVELOPMENT	21
<i>CTGF in Prenatal Skeletal Development</i>	22
<i>CTGF in Postnatal Bone Formation and Remodeling</i>	24
CTGF IN SKELETAL CELL DIFFERENTIATION AND FUNCTION	25
<i>Osteoblasts and CTGF</i>	25
<i>Chondrocytes and CTGF</i>	27
<i>Who have we forgotten? CTGF in Osteoclasts and Osteocytes</i>	29
CTGF AND ANIMAL MODELS: AN <i>IN AND EX VIVO</i> LOOK	32
<i>CTGF Global Ablation (Knockout) Models</i>	32
<i>Skeletal-Specific CTGF Conditional Knockout Models</i>	37
<i>Skeletal-Specific CTGF Overexpression (Transgenic) Models</i>	37
CLINICAL RELEVANCE OF CTGF IN HUMAN SKELETAL DEVELOPMENT AND FUNCTION	39
<i>CTGF Promoter Polymorphism and Systemic Sclerosis</i>	39
<i>WISP-3/CCN6 and Progressive Pseudorheumatoid Dysplasia</i>	40
<i>Targeting CTGF Clinically: FG-3019, a Potential Pyrrhic Victory in Bone?</i>	40
STUDIES OF THIS DISSERTATION	41
CHAPTER 2: THE SKELETAL SITE-SPECIFIC ROLE OF CONNECTIVE TISSUE GROWTH FACTOR IN PRENATAL OSTEOGENESIS*	46

INTRODUCTION	46
MATERIALS AND METHODS	49
<i>Animals</i>	49
<i>Tissue preparation and histology</i>	49
<i>Histomorphometry</i>	50
<i>Micro-computed tomography (micro-CT) analysis</i>	51
<i>Morphometric analysis of skull phenotypes</i>	52
<i>RNA Isolation and Quantitative Real-Time PCR (qPCR)</i>	55
<i>Statistical analysis</i>	56
RESULTS	58
<i>Multiple growth plate malformations occur in CTGF KO mice</i>	58
<i>CTGF KO mice have skeletal site-specific effects on bone formation</i>	60
<i>Skull phenotypes of CTGF KO mice</i>	65
<i>Differences in cranial shape in CTGF KO mice</i>	68
<i>Localized differences in craniofacial shape in CTGF KO mice</i>	70
<i>Morphologic traits unique to CTGF KO skulls</i>	74
<i>In vivo gene expression patterns in CTGF KO skeletal sites</i>	77
DISCUSSION.....	80
CHAPTER 3: AN ANALYSIS OF BONE CELL ULTRASTRUCTURE AND MATRIX COMPOSITION IN CONNECTIVE TISSUE GROWTH FACTOR KNOCKOUT (CTGF KO) MICE	88
INTRODUCTION	88
MATERIALS AND METHODS	90
<i>Animals</i>	90
<i>Electron Microscopy Tissue Preparation</i>	91
<i>FT-IRIS Tissue and Section Preparation</i>	92
<i>FT-IRIS Data Acquisition and Analysis</i>	93
<i>Statistical Data Analysis</i>	94
RESULTS	94
<i>Ultrastructure of Osteoblasts and Osteocytes in WT and CTGF KO Tibiae</i>	94
<i>Ultrastructure of Osteoclasts in WT and CTGF KO Tibiae</i>	101
<i>FT-IR Spectroscopy of Bone Matrix Properties in CTGF KO and WT Tibiae</i>	107
DISCUSSION.....	109
CHAPTER 4: SUMMARY.....	112
TGF- β -CTGF AXIS: A POTENTIAL MECHANISTIC EXPLANATION FOR THE CTGF KO	
CRANIOFACIAL PHENOTYPE	114
SOLVING THE RIDDLE OF THE KINKS	117
THE CLINICAL QUAGMIRE OF CTGF IN BONE.....	118
REFERENCES CITED	120

LIST OF FIGURES

FIGURE 1-1. STEPS IN ENDOCHONDRAL OSSIFICATION.....	8
FIGURE 1-2. DIVISIONS OF THE CRANIOFACIAL SKELETON.....	14
FIGURE 1-3. CTGF MODULAR STRUCTURE AND FUNCTION.....	20
FIGURE 1-4. CTGF SIGNALING IN CHONDROCYTES.....	31
FIGURE 1-5. COMPREHENSIVE SKELETAL PHENOTYPE CHARACTERIZATION OF CTGF KO MICE.....	43
FIGURE 2-1. GROWTH PLATE MALFORMATIONS IN CTGF KO MICE.....	59
FIGURE 2-2. SKELETAL SITE-SPECIFIC EFFECTS ON FORMED BONE IN CTGF KO APPENDICULAR SKELETON.....	61
FIGURE 2-3. SKELETAL SITE-SPECIFIC EFFECTS ON FORMED BONE IN CTGF KO AXIAL SKELETON.....	64
FIGURE 3-4. LANDMARKS COLLECTED FROM ISOSURFACES OF MICRO-CT RECONSTRUCTIONS OF P0 MURINE SKULLS.....	66
FIGURE 2-5. DIFFERENCES IN SKULL SHAPE IN CTGF KO MICE.....	69
FIGURE 2-6. LOCALIZED DIFFERENCES IN SKULL MORPHOLOGY IN CTGF KO MICE.....	72
FIGURE 2-7: MORPHOLOGIC TRAITS SEEN IN CTGF KO SKULLS.....	75
FIGURE 2-8. GENE EXPRESSION PATTERNS IN CTGF KO SKELETAL SITES.....	79
FIGURE 3-1. COMPARISON OF WT AND CTGF KO METAPHYSEAL OSTEOBLAST ULTRASTRUCTURE.....	97
FIGURE 3-2. ULTRASTRUCTURAL FEATURES OF CTGF KO DIAPHYSEAL OSTEOBLASTS ..	99
FIGURE 3-3. COMPARISON OF WILD-TYPE AND CTGF KO OSTEOCYTE ULTRASTRUCTURE	100
FIGURE 3-4. ANALYSIS OF WT OSTEOCLAST ULTRASTRUCTURE.....	103
FIGURE 3-5. ANALYSIS OF CTGF KO OSTEOCLAST ULTRASTRUCTURE	104
FIGURE 3-6. ULTRASTRUCTURAL DYSMORPHOLOGIES PREVALENT IN CTGF KO OSTEOCLASTS.....	105
FIGURE 3-7. FT-IR SPECTROSCOPY OF BONE MATRIX PROPERTIES IN WT AND CTGF KO TIBIAE.....	108

FIGURE 4-1: THE TGF- β -CTGF AXIS: A POTENTIAL MECHANISTIC EXPLANATION FOR
CTGF KO CRANIOFACIAL PHENOTYPE 116

LIST OF TABLES

TABLE 2-1. PRIMER SEQUENCES USED FOR QUANTITATIVE REAL-TIME POLYMERASE CHAIN REACTION (QPCR) ANALYSIS.....	57
TABLE 2-2. MICRO-CT ANALYSIS OF LONG BONE MICROARCHITECTURE IN WT AND CTGF KO FEMORA AND TIBIA.....	62
TABLE 2-3. CRANIOFACIAL LANDMARK ABBREVIATIONS AND DESCRIPTIONS.....	67
TABLE 2-4. RESULTS OF EDMA TESTING FOR SIGNIFICANT LOCALIZED DIFFERENCES IN CTGF KO SKULLS.....	73
TABLE 3-1. BONE PROPERTIES MEASURED BY FT-IR SPECTROSCOPY.	94

CHAPTER 1: REVIEW OF THE LITERATURE

The Skeletal System and its Roles

The adult human skeleton contains over 200 distinct pieces, or skeletal elements, and comprises two distinct tissues: cartilage and bone. Both cartilage and bone are specialized connective tissues, the differences between which are due to their respective components. In cartilage, the extracellular matrix (ECM) produced by chondrocytes (cartilage-forming cells), primarily consists of type II collagen and ground substance of proteoglycans. Bone, however, contains both organic and inorganic components; while the former is primarily composed of type I collagen, the latter contains calcium phosphate (Ca-PO_4) in the form of hydroxyapatite crystals (Junqueira and Carneiro, 2005). This calcified organic component provides the hardness of bones, allowing them to serve as scaffolding structures in three important functions: 1) providing the framework for the trunk and extremities in withstanding mechanical loads; 2) serving as levers for the locomotor function of skeletal muscle; and 3) affording protection for vulnerable viscera, such as the skull for the brain, the spine for the spinal cord, and the rib cage for the heart and lungs. In addition to the aforementioned structural roles, bone also provides an important role in hematopoiesis, occurring in the bone marrow, as well as a reservoir for calcium and phosphate. The resultant interplay between structural maintenance and balancing the “milieu intérieur” of ionized mineral homeostasis indicates that bone is a very dynamic tissue (Salter, 1999). It is not surprising then that the complexities of bone and the skeleton as an organ are reflected in its embryologic development.

Bone Cells

In order to accomplish the local (scaffolding) roles of bone, such as formation and mineralization, and the systemic (endocrine) roles, such as mineral homeostasis, bone contains three principal cell types: osteoblasts, osteocytes, and osteoclasts.

Osteoblasts

Osteoblasts are differentiated cells responsible for ECM production and mineralization. Osteoblast precursors originate from mesenchymal stem cells that are induced by master regulators, such as wingless-ints (Wnts) and bone morphogenetic proteins (BMPs), to become osteochondroprogenitor cells; these cells are upstream in the differentiation pathways of both chondrocytes and osteoblasts (Caplan and Bruder, 2001; Jiang et al., 2002b; Stein and Lian, 1993). A necessary event in the commitment to the osteoblast lineage is the activation of the transcription factor runt-related transcription factor 2 (Runx-2/Cbfa1). Indispensable to this process, Runx-2 ablation in mice yields a skeleton devoid of mineralized matrix, osteoblasts, and hypertrophic chondrocytes (Otto et al., 1997). Once expressing Runx-2, these “pre-osteoblasts” are now committed to the osteoblast lineage, and proceed through three distinct stages to become mature osteoblasts. Discerned based on changes in expression markers and phenotypic changes, these stages of maturation include the following: 1) proliferation, having cell expansion and expression markers indicative of cell division (e.g. c-Fos); 2) ECM production and maturation, expressing and actively secreting ECM proteins such as alkaline phosphatase (ALP) and collagen type I; and 3) ECM mineralization, secreting ECM proteins such as osteocalcin (OC) and osteopontin (OP) (Stein et al., 2004). When actively synthesizing proteins, mature osteoblasts take on a polarized, columnar ultrastructure with a well-

developed rough endoplasmic reticulum and Golgi network directed toward the surface of the newly produced bone matrix (Junqueira and Carneiro, 2005). Ultimately, mature osteoblasts will either become encased in their surrounding matrix and form osteocytes (described below) or will undergo apoptosis, demonstrated by upregulation of key players in the apoptotic cascades (e.g. Bcl-2) (Stein et al., 2004).

Osteocytes

Terminally differentiated osteoblasts can become encased in the ECM, resulting in their transformation into osteocytes (Manolagas, 2000). These cells make up over 90% of all bone cells and are dispersed throughout the mineralized matrix (Dallas and Bonewald, 2010). While the osteocyte cell body is encased in a lacuna, each cell sends out a vast network of dendritic processes through small canals, or canaliculi. The dendritic processes serve to maintain contact with other osteocytes, as well as the bone surface, vasculature, and even extend to the bone marrow. As a result, it is believed that these cells function in a concerted fashion as a network of sensory cells that respond to mechanical loading (Okada et al., 2002). Additionally, these cells play an important role in phosphate homeostasis (Dallas and Bonewald, 2010).

Osteoclasts

The third type of bone cell is the osteoclast, the role of which is bone resorption. Disparate in cellular origin from the osteoblast and osteocyte, the osteoclast is of myelomonocytic origin as its principal physiological precursor is the bone marrow macrophage (Karsenty et al., 2009; Karsenty and Wagner, 2002). During development, these precursor cells migrate through the mesenchyme surrounding the newly-formed bone where they are stimulated by several key cytokines to fuse and differentiate into mature

multinucleated osteoclasts (Karsenty and Wagner, 2002). It was noted from early *in vitro* experiments on osteoclasts in the 1980s that differentiation of precursor cells to functional osteoclasts requires the presence of osteoblast-lineage cells (Takahashi et al., 1988). Importantly, two key cytokines essential for osteoclastogenesis – receptor activator of nuclear factor kappa-B ligand (RANKL) and macrophage-colony stimulation factor (M-CSF) – are produced by osteoblasts. The process by which osteoblasts affect osteoclast formation is termed osteoblast-induced osteoclastogenesis and underscores the interplay between these two seemingly opposed cell types in proper bone maintenance (Suda et al., 1999; Teitelbaum, 2000). This interplay is critical in both bone development and postnatal remodeling, as will be discussed in subsequent sections.

Mature osteoclasts have a unique phenotype and expression pattern concomitant with their role as the cell responsible for bone resorption. Upon activation, osteoclasts adhere to mineralized bone matrix and take on a highly polarized morphology, in which mitochondria and nuclei are localized to the antiresorptive surface. The resorptive surface is characterized by a ruffled border or membrane, the appearance of which is due to the active resorption of the matrix (Novack and Teitelbaum, 2008). When actively resorbing bone, osteoclasts express several proteins, such as tartrate-resistant acid phosphatase (TRAP), cathepsin K, carbonic anhydrase II (CAII), H⁺-ATPase, and chloride channel-7 (CIC-7), all of which are required in acidifying the area of erosion (Howship's Lacuna) and degrading ECM components. The acidification by protons and concentration of enzymes in this region is made possible by the actin ring or sealing zone. Juxtaposed to the bone surface, this zone is composed of fibrillar actin that mediates integrin-dependent

contact with the matrix, allowing for a tightly sealed area in which bone erosion can occur (Karsenty and Wagner, 2002; Novack and Teitelbaum, 2008).

Prenatal Bone Development (Osteogenesis)

Mesenchymal Cell Condensations

Skeletogenesis is the process by which bone and cartilage form from mesenchymal cell precursors. This process can be divided into two general phases. During the first phase, the precursor mesenchymal cells aggregate and condense at the sites of future skeletal elements (Figure 1-1A-B). Influenced by both autocrine and paracrine factors, these condensations begin to form the shape of their adult skeletal counterparts (Karsenty et al., 2009). Because mesenchymal cells in various sites of the developing embryo arise from different lineages, the future sites of skeletal elements determines which cell lineage will contribute to the future skeleton. Neural crest and paraxial mesoderm cells contribute to the craniofacial bone, cells from the sclerotome of the ventral somite compartment contribute to the trunk axial skeleton, and cells from lateral plate mesoderm will contribute to the limb skeletons. Ultimately, mesenchymal cells within the condensations will begin to differentiate into osteochondroprogenitor cells (Zaidi, 2007).

Ossification Processes

The second phase of skeletogenesis involves the differentiation of the skeletal cell types involved in skeletal formation (osteoblasts, osteoclasts, chondrocytes), and the actual process of ossification. In a minority of future bones, such as the bones of the cranial vault and clavicle, these osteochondroprogenitor cells differentiate directly into

osteoblasts and commence osteogenesis; this process is called intramembranous ossification (Karsenty et al., 2009). It is termed thus as this process of ossification occurs within the mesenchymal condensations (Junqueira and Carneiro, 2005). However, in the majority of future skeletal sites, including long bones of the limbs (e.g. femora), vertebral bodies, and bones of the cranial base, bone is formed through endochondral ossification (Figure 1-1). In this process, osteochondroprogenitors first differentiate into chondrocytes, which produce an ECM composed of type II collagen and proteoglycans. Cells at the periphery of the mesenchymal condensations do not differentiate into chondrocytes, but rather form a structure called the perichondrium; this will exert an influence on both chondrocyte and osteoblast differentiation (Figure 1-1C) (Karsenty et al., 2009). Chondrocytes inside the cartilage undergo a tightly controlled process of proliferation and hypertrophy, which coincides with a change in expression from collagen type II to collagen type X (Figure 1-1D). Cells of the perichondrium will express Runx-2, causing this structure to eventually ossify, thus forming the bone collar; this will become the future cortical bone (Figure 1-1E). Furthermore, the cells within this cartilaginous anlage align to form the highly organized growth plates (Figure 1-1F). As this anlage expands, calcification of the matrix surrounding hypertrophic chondrocytes causes apoptosis of these cells (Figure 1-1G-H). These changes permit a vascular invasion, bringing with it osteoclast and osteoblast precursors that utilize this calcified matrix anlage as a scaffold for the deposition of future trabecular bone with an ECM rich in collagen type I (Figure 1-1I-J). This region is called the primary ossification center (Figure 1-1K) (Karsenty et al., 2009). Ultimately, the preformed cartilage scaffold, or anlage, is replaced entirely by bone.

While ossification in developing bones occurs through two distinct processes, intramembranous and endochondral, two important points must be noted concerning the bones formed by their processes. Firstly, both processes involve the laying down of osteoid matrix and calcification with crystalline apatite deposition, with the resulting adult osseous tissues indistinguishable based on ossification process. Secondly, both ossification processes can be involved in the formation of an individual future bone (Sperber et al., 2010). For example, in long bones such as the femur, the inner (trabecular) bone forms through endochondral ossification while the periosteal bone collar forms through intramembranous ossification.

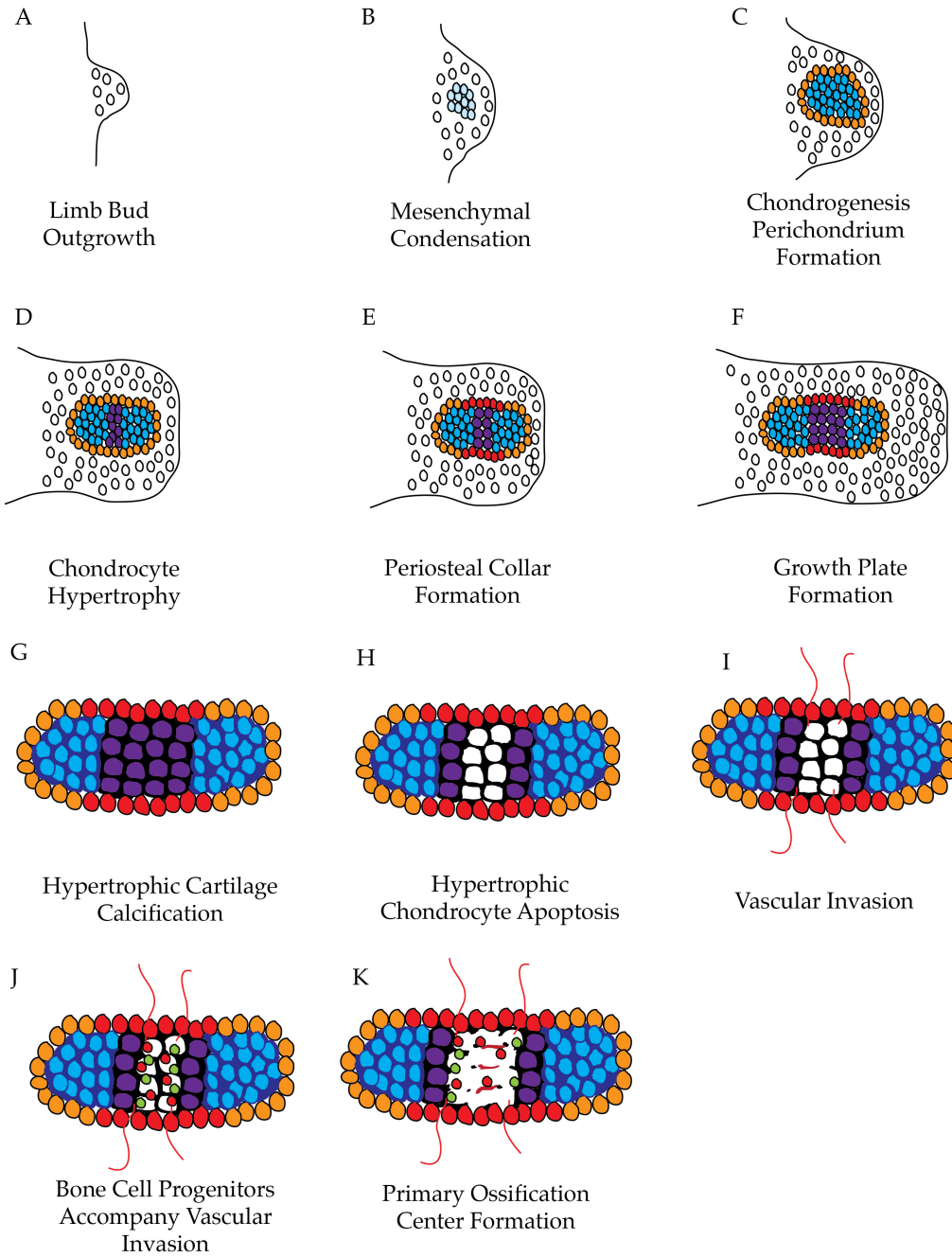


Figure 1-1. Steps in endochondral ossification.

This illustration demonstrates the requisite steps in endochondral ossification of long bones. Depicted are the key steps in endochondral ossification using the formation of long bones of the limbs as an example.

Congenital Defects involving Individual Ossification Processes

Congenital inherited bone defects can arise from mutations in genes necessary for proper bone formation. Interestingly, certain defects are confined to a specific type of ossification, while others can affect global bone formation. Inherited syndromes affecting a unique process of bone formation include Achondroplasia, caused by mutations in the *FGFR3* gene and affecting only endochondral ossification, and Cleidocranial dysostosis, caused by mutations in the *RUNX2* gene and affecting only intramembranous ossification. However, a condition such as Osteogenesis imperfecta, caused by mutations in type I collagen genes, will impact global osteogenesis, regardless of the specific ossification process (Sperber et al., 2010). Therefore, the complexity of bone formation, particularly in long bones, requires an equally diverse approach to studying it. One must choose carefully not only specific bones, but also regions within these bones in order to discern important information regarding the distinct processes of ossification.

The Growth Plate and its Regulation

Proliferating and hypertrophic chondrocytes of the developing long bone cartilage become arranged in distinct zones as part of an avascular structure called the growth plate. The growth plate consists of the following zones: 1) the resting zone, with typical chondrocytes; 2) the proliferation zone, where chondrocytes divide rapidly and align in stacks along the longitudinal axis of the bone; 3) the early hypertrophic zone, a transition zone in which chondrocytes begin undergoing hypertrophy due to intracellular glycogen accumulation; 4) the late hypertrophic zone, where chondrocytes calcify the ECM followed by apoptosis of these cells; and 5) the ossification zone, in which osteoblast

progenitors invade, differentiate into osteoblasts, and begin laying down bone (Junqueira and Carneiro, 2005; Karsenty, 2003; Karsenty et al., 2009; Kronenberg, 2003).

The rapid lengthening of long bones during fetal life is attributed to the progression of chondrocytes from the proliferative to hypertrophic zone (Karsenty and Wagner, 2002; Noonan et al., 1998). Two main proteins are responsible for controlling progression of chondrocytes through the different zones; these are parathyroid hormone-related protein (PTHrP) and Indian hedgehog (Ihh) (Kronenberg, 2003). PTHrP is produced by cells near the ends of developing bones and positively maintains a pool of proliferating chondrocytes through progression from resting to proliferative zones, and prevention of transitioning from proliferative to hypertrophic zones (Karaplis et al., 1994; Lanske et al., 1996). However, once the proliferating chondrocytes become sufficiently distant from the PTHrP-producing cells, Ihh production begins as the chondrocytes undergo hypertrophy. Ihh functions to keep chondrocytes proliferating and stimulate PTHrP-producing cells, thereby preventing early transition to hypertrophy (St-Jacques et al., 1999; Vortkamp et al., 1996). The cooperation of these two proteins maintains adequate progression of chondrocytes through the zones of the growth plate (Kronenberg, 2003).

Craniofacial Bone Development

Craniofacial bone development involves the integration of individual skeletal elements undergoing both ossification processes and deriving from several cell lineages. However, the embryonic origins of the skull can be divided into three developmental divisions: the cranial vault or calvaria, the cranial base, and the facial skeleton (Figure 1-

2). The proper amount and direction of growth of these elements is necessary for the stability of the future skull (Sperber et al., 2010).

The Calvaria (Desmocranum)

The role of the calvaria, cranial vault, or desmocranum is to protect the brain. The etymology of the term desmocranum comes from “desmos” (membrane) and “cranium” (skull), and denotes the formation of this craniofacial division through intramembranous ossification (Sperber et al., 2010; Toma et al., 1997). As the fetal brain develops, a dual-layered, capsular membrane surrounds it. This membrane has an inner endomeninx, which is of neural crest origin and will form the two inner meninges, the pia mater and arachnoid. The outer ectomeninx, of both paraxial mesoderm and neural crest origin, differentiates into the third meninx, the dura mater, and an outer membrane with chondro- and osteogenic properties. In the region of the future calvaria, this outer membrane undergoes intramembranous ossification to form the bones of the cranial vault, while this membrane undergoes endochondral ossification at the region of the future cranial base (Sperber et al., 2010). Due to the involvement of cells of both mesodermal and neural crest origin, the resulting bones will be of mixed embryonic cell origin (Lenton et al., 2005). Ossification of the calvarial bones is influenced by the underlying dura mater, acting as a periosteum, and requires the developing brain. Fetal development lacking a brain, such as the syndrome anencephaly, results in the absence of an ossified calvaria (Harris et al., 1993; Mandarim-de-Lacerda and Alves, 1992; Sperber et al., 2010).

The Cranial Base (Chondrocranium)

The cranial base derives from the phylogenetically ancient cranial floor. The etymology of the term chondrocranium comes from “chondros” (cartilage) and cranium,

and denotes the formation of this craniofacial division through endochondral ossification. This portion of the cranial skeleton forms as the ectomeninx undergoes chondrogenesis first, followed by ossification (McBratney-Owen et al., 2008). The cranial base derives from two cell types and the resulting bones can be divided into two regions: the anterior prechordal region of neural crest origin, and the posterior region of mesodermal origin. Ultimately, the junction of the future basisphenoid and basioccipital bones delineates the boundary between these regions (McBratney-Owen et al., 2008; Sadler and Langman, 2009). Unlike the desmocranum, which rapidly expands in tandem with the growing brain, the chondrocranium has relative stability in growth; this serves to maintain the relationships of blood vessels, cranial nerves, and the spinal cord running through it. In addition to being affected by conditions of abnormal fetal brain development, cranial base development can also undergo developmental aberrations due to afflictions of cartilage growth (Sperber et al., 2010).

The Facial Skeleton (Viscerocranium)

The facial skeleton derives from the phylogenetically ancient branchial arches. The etymology of the term viscerocranium comes from “viscus” (organ) and cranium, and forms the aditus for the visual, aural, and respiratory systems, as well as comprises the oromasticatory apparatus. As a whole, the facial skeleton forms from intramembranous ossification of cells of neural crest origin (Jiang et al., 2002a). This craniofacial element is typically divided into three regions – the upper, middle, and lower – corresponding to the embryologic frontonasal, maxillary, and mandibular prominences, respectively. The upper division of the face is primarily of neurocranial composition, owing to the contribution of the frontal bone of the calvaria also forming the forehead.

The middle division, the most complex of the three, involves an attachment to the cranial base, nasal extension from the upper division, and part of the masticatory apparatus. The lower division includes the remaining masticatory apparatus, as it is composed of the mandible and its dentition. As the facial skeleton derives entirely from neural crest origin, congenital abnormalities involving this craniofacial element are often due to aberrations in neural crest tissue (neurocristopathy) (Sperber et al., 2010). In fact, cleft lip and palate disorders, the most common craniofacial birth defects in the United States, are typically due to insufficiencies of neural crest tissue in the frontonasal prominence during development (Arosarena, 2007).

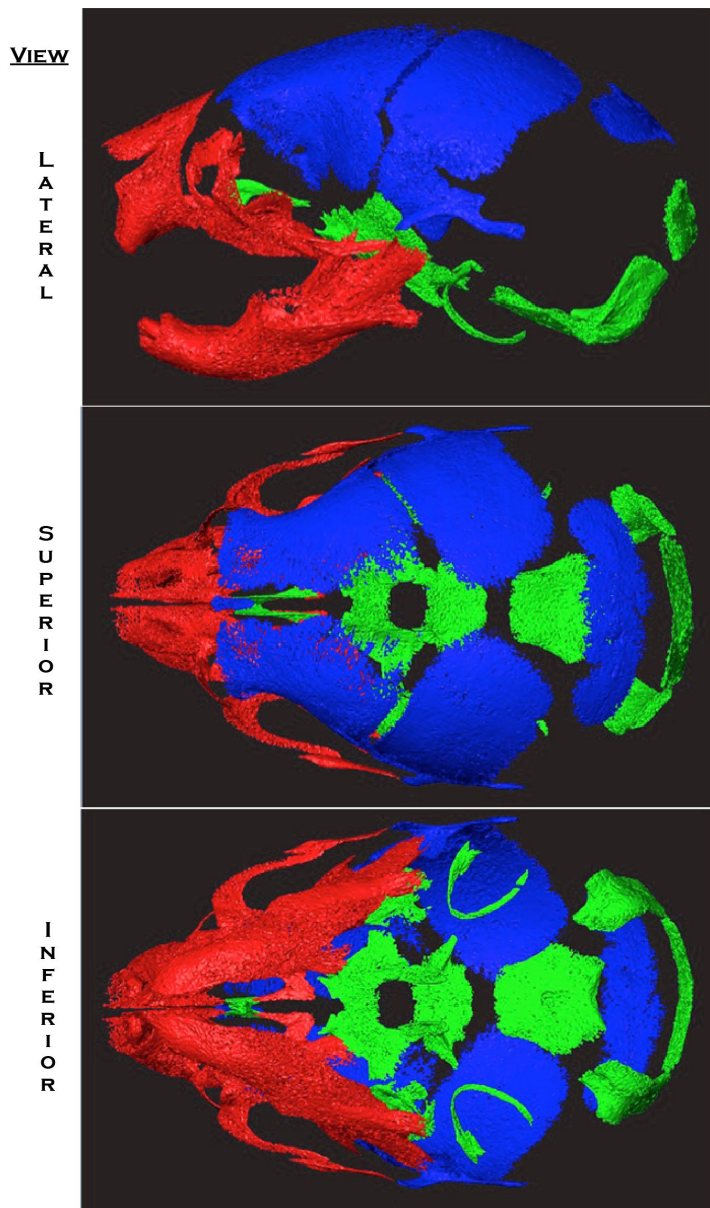


Figure 1-2. Divisions of the craniofacial skeleton.

The craniofacial skeleton is subdivided into three distinct regions based on embryologic and phylogenetic origins. These regions are the calvaria or *desmocranum* (blue), the cranial base or *chondrocranium* (green), and the facial skeleton or *viscerocranum* (red). Collectively, the *desmocranum* and *chondrocranium* make up the *neurocranium*. Divisions are shown on a 3D micro-CT reconstruction of a newborn murine skull.

Postnatal Bone Growth, Remodeling, and Healing

Newborn Bone Development

The period immediately after birth involves significant changes in all of the organ systems, including bone, due to the lack of placental nutrients. Skeletal development particularly slows during this period, as the body must adapt to obtaining calcium through dietary sources, such as milk intake (Rauch and Schoenau, 2001a). Once the neonate adapts to these conditions, regular and rapid bone growth ensues, characterized by active bone formation and resorption; the net balance of the two favors bone formation. Additionally, there is a decrease in volumetric density in long bones, as the marrow cavity expands. These changes have been termed “physiologic osteoporosis of infancy”, where the term osteoporosis denotes a general decrease in bone density. However, the decrease in bone density is not accompanied by a decrease in bone strength as a redistribution of bone mineral density occurs favoring the periosteal surface (Rauch and Schoenau, 2001a, b).

Ossification Centers and Long Bone Expansion

As discussed above, a vascular invasion of the cartilage anlagen of future long bones is necessary to allow osteoblast precursors to migrate to the site for bone formation. This initial nidus for osteogenesis is termed the primary center of ossification. Most of these centers appear before birth (Sperber et al., 2010). Additionally, secondary centers of ossification will appear in growing bones peri- and postnatally (Burkus et al., 1993). Appearing at the ends, or epiphyses, of long bones, secondary ossification centers are bounded above and below by the articular cartilage and growth plate, respectively (Junqueira and Carneiro, 2005). Both ossification centers expand and eventually produce

cavities that are filled with bone marrow (Karsenty and Wagner, 2002). The highly organized growth plate cartilage (discussed above) is responsible for the longitudinal growth of long bones. Ultimately, the growth plate cartilage disappears in long bones by young adulthood, at which point longitudinal growth of these bones ceases; this event is called epiphyseal closure. While longitudinal growth is impossible at this point, bone widening may still occur at the periosteum through intramembranous ossification (Duan et al., 2003; Garn, 1972).

Bone Remodeling

Bone undergoes a constant process of tissue renewal for a variety of physiologic reasons, such as the extrusion of calcium necessary for normal mineral homeostasis. It does this through the process of bone remodeling, where osteoclast resorption is coupled tightly with osteoblast bone deposition (Confavreux, 2011). During longitudinal bone growth, remodeling occurs to the extent that the newly formed bone is shaped properly (Salter, 1999). In healthy adults, bone remodeling maintains a delicate balance of bone formation and resorption (Confavreux, 2011). However, in old age, bone deposition cannot keep pace with osteoclast-mediated bone resorption. Therefore, elderly persons are typically in a state of negative bone balance (Salter, 1999), which can lead to the prevalent, age-related disease osteoporosis, characterized by unbalanced bone remodeling, with low bone mass and altered architecture, resulting in increased susceptibility to bone fracture (Confavreux, 2011).

Bone Healing and Fracture Repair

Bone repair is necessary for restoration of skeletal integrity following insult, either by trauma or skeletal surgery. The reparative process begins immediately after fracture

occurs in a bone, and involves both intramembranous and endochondral ossification processes (Einhorn, 1998; Gerstenfeld et al., 2003). Initially, when a bone is fractured, blood vessels are damaged and produce a localized hematoma. Infiltration of blood at the fracture site brings inflammatory cells and related cytokines and growth factors that recruit local mesenchymal stem cell (MSC) progenitors, mainly from the periosteal cambium layer (Allen et al., 2004; Le et al., 2001; Orwoll, 2003). The blood clot from the hematoma and adjacent matrix are removed by infiltrating macrophages and osteoclasts, respectively, and are replaced by a soft procillus of fibrocartilage tissue near the fracture site. Nearest to the fracture site, endochondral bone formation occurs as this region is furthest from oxygenated blood supply and cartilage formation requires low oxygen tension (Schipani, 2005). Intramembranous bone formation takes place furthest from the fracture site, where intact blood vessels are still present (Thompson et al., 2002). Vascular invasion into the soft procillus allows osteoblast precursors to invade and replace the cartilage with a hard callus formed of primary (woven) bone. Ultimately, this primary bone is remodeled into its normal cortical (compact) and trabecular (cancellous) bone and skeletal integrity is regained (Einhorn, 1998; Gerstenfeld et al., 2003; Le et al., 2001).

CTGF and the CCN Family of Proteins

CTGF's Modular Structure and Function

Connective tissue growth factor (CTGF/CCN2) is a 38kDa, cysteine rich, extracellular matrix protein that belongs to the CCN family of proteins. This family was named after the three original members: Cysteine-rich 61 (Cyr61/CCN1), CTGF/CCN2, Nephroblastoma overexpressed (Nov/CCN3) (Bork, 1993). More recent members include

the Wnt-induced secreted proteins-1 (WISP-1/CCN4), -2 (WISP-2/CCN5) and -3 (WISP-3/CCN6) (Brigstock, 2003). To date, a total of six distinct members have been identified and a nomenclature committee named them CCN1-6 according to the order in which they were discovered (Brigstock et al., 2003). Members of the CCN family are multi-modular proteins containing four conserved modules (with the exception of CCN5 which lacks the C-terminal or fourth module) that are also present in other unrelated extracellular proteins (Brigstock, 1999; Lau and Lam, 1999; Perbal, 2001). The CTGF gene consists of 5 exons, the first coding for a signal peptide (for secretion) and exons 2-5 coding for each of the four different modules. Module 1 is an insulin-like growth factor binding protein (IGFBP) domain, module 2 is a von Willebrand type C (VWC) domain, module 3 is a thrombospondin-1 (TSP-1) domain, and module 4 is a C-terminal (CT) domain containing a putative cysteine knot (Figure 1-3A) (Brigstock, 2003; de Winter et al., 2008; Perbal, 2004).

CTGF has been shown to regulate a diverse array of cellular functions including proliferation, migration, adhesion, survival, differentiation and synthesis of extracellular matrix (ECM) proteins in various cell types (Brigstock, 2003; de Winter et al., 2008; Perbal, 2001, 2004). CTGF has also been implicated in more complex biological processes such as angiogenesis, chondrogenesis, osteogenesis, wound healing, fibrosis and tumorigenesis (Figure 1-3B) (Cicha and Goppelt-Struebe, 2009; de Winter et al., 2008; Perbal, 2001, 2004). The diverse biological activities of CTGF are consistent with its modular structure. Recent studies have shown that individual domains can regulate different cellular functions (Grotendorst and Duncan, 2005), certain modules can act interdependently (Brigstock, 2003), and the presence or absence of other growth factors

can influence the biological response of the target cell (Cicha and Goppelt-Strube, 2009; Grotendorst and Duncan, 2005; Grotendorst et al., 2004).

Matricellular Interactions of CTGF

CTGF was first identified in the conditioned media of human umbilical vein endothelial cells (Bradham et al., 1991). The direct stimulation of CTGF by transforming growth factor beta (TGF- β), the most potent inducer of CTGF expression, was first demonstrated in human skin fibroblasts, and during wound repair *in vivo* where there is a coordinated up-regulation of TGF- β followed by CTGF expression (Igarashi et al., 1993). In addition to TGF- β , CTGF is also induced by other growth factors and secreted into the ECM, where it associates with cell surface proteins and extracellular matrix components (Cicha and Goppelt-Strube, 2009). Studies have demonstrated that CTGF binds to specific cell surface integrins via its C-terminal module in a cell type-dependent manner (Gao and Brigstock, 2004, 2006; Hoshijima et al., 2006). This interaction with cell surface integrins can account for some of its functions such as cell adhesion, migration and extracellular matrix protein deposition, events that are mediated by the activation of focal adhesion kinase (FAK) and other intracellular signaling molecules (Chen et al., 2001; Ono et al., 2007; Tan et al., 2009). It has also been shown that CTGF can interact with other growth factors, and therefore, positively or negatively modulate growth factor signaling (Cicha and Goppelt-Strube, 2009). For example, CTGF can bind to TGF- β_1 and enhance TGF- β receptor signaling while inhibiting bone morphogenetic protein (BMP) receptor signaling through its interaction with BMP-4 (Abreu et al., 2002).

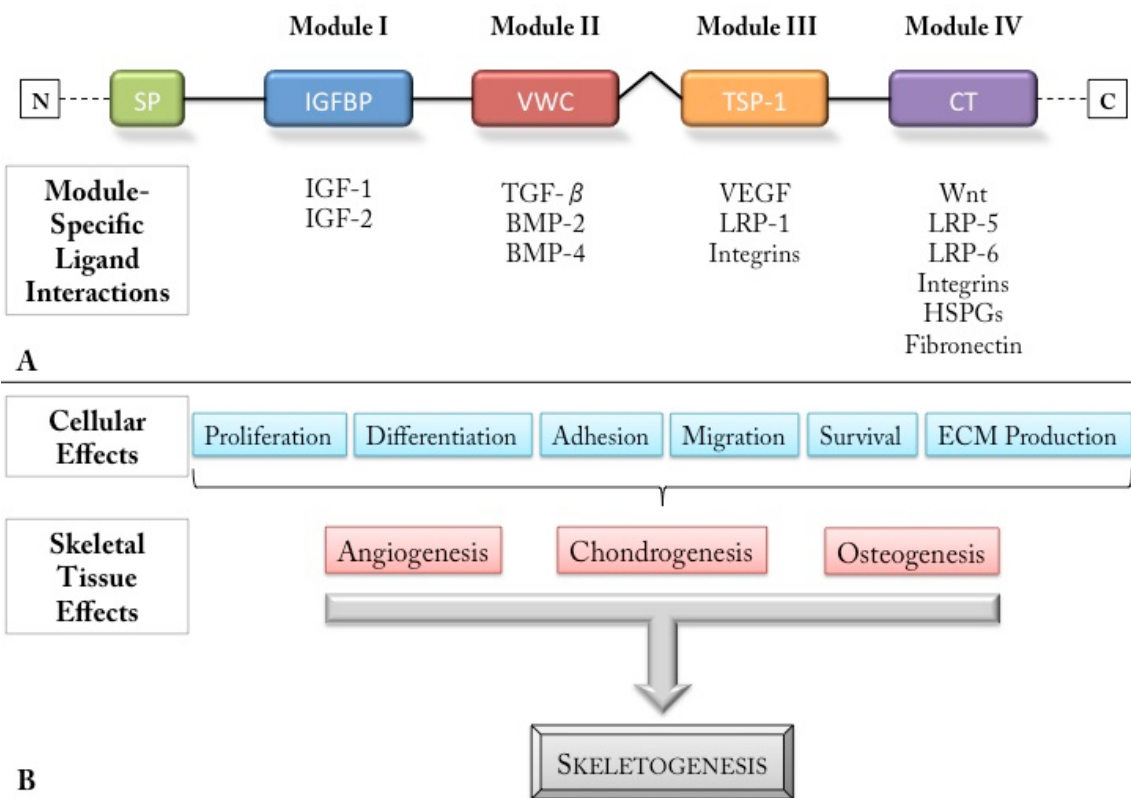


Figure 1-3. CTGF modular structure and function.

- A) The CTGF transcript contains a signal peptide (SP) as well as four modules: module 1 is an insulin-like growth factor (IGF)-binding protein domain; module 2 is a von Willebrand type C domain; module 3 is a thrombospondin-1 domain; and module 4 is a C-terminal domain containing a putative cysteine knot. Modules II and III are separated by a variable hinge region susceptible to enzymatic cleavage. Also shown below each module are molecules known to interact with this region of the secreted CTGF protein.
- B) The mosaic structure of these proteins allows for their involvement in many normal cellular events that contribute to key physiologic processes necessary for skeletogenesis (Note: This figure was adapted from (Arnott et al., 2011)).

The Role of CTGF in Skeletal Development

A role for CTGF in the skeletal tissues began to emerge in studies demonstrating its expression in developing cartilage, bone and teeth (Friedrichsen et al., 2003; Ivkovic et al., 2003; Safadi et al., 2003; Shimo et al., 2002). Studies have shown that CTGF expression is markedly increased during the repair or regeneration of skeletal tissues (Kadota et al., 2004; Nakata et al., 2002; Safadi et al., 2003; Yamashiro et al., 2001). Culture studies using chondrocytes, osteoblasts or surrogate cell lines demonstrated that treatment with recombinant forms of CTGF stimulates the proliferation and differentiation of these cells (Nakanishi et al., 2000; Nishida et al., 2000; Safadi et al., 2003; Yosimichi et al., 2006; Yosimichi et al., 2001). The importance of CTGF in skeletogenesis was confirmed in CTGF-null mice that exhibited multiple skeletal dysmorphisms as a result of impaired growth plate chondrogenesis, angiogenesis, and bone formation and mineralization (Ivkovic et al., 2003). It has been implied that the effects of CTGF on osteogenesis are largely secondary to its chondrogenic effects, such as those during endochondral ossification (Katsume et al., 2009; Kubota and Takigawa, 2007). However, there is an ever-increasing number of studies that demonstrate a direct and important role for CTGF in regulating bone cell development and function that is independent of its chondrogenic effects. In fact, the levels of CTGF expressed in and produced by osteoblasts and their progenitors at active bone forming sites *in vivo*, as well as in culture, are equivalent to or greater than those in cartilage (Arnott et al., 2007; Friedrichsen et al., 2003; Safadi et al., 2003; Xu et al., 2000; Yamashiro et al., 2001).

CTGF in Prenatal Skeletal Development

During embryogenesis, CTGF is expressed at different times and places in the developing skeleton. It is initially expressed during condensation of mesenchymal cells that will form the cartilaginous anlagen of the endochondral bones (Friedrichsen et al., 2003; Ivkovic et al., 2003; Song et al., 2007), and in developing Meckel's cartilage (Shimo et al., 2004). The mesenchymal progenitor cells must proliferate and migrate to the sites of future endochondral bones. Cell motility occurs via the activation of the FAK/Src signaling pathway, which is the first step in cell condensation (Bang et al., 2000). Once these motile cells aggregate into pre-cartilage condensations, FAK is down-regulated and cell-cell contacts are highly favored. Condensation has been shown to be directed by TGF- β , a signaling protein that regulates this process through its simultaneous regulation of fibronectin and several cell adhesion molecules, such as N-CAM, necessary for cell-cell communication (Goldring et al., 2006; Hall and Miyake, 2000). Recent studies have shown that CTGF is also essential for the formation of pre-cartilage condensations. Studies have demonstrated that CTGF stimulates mesenchymal cell proliferation, migration and aggregation (condensation), while knockdown of CTGF or application of CTGF neutralizing antibodies prevented these effects (Shimo et al., 2004; Song et al., 2007). Silencing of CTGF using siRNA and antisense oligonucleotide approaches demonstrated that TGF- β -induced condensation of C3H10T1/2 mesenchymal cells was inhibited in micromass cultures (Song et al., 2007). Cell proliferation and migration, two crucial events for condensation, were also significantly reduced in these cells. In another study, mesenchymal cells isolated from E10 first branchial arches formed increased numbers of cellular aggregates (nodules) in micromass cultures treated

with recombinant CTGF (rCTGF) and this effect was blocked in the presence of CTGF neutralizing antibodies (Shimo et al., 2004). In a study using E13.5 CTGF-null mesenchymal cells obtained from CTGF-null mice, when plated at high density the cells failed to undergo condensation and exhibited a decrease in proteoglycan synthesis (marker of the initiation of cell differentiation) compared to mesenchymal cells from wild-type mice (Pala et al., 2008). Additionally, the loss of FAK induced the expression of a few chondrogenesis markers, including L-SOX-5, Col2a1 and CTGF (Pala et al., 2008). The data from these studies reveal that proper timing and regulation of CTGF expression is important for cell condensation and subsequent chondrocyte differentiation during chondrogenesis (Pala et al., 2008; Shimo et al., 2004; Song et al., 2007).

Immunofluorescent localization of CTGF, TGF- β 1 and SOX-9 during development of vertebral bodies in mice demonstrated that both CTGF and TGF- β 1 were highly expressed and co-localized in mesenchymal cell condensations at E10.5 (Song et al., 2007). On the contrary, the expression of SOX-9 and CTGF were inversely related, with SOX-9 being highly expressed in chondrocytes of developing cartilage at E12.5 while CTGF expression was low in chondrocytes but high in the surrounding perichondrium (Song et al., 2007). Although CTGF appears to play an important role in mesenchymal cell condensation, the absence of its expression in differentiating chondrocytes suggests that its down-regulation is required for chondrocyte differentiation to proceed. Future studies could examine whether sustained CTGF expression in mesenchymal cells blocks subsequent chondrocyte differentiation following condensation.

In addition to its role during cell condensation and subsequent chondrocyte differentiation, CTGF is also expressed in the growth plate, in the periosteum, and in

osteoblasts of developing endochondral bones (Friedrichsen et al., 2003; Ivkovic et al., 2003; Xu et al., 2000). In the growth plate, it is expressed at moderate levels in the proliferative zone and at high levels in the hypertrophic zone (Ivkovic et al., 2003; Kawaki et al., 2008a). Corresponding to its expression in hypertrophic chondrocytes, absence of CTGF results in inhibition of terminal chondrocyte differentiation (Ivkovic et al., 2003; Kawaki et al., 2008a).

CTGF in Postnatal Bone Formation and Remodeling

A role for CTGF in osteogenesis was first appreciated when it was discovered by virtue of its dramatic over-expression in osteopetrosic bone (Xu et al., 2000). Since then, several studies have demonstrated increased CTGF expression accompanying active bone formation. During postnatal bone growth, CTGF is highly expressed in active osteoblasts lining osteogenic surfaces (Safadi et al., 2003). CTGF is expressed at moderate levels in osteoblasts and osteocytes in alveolar bone adjacent to the periodontal ligament as a result of bone forming activity associated with physiological tooth movement (Yamashiro et al., 2001). The mechanical stimulation of bone caused by experimental tooth movement dramatically increased the expression of CTGF in osteoblasts and osteocytes around the periodontal ligament (Yamashiro et al., 2001). In a model for distraction osteogenesis, CTGF expression was increased in mesenchymal cells, hypertrophic chondrocytes and osteoblasts in the area of new bone formation, suggesting that CTGF plays an anabolic role in endochondral and intramembranous bone forming processes (Kadota et al., 2004; Nakata et al., 2002). CTGF expression was dramatically increased in active osteoblasts during formation of the hard (bony) callus in studies of fracture healing (Nakata et al., 2002; Safadi et al., 2003).

CTGF in Skeletal Cell Differentiation and Function

Osteoblasts and CTGF

CTGF AND OSTEOBLAST DIFFERENTIATION AND FUNCTION

CTGF is produced and secreted by osteoblasts in culture (Parisi et al., 2006; Safadi et al., 2003). Analysis of the temporal pattern of CTGF expression in primary osteoblast cultures revealed that CTGF levels were high during the proliferative phase, abated in confluent cultures, and increased again to maximal levels during matrix production and maturation, remaining at high levels during mineralization (Safadi et al., 2003). Different groups have also demonstrated that CTGF stimulates osteoblast proliferation, matrix production and differentiation in cultures of osteoblasts (Arnott et al., 2007; Nishida et al., 2000; Safadi et al., 2003; Takigawa et al., 2003; Xu et al., 2000). Treatment of primary osteoblasts or osteoblastic cell lines (Saos-2 or MC3T3-E1) with rCTGF promotes proliferation, up-regulates the expression of various markers of osteoblast differentiation, including type I collagen (Col1A1), alkaline phosphatase (ALP), osteopontin (OP) and osteocalcin (OC), and stimulates matrix mineralization and mineralized nodule formation (Nishida et al., 2000; Safadi et al., 2003). On the contrary, calvarial osteoblasts and stromal cells isolated from CTGF transgenic mice displayed decreased ALP and OC mRNA levels (see section on CTGF and Animal Models) (Smerdel-Ramoya et al., 2008).

CTGF levels in osteoblasts are stimulated by TGF- β_1 and BMP-2 (Arnott et al., 2007; Nakanishi et al., 1997; Parisi et al., 2006), a finding that is consistent with a role for CTGF in the effects of these proteins on osteoblast growth and differentiation. Mesenchymal cells stimulated with Wnt-3A and BMP-9 identified CTGF as a target

during osteoblast lineage-specific differentiation (Luo et al., 2004). At the early stages of osteoblast differentiation, CTGF was up-regulated by Wnt-3A and BMP-9, and CTGF silencing blocked BMP-9-induced osteogenic differentiation. This up-regulation of CTGF was not evident at later stages of osteoblast differentiation. Furthermore, constitutive expression of CTGF had the opposite effect, inhibiting both Wnt-3A and BMP-9-induced osteoblast differentiation. These results suggest that CTGF plays a role in early events of osteogenic differentiation, such as proliferation and recruitment of osteoprogenitors (Luo et al., 2004). The tight regulation of CTGF expression and the precise temporal interactions between CTGF and other osteogenic growth factors appear to be critical for normal osteoblast differentiation and additional studies are needed to elucidate the role of CTGF in this process.

THE OSTEOINDUCTIVE PROMISE OF CTGF

Considering the apparent beneficial effects of CTGF on osteoblast differentiation and bone formation, recent studies have tested applications of its use in bone regeneration to promote bone healing or new bone formation. Injection of rCTGF injection into the marrow cavity of rat femurs elicited an osteoinductive response in the form of osteoblast differentiation and active bone formation (Safadi et al., 2003; Xu et al., 2000). When a hydroxyapatite carrier loaded with CTGF was implanted into bone defects within a rabbit mandible, CTGF significantly enhanced the proliferation and migration of human bone marrow stromal cells, induced cell invasion and enhanced bone formation compared with the carrier alone (Ono et al., 2008). Using the intractable bone defect model, treatment with rCTGF induced the osteoblast mineralization markers and enhanced the bone regeneration (Kikuchi et al., 2008). The majority of *in vivo* and *in vitro* studies support an

anabolic role for CTGF on bone formation, and therefore, this factor is a candidate for the development of novel clinical therapeutic approaches to stimulate bone formation.

Information concerning possible molecular mechanisms for CTGF actions and its regulation in bone are reviewed in subsequent sections.

Chondrocytes and CTGF

CTGF IN CHONDROCYTE DIFFERENTIATION

In 1997, differential display PCR studies revealed that the gene, Hcs24, was expressed in human chondrosarcoma-derived chondrocytes (HCS-2/8 cell line) and that this gene is identical to CTGF (Nakanishi et al., 1997). It was subsequently shown that when treated with rCTGF, HCS-2/8 chondrocytic cells and primary rib growth plate chondrocytes (RGCs) demonstrated increases in both cell proliferation and proteoglycan synthesis (Nakanishi et al., 2000). Furthermore, it was shown that CTGF promotes chondrocyte maturation hypertrophy, exhibited by an increase in ALP activity in treated RGCs (Nakanishi et al., 2000). A closer look at the synthesis, processing and secretion of CTGF in HCS-2/8 chondrocytic cells, revealed differences depending on the stage of maturation of the cells (Kubota et al., 2001). In proliferating chondrocytes, CTGF was immediately released upon synthesis, and most of the secreted CTGF was free in the culture supernatant. After the cells reached confluence, secretion slowed as the cells matured, and most of the secreted CTGF accumulated in the ECM surrounding the cells (Kubota et al., 2001). These data demonstrated differential regulation of CTGF secretion and processing depending on the status of cell growth and differentiation.

SIGNALING OF CTGF IN CHONDROCYTES

To elucidate a mechanism through which CTGF regulates chondrocyte proliferation and differentiation, investigators have examined its interaction with BMPs as well as mitogen-activated protein kinase (MAPK) signaling pathways, as both have been shown to play a significant role in skeletal development (Wan and Cao, 2005). Biochemical studies have shown that CTGF directly interacts with BMP-4 via its cysteine-rich domain (domain 4) and prevents BMP-4 from binding to its receptor, thereby inhibiting BMP signaling (Abreu et al., 2002). A more recent study demonstrated that CTGF also interacts with BMP-2 via its fourth domain (Maeda et al., 2009). When examining the combined effect of CTGF and BMP-2 on chondrocyte proliferation and differentiation using HCS-2/8 chondrocytic cells, there was no synergistic effect on proliferation compared to separate treatment with each growth factor (Maeda et al., 2009). However, combined treatment did enhance proteoglycan synthesis, indicative of chondrocyte differentiation. This was further demonstrated in primary mouse chondrocytes where treatment with both growth factors simultaneously increased cartilage differentiation markers, such as type II collagen, aggrecan, type X collagen, and Runx-2/Cbfa1 (Maeda et al., 2009).

In addition to BMP signaling, CTGF has also been shown to regulate the proliferation and differentiation of chondrocytes via Protein Kinase and MAPK signaling pathways (Yosimichi et al., 2006; Yosimichi et al., 2001). Involvement of protein kinase C (PKC) in CTGF-mediated signaling in chondrocytes was demonstrated by inhibition of PKC in rCTGF-treated HCS-2/8 chondrocytic cells. These cells demonstrated significantly reduced proliferation and differentiation (Figure 1-4). Furthermore, PKC is

an important upstream protein in CTGF-mediated signaling to multiple kinase signaling pathways; these include MEK/ERK, p38, and protein kinase B (PKB) (Yosimichi et al., 2006; Yosimichi et al., 2001). Using specific inhibitors, it was shown that CTGF-mediated activation of MEK/ERK, p38, or PKB causes selective stimulation of chondrocyte proliferation, maturation, or terminal differentiation, respectively (Figure 1-4). CTGF also activates JNK, another member of the MAPK family, and JNK activation is involved in the proliferation and maturation of RGCs and HCS-2/8 chondrocytic cells (Figure 1-4). Lastly, a role for phosphatidylinositol 3-kinase (PI3K), an upstream kinase to PKB, was also identified. Treatment of RGCs with CTGF and specific inhibitors of PI3K and PKC inhibited ALP activity, suggesting that both PKC and PI3K are involved in terminal differentiation of chondrocytes (Figure 1-4). These studies demonstrate that CTGF is an important regulator of chondrocyte proliferation and differentiation.

Who have we forgotten? CTGF in Osteoclasts and Osteocytes

CTGF AND OSTEOCLAST DIFFERENTIATION AND FUNCTION

As mentioned previously, studies have demonstrated a marked increase in CTGF expression during the repair or regeneration of skeletal tissues, such as in the bony callous produced during fracture repair (Kadota et al., 2004; Nakata et al., 2002; Safadi et al., 2003; Yamashiro et al., 2001). Additionally, perturbations in the hypertrophic regions of growth plates occur in CTGF-null long bones (discussed below) (Arnott et al., 2011; Ivkovic et al., 2003), which could be partly due to defects in osteoclast-mediated cartilage degradation. It has been shown that osteolytic metastases of human breast cancer cells (MDA231) in mice was decreased by a CTGF blocking antibody. Upon histologic inspection, these metastases had decreased mature osteoclast numbers (Shimo et al.,

2006). Expression of CTGF in osteoclast-like cells increases as these cells undergo maturation *in vitro*. When treated in rCTGF, these cells demonstrate significantly enhanced tartrate-resistant acid phosphatase (TRAP)-positive multinucleated cell formation, possibly due to their interaction with dendritic cell-specific transmembrane protein (DC-STAMP), a protein involved in cell-cell fusion (Nishida et al., 2011).

EXPRESSION OF CTGF IN OSTEOCYTES

Very little has been done to study the role of CTGF in osteocyte development or function. Immunostaining for CTGF in postnatal day 3 (P3) murine parietal bone sections has revealed the expression of CTGF in osteocytes near the bone surface. However, this expression was gone as the osteocytes moved further (30 μ m depth) from the bone surface (Kawaki et al., 2011). This would suggest a role in osteoblast-osteocyte transition but not in mature osteocyte function. Further studies are needed to elucidate any potential effects of exogenous CTGF administration or blockade in osteocyte development and function.

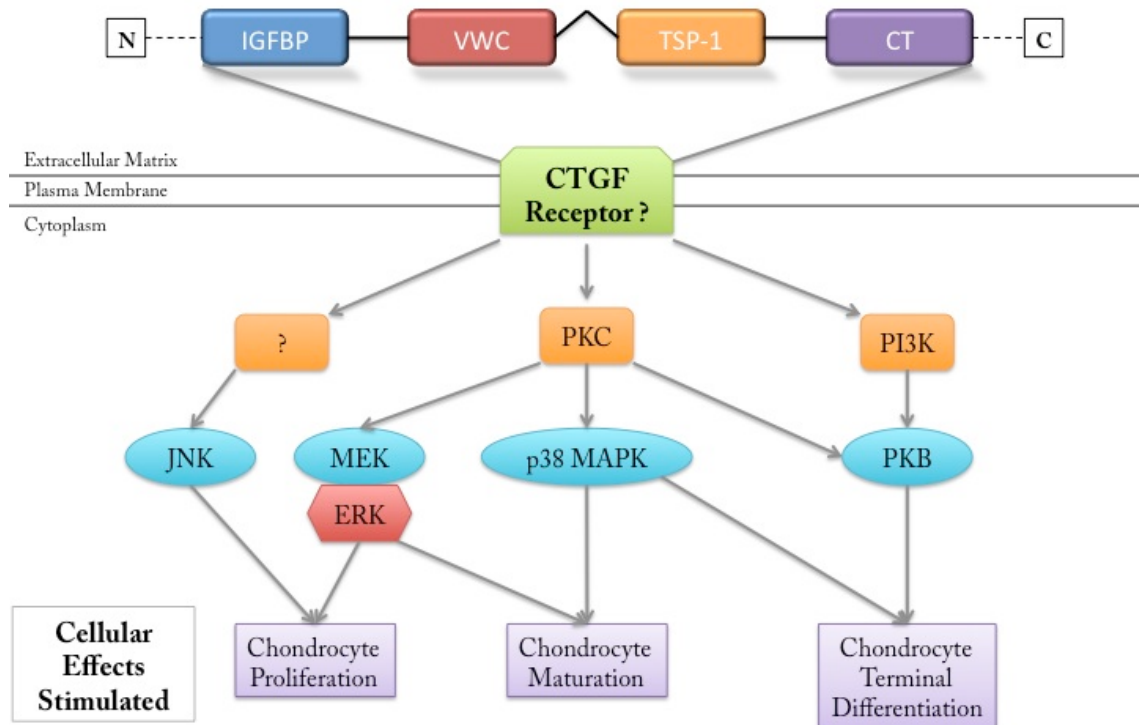


Figure 1-4. CTGF signaling in chondrocytes

CTGF interacts with (an) unknown receptor(s) on the surface of chondrocytes via binding of one or more of its four distinct modules. This interaction triggers various intracellular pathways. PKC plays an important upstream role in chondrocyte proliferation, maturation, and terminal differentiation via its activation of MEK, p38, and PKB, respectively. CTGF-activated activation of PI3K also stimulates chondrocyte terminal differentiation via PKB. This figure was adapted from Yosimichi, G., et al., (2006). *Bone*, 38(6), 853-863 (Yosimichi et al., 2006).

CTGF and Animal Models: An *In* and *Ex Vivo* Look

Elucidating the *in vivo* importance of CTGF in skeletogenesis has required a multifaceted approach utilizing overexpressing transgenic as well as knockout mice. The action of many growth factors requires an appropriate balance in physiologic levels, where either too much or too little can be deleterious. Therefore, an essential approach to characterizing the effects of CTGF on skeletal formation requires the generation of genetically engineered animal models where the physiologic scale is tipped in either direction. Here we provide an overview of the studies and findings to date using animal models to study the role of CTGF in skeletogenesis; these include global and conditional knockout models, as well as transgenic models. We will discuss both *in vivo* findings, as well as *ex vivo* studies that utilized skeletal cells derived from these genetically engineered animal models.

CTGF Global Ablation (Knockout) Models

THE TWO KNOCKOUT MODELS FOR CTGF ABLATION

A role for CTGF in skeletal development has been illustrated in studies using one of two global knockout models, both of which appear to produce a similar skeletal phenotype (as described below) (Crawford et al., 2009; Ivkovic et al., 2003). The first model described in 2003 in the context of growth plate chondrogenesis and endochondral bone formation, was generated by replacing a fragment containing exon 1 (signal peptide), the TATA box and the transcription start site with the neomycin-resistance gene. Due to the design of the construct, Southern blot analysis could be used to genotype resulting litters when crossing heterozygous parents, and therefore discern wild-type

(WT, +/+)¹, heterozygous (+/-) and null (-/-) offspring (Ivkovic et al., 2003). The second model, described in 2008 in the context of pancreatic islet development, was generated by replacing the coding sequence of CTGF within exons 3 through 5 with a transmembrane domain-lacZ/Neomycin phosphotransferase cassette.(Crawford et al., 2009) While a single RT-PCR amplification is not possible to discern the three genotypic possibilities from crossing two heterozygous parents (CTGF +/+, +/-, -/-), a clear advantage of this model is the ability to utilize an antibody to β-gal and/or X-gal staining to determine the location and distribution of the CTGF-β-gal fusion protein in heterozygous and null offspring. To date, much of the *ex vivo* work done with cells isolated from global CTGF knockout mice has utilized the former model; the details of which will be discussed subsequently (Baguma-Nibasheka and Kablar, 2008; Chen et al., 2004; Crawford et al., 2009; Kawaki et al., 2008a; Kawaki et al., 2008b; Kuiper et al., 2007; Mori et al., 2008; Nishida et al., 2011; Nishida et al., 2007; Pacheco et al., 2008).

SKELETAL PHENOTYPE OF CTGF NULL MICE

The importance of CTGF in skeletogenesis was first demonstrated by Lyons and colleagues in CTGF null mice, which showed defects in growth plate chondrogenesis, angiogenesis, bone formation/mineralization, and ECM production. While skeletal defects were region specific, they reproducibly included kinked ribs, tibiae, radii and ulnae, as well as craniofacial abnormalities (Ivkovic et al., 2003). Ultimately, global ablation of CTGF results in neonatal lethality caused by respiratory failure secondary to misshapen ribs and pulmonary hypoplasia (Baguma-Nibasheka and Kablar, 2008;

¹ Unless otherwise specified, CTGF ‘WT’ mice includes both CTGF +/+ and +/- genotypes.

² For ultrastructure studies, trabecular bone (TB) under the growth plate comprises newly

Ivkovic et al., 2003). The neonatal lethality of these knockout mice represents a challenge in studying the full role of CTGF in skeletogenesis, namely the inability to study the effects of CTGF ablation during postnatal skeletal development, maintenance, and aging.

EFFECTS OF CTGF ABLATION ON OSTEOGENESIS

Further *in vivo* analysis of skeletogenesis in CTGF KO mice has focused on embryonic development at E15.5, 16.5 and 18.5. At E15.5 only the periosteal bone collar is visible microscopically in extremity long bones, and at E16.5 trabecular bone is just beginning to form in the primary centers of ossification (Kawaki et al., 2008b; Theiler, 1989). Therefore, studies at these times have provided information that is perhaps more applicable to the role of CTGF in bone formed by intramembranous ossification. Using these time points, it was demonstrated that CTGF KO mice have delays in craniofacial ossification, collagen deposition, osteoblast proliferation, and mineralization, as well as decreased tibial trabecular collagen deposition (also at E18.5), ALP activity, periosteal collar mineralization and osteoblast proliferation (Kawaki et al., 2008b). *Ex vivo* studies of CTGF KO and WT primary osteoblasts also showed less Col1A1, ALP and OC expression levels, as well as decreased ALP activity and osteoblast proliferation. Furthermore, it was shown that rCTGF could rescue defects in osteoblast proliferation, mineralization and ALP activity in the CTGF-null osteoblasts (Kawaki et al., 2008b). Lastly, it has been shown that the ossified area in CTGF KO tibiae (E18.5) was reduced in length when compared to WT littermates, while total bone length did not appear different (Kawaki et al., 2008a). Despite the initial 2003 findings of striking skeletal defects, a more in depth, quantitative analysis of the effect of CTGF ablation on bone formation is warranted.

EFFECTS OF CTGF ABLATION ON CHONDROGENESIS

A critical role for CTGF in growth plate chondrogenesis has been more extensively examined in global ablation studies where CTGF-null mice display chondrodysplasia in limb and rib cartilage, as well as deformations in Meckel's cartilage (Ivkovic et al., 2003). It had previously been shown that rCTGF stimulated chondrocyte proliferation *in vitro* (Nakanishi et al., 2000). This was confirmed in CTGF-null chondrocytes, which had an impaired ability to proliferate *in vivo* beginning at E14.5, the time at which CTGF is upregulated in prehypertrophic and hypertrophic chondrocytes, and this resulted in fewer chondrocytes by E18.5 (Ivkovic et al., 2003; Kawaki et al., 2008a). *Ex vivo* studies using CTGF-null primary chondrocytes have confirmed decreased chondrocyte proliferation, as well as shown decreased α_5 integrin expression (Nishida et al., 2007). The α_5 integrin is important in pre-hypertrophic chondrocyte differentiation and its expression overlaps that of CTGF in cartilage (GarciaDiego-Cazares et al., 2004; Nishida et al., 2007). Additional studies revealed a potential role for Nov/CCN3 in the CTGF-null developing cartilage, as CCN3 mRNA is elevated in null chondrocytes, despite decreased levels of CCN6, SOX-9, aggrecan, and Col2a1 mRNA (Kawaki et al., 2008a).

The apparent *in vivo* defects of chondrocyte proliferation at E14.5 also coincided with an increased expansion in the hypertrophic zone of certain bones (e.g. humeri) in CTGF-null mice; this expansion continued until birth (Ivkovic et al., 2003). The noticeable expansion of the hypertrophic zone in CTGF KO mice warranted a closer look as to whether defects in angiogenesis were present in these growth plates. It had previously been shown that defects in vascular endothelial factor (VEGF)- and matrix

metalloproteinase 9 (MMP-9)-mediated angiogenesis resulted in lengthened hypertrophic zones (Gerber et al., 1999; Haigh et al., 2000; Vu et al., 1998). In CTGF KO mice, immunostaining demonstrated that while blood vessels were present in the metaphyseal intertrabecular spaces, the overall network of capillaries in the ossification zone adjacent the hypertrophic zone, was less extensive in the mutant bones (radii) compared to WT littermates (Ivkovic et al., 2003). Further analysis revealed decreased MMP-9 and VEGF expression levels (Ivkovic et al., 2003). Taking into account previous findings that impaired angiogenesis was concomitant with decreased trabecular bone density (Gerber et al., 1999), as well as the appearance of decreased trabecular bone and thinner bone collars in CTGF KO mice, it was concluded that growth plate angiogenesis was indeed defective in these mice (Ivkovic et al., 2003). However, using metatarsals isolated from CTGF WT (+/+), heterozygous (+/-), and KO (-/-) embryos, it was later demonstrated that *in vitro* angiogenesis was not significantly different between these groups (Kuiper et al., 2007). Further studies are necessary to clarify the extent to which angiogenesis is impaired in the CTGF-null growth plates.

HAPLOINSUFFICIENCY OF CTGF IN OSTEOGENESIS

Despite the inability to study CTGF-null mice postnatally, some knowledge on the effects of CTGF ablation has been garnered using CTGF heterozygous mice. It has been shown that CTGF haploinsufficiency results in roughly 50% normal protein levels (Kuiper et al., 2007). When compared to CTGF wild-type (+/+) littermates, heterozygous (+/-) mice are phenotypically normal, lacking any of the aforementioned skeletal defects seen in the null (-/-) mice (Lambi, Popoff, unpublished data; (Canalis et al., 2010)). Furthermore, CTGF heterozygous mice demonstrated reduced trabecular number and

resultant transient osteopenia at 1 month of age, which was not observed in 4- and 6-month old CTGF heterozygous mice (Canalis et al., 2010).

Skeletal-Specific CTGF Conditional Knockout Models

Additional information on CTGF ablation has been obtained through generation of two bone-specific conditional CTGF knockout models. The first of which was constructed using the 2.4-kb paired-related homeobox gene 1 (Prx1) enhancer, previously shown to drive expression beginning in E10.5 limb buds and later in E15.5 tendons and periosteum of fore- and hindlimbs (Logan et al., 2002; Martin and Olson, 2000). Conditional CTGF-null mice under this model demonstrated an osteopenic phenotype at 1 month of age only in male mice (Canalis et al., 2010). Bone parameters were normal at the other ages examined in male mice and at all ages examined in female mice. The second model was constructed using the 3.9-kb human OC promoter capable of driving expression in terminally differentiated (mineralizing) osteoblasts (Canalis et al., 2010; Zhang et al., 2002). Conditional CTGF-null mice under the control of the OC promoter demonstrated an osteopenic phenotype at 6 months of age, but again only in male mice (Canalis et al., 2010). These results suggest that CTGF has a more important role in prenatal skeletal development rather than postnatal bone maintenance. Since the phenotype in conditional knockout mice can vary depending on the promoter being used to target specific cell populations, additional studies utilizing other established skeletal cell-specific promoters are warranted.

Skeletal-Specific CTGF Overexpression (Transgenic) Models

While the majority of the research involving CTGF and skeletogenesis has relied on CTGF ablation, several studies have utilized overexpressing transgenic lines to

provide more information of CTGF's role in bone formation. A model of CTGF overexpression under the control of the type XI collagen promoter (ColXIA1), localized to chondrocytes (Yoshioka et al., 1995), resulted in a decreased size of transgenic mice compared to WT littermates, as well as decreased bone density in the hindlimbs of transgenic mice (Nakanishi et al., 2001). A subsequent study generated bone-specific CTGF overexpression under the control of a 3.8-kb OC promoter (Smerdel-Ramoya et al., 2008). These transgenic mice displayed decreased bone mineralization and trabecular bone volume, as well as decreased rates of bone formation and mineral apposition. *Ex vivo* studies of calvarial osteoblasts and stromal cells isolated from these animals demonstrated decreased ALP and OC mRNA levels in cells from transgenic mice, as well as varying effects on BMP/Smad, Wnt/β-catenin, and insulin-like growth factor (IGF-1) / AKT signaling (Smerdel-Ramoya et al., 2008). These results are contrary to previously reported *in vitro* studies where rCTGF increased the expression of ALP, OC, and other markers of osteoblast differentiation in MC3T3-E1 osteoblastic cells and primary calvarial osteoblasts (Nishida et al., 2000; Safadi et al., 2003). Perhaps the conflicting results from these experiments are caused by differences in the magnitude of CTGF over-expression and/or from differences between intermittent (short-term) exposure to exogenously added rCTGF versus continuous (long-term) exposure from endogenous, over-expression. Such discrepancies highlight yet another area where future studies are necessary, not only utilizing various skeletal cell-specific promoters, but also inducible constructs.

From the studies to date concerning the effects of CTGF on skeletogenesis, one broad conclusion can be drawn: appropriate physiological levels of CTGF are necessary

for normal skeletal development, as animal models with either ablation or overexpression of CTGF have demonstrated phenotypes related to cartilage and/or bone development.

Clinical Relevance of CTGF in Human Skeletal Development and Function

CTGF Promoter Polymorphism and Systemic Sclerosis

While there is no currently identified clinical syndrome directly resulting from a mutation in the CTGF protein, recent evidence demonstrates a polymorphism in the CTGF promoter is associated with a susceptibility to systemic sclerosis (SSc). The polymorphism constitutes a G-945C substitution, the effect of which is to decrease the binding of the key transcriptional repressor, SP3, resulting in increased expression of CTGF (Fonseca et al., 2007). However, this (G-945C) polymorphism does not correlate with increased plasma CTGF levels (Dendooven et al., 2011). SSc, also known as scleroderma, is a heterogenous disorder of the connective tissue and includes in its disease progression immune activation, vascular damage, and eventual tissue fibrosis (Denton et al., 2006). Due to the lack of efficient antifibrotic therapeutics, severe SSc results in mortality due to the fibrosis and subsequent loss of function of skin, vasculature, musculoskeletal system, and internal organs (Denton et al., 2006; Fonseca et al., 2007). In addition to the well-known fibrotic changes seen in SSc, bone mineral density (BMD), bone mass, and bone quality in these patients are deleteriously affected (Frediani et al., 2004a; Frediani et al., 2004b), including both trabecular and cortical bone (Souza et al., 2006). Further studies are necessary to determine if there is a direct link between the G-945C CTGF promoter polymorphism and effects on bone in SSc patients.

WISP-3/CCN6 and Progressive Pseudorheumatoid Dysplasia

Members of the CCN family, such as CTGF, may play a role in regulating the expression of other family members. Importantly, this has been suggested from studies using the CTGF KO mouse in which Nov/CCN3 expression increased in chondrocytes in the absence of CTGF (Kawaki et al., 2008a). Therefore, it is becoming increasingly evident that examining the expression levels of all six CCN family members is prudent in cases of individual mutations causing skeletal abnormalities. In 1999, mutations in Wisp-3/CCN6 were identified as the molecular cause for the syndrome Progressive Pseudorheumatoid Dysplasia (PPD). PPD is an autosomal recessive disorder characterized by juvenile onset arthropathies and progressive erosive bone and joint changes (Hurvitz et al., 1999). However, when mice were generated with the mutations seen in human PPD, the skeletal function was normal (Kutz et al., 2005). This highlights the fact that murine models involving genetic mutations in CCN proteins do not always recapitulate human pathologies. Further investigation is necessary to determine if any CTGF expression is affected as a result of Wisp-3 mutations in PPD.

Targeting CTGF Clinically: FG-3019, a Potential Pyrrhic Victory in Bone?

Levels of CTGF have been shown to be markedly elevated in various injured tissues that develop fibrosis including the skin, kidney, liver and lung (Igarashi et al., 1996; Igarashi et al., 1995; Ito et al., 1998; Lasky et al., 1998; Paradis et al., 2002). More recently, CTGF over-expression has been implicated in the pathophysiology of dystrophic skeletal muscles where it is believed to contribute to the deterioration of skeletal muscles and their function in addition to mediating the ensuing fibrosis of the damaged muscle tissue (Morales et al., 2011). Clinical trials are currently underway using

a fully human IgG_{1K} monoclonal antibody (FG-3019) that recognizes module II of human and rodent CTGF as a novel therapy to treat patients with diabetes, advanced kidney disease, pancreatic cancer and idiopathic pulmonary fibrosis (FibroGen, 2012). This antibody has also been used to treat CTGF-expressing tumors in mice, where it abrogated CTGF-dependent pancreatic tumor growth and lymph node metastasis without any toxic side effects in mice (Dornhofer et al., 2006). FG-3019 has also been used as a therapy in a mouse model of Duchenne muscular dystrophy, where it reversed the fibrosis of muscular tissue and even allowed return of skeletal muscle function (personal communication, Dr. Enrique Brandan). These studies support the concept of using drugs that specifically target CTGF as a treatment for various human diseases. However, the effects of FG-3019 on underlying bone have not yet been investigated. As mentioned previously, CTGF expression increases during fracture repair (Kadota et al., 2004; Nakata et al., 2002; Safadi et al., 2003; Yamashiro et al., 2001). Therefore, it is possible that anti-CTGF therapy could result in delayed or aberrant fracture healing after skeletal injury. This would present a serious detractor to FG-3019 therapy, particularly in post-menopausal women, and presents an area ripe with research potential.

Studies of this Dissertation

It is undoubtedly true that CTGF is necessary for proper skeletal development and function. The neonatal lethality that results from CTGF ablation *in vivo* highlights a critical role for this protein during development of the skeleton. However, a global decrease in bone formation would not account for the unique phenotype seen in CTGF KO mice, and therefore represents an oversimplification of the skeletal defects seen therein. Taking into account the juxtaposition of phenotypically normal and abnormal

bones in a highly reproducible fashion in CTGF KO mice, **we hypothesized that the role of CTGF in bone development is skeletal site specific, such that its loss results in dysregulation of local bone formation in a bone specific fashion.** Osteogenesis of individual bones requires proper regulation of osteogenic differentiation and formation through intramembranous (*de novo* bone formation) and/or endochondral (through preexisting cartilage anlage) ossification processes. Therefore, to draw conclusions as to the extent to which either of these processes is being affected in CTGF KO mice, individual bones or regions within bones forming by a specific ossification process must be isolated and examined. Performing a comprehensive skeletal phenotype characterization of newborn CTGF KO mice compared to their wild-type (WT) littermates, we determined the exact bones affected in the CTGF KO model and the degree to which they are. This involved a thorough analysis of multiple skeletal sites, including both appendicular and axial skeletal divisions, as well as phenotypically normal and abnormal bones (Figure 1-5). We proceeded in a tiered fashion from analysis of the bone volume and microarchitecture by micro-computed tomography (micro-CT), to the bone structure by histomorphometry and immunostaining, to the ultrastructure of bone cells by electron microscopy, and ultimately to the molecular composition of these bones by fluorescent transform infrared (FTIR) spectroscopy.

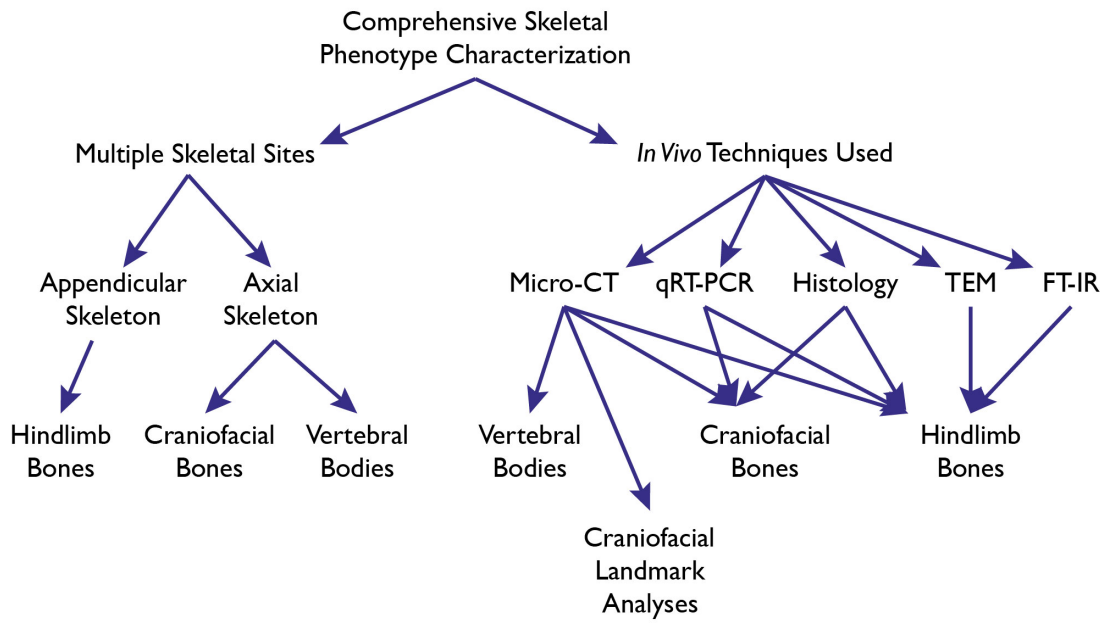


Figure 1-5. Comprehensive Skeletal Phenotype Characterization of CTGF KO Mice

Multiple skeletal sites and *in vivo* techniques were used to produce a comprehensive characterization of the skeletal phenotype seen in CTGF KO mice. Techniques included micro-computed tomography (micro-CT) for bone volume and microarchitecture, quantitative real-time polymerase chain reaction (qRT-PCR) for expression patterns, histomorphometry and immunostaining (histology), transmission electron microscopy (TEM) for bone cell ultrastructure, and Fourier transform infrared (FT-IR) spectroscopy for the molecular composition properties of these bones. A craniofacial landmark analysis was used to define the extent of skull dysmorphology in CTGF KO mice.

In addition to our studies of aberrant appendicular skeleton development in CTGF KO mice, we pursued an in-depth study of the skull dysmorphology seen in this model. It was previously reported that CTGF KO mice demonstrate several craniofacial abnormalities, however, many of the specific bones affected were not identified and no morphologic measurements of size and shape were taken (Kawaki et al., 2008b). Therefore, we established a collaboration with the laboratory of Dr. Joan Richtsmeier, a professor of anthropology at Pennsylvania State University and an expert in craniofacial development. Using a system of cranial Landmark Analysis developed in her laboratory, we marked biologically pertinent loci as anatomic landmarks on three-dimensional micro-CT reconstructions WT and CTGF KO skulls, as previously described (Martinez-Abadias et al., 2010; Wang et al., 2010). Having landmarked the skulls, we computed differences in skull morphology using Euclidean Distance Matrix Analysis (EDMA), also developed by Dr. Richstmeier and colleague (Richtsmeier and Lele, 1993). These tools allowed us to generate a truly unprecedented look at the skull dysmorphology in CTGF KO mice.

Studying the cranial aberrations in CTGF KO mice provided a unique perspective on the role of CTGF in skeletal development. In addition to the cranial abnormalities of CTGF KO mice demonstrating another example of the site-specific effects of CTGF in bone development, the craniofacial bones are distinct from other skeletal sites in that they originate from multiple embryonic cell lineages: neural crest (NC) and paraxial mesoderm (PM) cells. Conventional analysis of craniofacial skeleton development involves the subdivision of the skull into three regions, based on the phylogenetic and embryologic origins: 1) the facial skeleton; 2) the cranial vault or calvaria; and 3) the

cranial base (McBratney-Owen et al., 2008; Noden and Trainor, 2005; Sperber et al., 2010). Ultimately, the craniofacial skeleton develops from the interaction and differentiation of these cell types, as well as both ossification processes, to yield a highly organized concrescence of smaller skeletal units (Noden and Trainor, 2005). Therefore, global and regional skull analyses of CTGF KO mice yield information regarding the potential effects of CTGF in regulating craniofacial bone formation in an embryonic cell specific fashion.

The data obtained from the studies of this dissertation generated novel information regarding the global effects of CTGF in regulating skeletal development *in vivo*. There is an increasing need to comprehensively define the role of CTGF in bone formation and maintenance. Osteoporosis is a worldwide syndrome that comprises a decrease in bone mass, resulting in increased bone fragility and a consequent increase in fracture risk (van den Bergh et al., 2012). Understanding the mechanisms by which CTGF regulates bone formation could help generate novel therapies for treating patients with bone diseases, such as osteoporosis. Additionally, a humanized monoclonal antibody (FG-3019) that globally blocks CTGF is currently in several clinical trials for the treatment of pancreatic cancer, idiopathic pulmonary fibrosis, and liver fibrosis due to chronic hepatitis B infection (FibroGen, 2012). However, any effects on skeletal formation, maintenance, and healing in the presence of FG-3019 have yet to be studied. Therefore, it is imperative that we fully understand the role of CTGF in bone formation not only to further the development of novel therapeutic strategies in bone disease, but also to identify potential effects of clinically blocking CTGF in the body.

CHAPTER 2: THE SKELETAL SITE-SPECIFIC ROLE OF CONNECTIVE TISSUE GROWTH FACTOR IN PRENATAL OSTEODEVELOPMENT*

*Extracted from previously published work: Lambi, A.G., Pankratz, T.L., Mundy, C., Gannon, M., Barbe, M.F., Richtsmeier, J.T., & Popoff, S.N. (2012) *Developmental Dynamics* 241, 1944-59.

Introduction

Connective tissue growth factor (CTGF) is a matricellular protein with a multi-modular structure that affords it multiple roles in normal and pathologic development. Because of its unique modular structure, CTGF has been grouped with other proteins in the CCN family. Named for the first three members to be described in the literature – Cysteine-rich 61 (Cyr61/CCN1), CTGF (CCN2), and Nephroblastoma overexpressed protein (Nov/CCN3) – the CCN family has since been extended to include the Wnt-induced secreted proteins-1 (Wisp-1/CCN4), -2 (Wisp-2/CCN5), and -3 (Wisp-3/CCN6) (Brigstock et al., 2003). CCN proteins are 30-40kDa proteins that are cysteine-rich, and are composed of the following four conserved modules: module 1 is an insulin-like growth factor (IGF)-binding domain; module 2 is a von Willebrand type C domain; module 3 is a thrombospondin-1 domain; and module 4 is a C-terminal domain containing a putative cysteine knot (Bork, 1993; Brigstock, 1999; Lau and Lam, 1999; Perbal, 2001). The mosaic structure of these proteins allows for their involvement in crucial cellular (mitosis, adhesion, extracellular matrix production) and physiologic (angiogenesis, chondrogenesis, osteogenesis) processes necessary for skeletal development (Brigstock, 2003; Dhar and Ray, 2010).

Matricellular proteins, such as CTGF, are a subset of extracellular matrix (ECM) proteins that are dynamically regulated and serve a complex role in their local

environment. In addition to having direct ECM-related scaffolding functions, CTGF also modulates cellular responses to local environmental cues through functional interactions with cell surface integrins, growth factors, proteases, cytokines, or other ECM proteins (Arnott et al., 2011; Cicha and Goppelt-Strube, 2009; Rachfal and Brigstock, 2005). Because the effects of CTGF are determined by the relative presence or absence of the aforementioned extracellular components in the local milieu, its functions are context dependent (Cicha and Goppelt-Strube, 2009). As a result, the effects of CTGF on physiologic processes, such as osteogenesis, may differ depending on the skeletal site being investigated.

The importance of CTGF in skeletal development has been established from studies using the global CTGF ablation (knockout, KO) model in mice. First described in 2003, it was shown that CTGF KO mice had defects in growth plate chondrogenesis, angiogenesis, endochondral bone formation, and ECM production (Ivkovic et al., 2003). CTGF KO mice displayed chondrodysplasia in limb and rib cartilage, deformations in Meckel's cartilage, and aberrations in growth plate organization in endochondral bones (Ivkovic et al., 2003). Interestingly, the gross skeletal defects seen in the CTGF KO mice were consistent and presented as kinking of the ribs, tibiae, fibulae, radii, and ulnae, as well as craniofacial abnormalities. Due to misshapen ribs and pulmonary hypoplasia, respiratory failure occurred shortly after birth resulting in neonatal lethality (Baguma-Nibasheka and Kablar, 2008; Ivkovic et al., 2003). This constitutes the chief difficulty in studying the role of CTGF in bone development, formation, and function: the inability to study CTGF KO mice at postnatal time points.

As bone formation occurs through both endochondral (replacing a preexisting cartilage anlage) and intramembranous (*de novo*) ossification processes, additional studies have been conducted to elucidate the effects of CTGF on prenatal skeletal development. *In vitro* studies using CTGF-null chondrocytes demonstrated decreased proliferation and deregulation of Indian hedgehog (Ihh) and parathyroid hormone-related peptide (PTH-rP), two critical players in proper growth plate organization and endochondral ossification (Kawaki et al., 2008a). Taking into account original evidence of defects in growth plate cartilage, it was concluded that endochondral ossification is negatively affected in the absence of CTGF. Implied in this conclusion is that bone formed as a result of the endochondral process is also affected in CTGF KO mice. To date, the studies examining the bone phenotype in these mice have been largely qualitative, and demonstrate decreased ossification of intramembranous (cranial vault) and endochondral (metaphyseal trabeculae) bones (Ivkovic et al., 2003; Kawaki et al., 2008a; Kawaki et al., 2008b). Furthermore, *in vitro* studies of CTGF-null osteoblasts have demonstrated that their differentiation and function were decreased compared to wild-type osteoblasts (Kawaki et al., 2008b).

In this study, we extended previous studies to provide an in-depth characterization of appendicular, axial, and craniofacial skeletal phenotypes of CTGF KO mice. We hypothesized that the effect of CTGF on skeletogenesis would be context dependent, and therefore, ablation of CTGF would result in skeletal site-specific aberrations in bone formation. Based on this hypothesis, we selected and analyzed several skeletal sites (bony elements) based on the ossification process(es) through which they form, as well as their location in either the appendicular or axial skeleton. The sites analyzed included femora

and tibiae, vertebral bodies, and the craniofacial skeleton. Techniques utilized included micro-CT, histomorphometry, craniofacial landmark analyses, and quantitative real-time RT-PCR (qPCR).

Materials and Methods

Animals

CTGF heterozygous mice ($\text{CTGF}^{+/LacZ}$) were used as breeders to obtain CTGF KO ($\text{CTGF}^{LacZ/LacZ}$) mice as previously described (Crawford et al., 2009). Newborn animals used for this study were sacrificed at birth (P0). Genotype was determined as previously described (Crawford et al., 2009), and animals were split into three groups: wild-type (CTGF^{++}), heterozygous ($\text{CTGF}^{+/LacZ}$), and knockout ($\text{CTGF}^{LacZ/LacZ}$). For our studies, CTGF^{++} were used as wild-type (WT) controls.

All animals were maintained and used according to the principles in the NIH Guide for the Care and Use of Laboratory Animals (U.S. Department of Health and Human Services, Publ. NO. 86-23, 1985) and guidelines established by the IACUC of Temple University.

Tissue preparation and histology

Animals used for this study were euthanized at birth (P0). Subsequently, tails were removed and used for DNA extraction and PCR amplification (Sigma, St. Louis, MO), or X-gal staining (Qiagen, Valencia, CA). Skulls, forelimbs, hindlimbs and vertebral columns were dissected in PBS and fixed immediately in 4% paraformaldehyde (PFA) for 24h at 4°C, and replaced with fresh PFA at 48h and 72h. Specimens for micro-CT scanning were placed in PBS 3h prior to scanning.

For histology, specimens were fixed with 4% PFA, decalcified with Formical-2000 (Decal Chemical, Tallman, NY), and embedded in paraffin. Specimens for plastic embedding were fixed in 4% PFA, dehydrated and cleared, followed by infiltration with and embedding in methylmethacrylate resin (Osteo-Bed Bone Embedding Kit, Polysciences, Warrington, PA). Five μm sections were obtained from the polymerized resin blocks, then de-plasticized and stained with von Kossa staining technique, for mineralization, and counterstained with toluidine blue (Abdelmagid et al., 2010; Ivkovic et al., 2003; Zhou et al., 2010). High-resolution images were captured with a digital camera attached to a Nikon Eclipse E-600 microscope.

Histomorphometry

Growth plate zones were quantified using a microscope (Nikon E800) interfaced with a digital camera (QImaging cooled Retiga camera, Surrey, BC, Canada) and bioquantification software system (BioquantOsteo II, Bioquant, Nashville, TN). The zones were identified based on previously established morphologic criteria (Farnum and Wilsman, 1987; Hunziker and Schenk, 1989; Hunziker et al., 1987; Kerkhofs et al., 2012). Briefly, the PZ was determined using the broad, flattened morphology of proliferating chondrocytes arranged in columns. The upper margin of the PHZ is determined as chondrocytes cease proliferating and undergo cytoplasmic expansion. This PHZ exhibits great variation in the morphology of the cells therein as it is a transition zone between the PZ and HZ. The separation of the lower PHZ from the upper HZ is determined by the increased size of hypertrophic chondrocytes and a lack of longitudinal space between neighboring chondrocytes in the HZ. Lengths of specific zones were measured using the

auto-width tool of the Bioquant Image Analysis program in which the inner and outer boundaries of structures were traced, and then mean layer thicknesses were automatically generated, using similar methods as previously described (Bove et al., 2009). The assessment and analysis of the data were carried out in a blinded fashion. Three different sections were measured per bone for WT (n=9) and CTGF KO (n=7) mice, and the mean values \pm SEM are reported.

Micro-computed tomography (micro-CT) analysis

Bones were scanned in air with a Skyscan 1172, 11 MPix camera model, high-resolution cone-beam micro-CT scanner. Long bone images were scanned at a pixel size of 5.2 μm with an X-ray tube potential of 40 kV and X-ray intensity 250 μA . Entire hind limbs were scanned, with each slice equal to 5 μm . A 0.5mm aluminum filter was used to remove image noise, with a ring artifact correction of 10 and a beam hardening correction of 40%. Skulls were scanned at a pixel size of 9.4 μm with an X-ray tube potential of 80 kV and X-ray intensity 125 μA , with each slice equal to 9 μm . A 0.5mm aluminum filter was used to remove image noise, with a ring artifact correction of 15 and a beam hardening correction of 40%. After scanning, 3D microstructural image data was reconstructed using the SkyscanNRecon software.

Volumes of interest were isolated and structural indices calculated using the Skyscan CT Analyzer (CTAn) software. For long bones, cortical and trabecular bone were separated manually at 15 μm away from the endocortical surface with an irregular region of interest (ROI) tool. For vertebral bodies, mandibles, and parietal bones, individual bones were isolated using an irregular ROI tool. Left parietal bones and mandibles were used for analysis. Morphometric traits were computed from binarized

images using direct 3D techniques, which do not rely on prior assumptions from the underlying structures. The volume of interest for trabecular microarchitectural variables, started 10 μm below the transition into the zone of ossification from the femoral distal epiphysis or tibial proximal epiphysis, and then extended 250 μm toward the diaphysis. An upper threshold of 255 and a lower threshold of 121 were used to delineate each pixel as “bone” or “non-bone”. Trabecular bone volume (BV), trabecular BV per total volume (BV/TV), mean trabecular thickness (Tb.Th), mean trabecular number (Tb.N), and mean trabecular separation (Tb.Sp) indices were computed using a marching-cubes algorithm in 3D. Morphological traits of the mid-diaphyseal region were identified at a site equidistant from the aforementioned starting points, and then extending from this position 50 slices in the proximal and distal directions, totaling 500 μm . Threshold values were identical to trabecular analysis, and BV, TV, BV/TV, and periosteal perimeter (Ps.Pm) indices were computed using a marching-cubes algorithm.

Morphometric analysis of skull phenotypes

Isosurfaces were reconstructed for the CTGF KO (N=10) and WT (N=11) mice from the microCT data to characterize all cranial bone using the software package Avizo 6.0 (Visualization Sciences Group, VSG, Burlington, MA). To statistically determine differences in shape of the skulls of CTGF KO mice, 3D coordinate locations of 32 cranial landmarks were recorded using Aviso 6.0. Landmarks were identified on endo- and ectocranial surfaces of cranial bones and used in morphometric analysis. Each specimen was digitized twice by the same observer (TP) and measurement error was minimized by averaging the coordinates of the two trials (Aldridge et al., 2005; Richtsmeier et al., 1995). To ascertain the accuracy and reproducibility of landmark

placement, intraobserver error (i.e. absolute difference between the two trials) was estimated for every landmark. If landmark placement differed by more than 0.05 mm, the landmark was remeasured. Landmark definitions are provided in Table S1 and detailed on the website http://www.getahead.psu.edu/landmarks_new.html.

Variations in skull phenotype were evaluated by analyzing 3D landmark data using two methods of analysis. Generalized Procrustes analysis was used to compare craniofacial shape as defined by landmark coordinate data (Dryden and Mardia, 1998; Rohlf and Slice, 1990). This method superimposes the coordinate data and adopts a single orientation for all specimens by shifting the landmark configurations to a common position, scaling them to a standard size and rotating them until a best fit of corresponding landmarks is achieved. We estimated landmark configurations of global skull using all landmarks, and separately estimated cranial vault, facial, and cranial base configurations by superimposition of specific landmark subsets (Figure 3) using MorphoJ (Klingenberg, 2008). This procedure reduces the effects of scale (Rohlf and Slice, 1990), but does not eliminate the allometric shape variation that is related to size. To estimate the effect of allometry on shape information, we computed a regression of shape (represented by Procrustes coordinates) on centroid size (Drake and Klingenberg, 2008), estimated as the square root of the summed distances between each landmark location and the centroid of the landmark configuration (Dryden and Mardia, 1998). We explored the variation in the various data sets (global skull, vault, cranial base, facial skeleton) using a Principal Component Analysis (PCA), which performs an orthogonal decomposition of the data and transforms the resulting Procrustes coordinates into a smaller number of uncorrelated variables called principal components (PCs). For each

landmark configuration PCA performs a coordinate rotation that aligns the transformed axes (PCs) with the directions of maximum variation. The first PC (PC1) accounts for the largest amount of variation in the data set, the second PC (PC2) accounts for the second largest amount of variation, and so on (Reyment et al., 1984).

To statistically determine localized shape differences between KO and WT groups we used EDMA, Euclidean Distance Matrix Analysis (Lele and Richtsmeier, 1995b, 2001). EDMA converts 3D landmark data into a form matrix consisting of all possible linear distances between unique landmark pairs, computes a relative comparison of form matrices for the samples of interest, and statistically tests for differences in shape between samples using nonparametric confidence intervals (Lele and Richtsmeier, 1995a; Lele and Richtsmeier, 2001). We tested for morphological differences in CTGF mice relative to their WT littermates for groups of landmarks that define the whole skull (global skull) and specific regions (facial skeleton, cranial base, cranial vault). Within each group (WT, nonmutant littermates), for each landmark set, an average form matrix, consisting of the linear distance for all unique linear distance pairs, is estimated using the 3D landmark data. Differences in three-dimensional size and shape are statistically compared as a matrix of ratios of all like linear distances in the two samples. The null hypothesis for each comparison is that there is no difference in shape between groups. For each linear distance, a ratio of the average values of that distance for the WT and the KO is computed. A ratio of 1 indicates that the two groups are similar for that measure; whereas a ratio significantly greater or less than 1 shows that they are different. The null hypothesis of similarity in shape for groups of landmarks representing the various landmark subsets is initially evaluated by a bootstrap approach providing an overall

indication of difference in shapes between the samples (Lele and Richtsmeier, 2001). Confidence intervals for the null hypothesis of similarity in shape were also evaluated for each linear distance using 100,000 pseudo-samples generated from the data using a non-parametric bootstrapping algorithm. For each linear distance the null hypothesis is rejected if the 90% confidence interval does not include 1.0. Rejection of the null hypothesis enables localization of differences to specific landmarks and linear distances (Lele and Richtsmeier, 1995b, 2001). EDMA analyses were performed using WinEDMA (Cole, 2002).

RNA Isolation and Quantitative Real-Time PCR (qPCR)

Total RNA was isolated from P0 calvaria (parietal bones) from WT and CTGF KO mice as described previously (Abdelmagid et al., 2010). Briefly, bones from neonatal mice pups were dissected free from soft tissues and placed immediately in TRizol (Invitrogen, Austin, TX). Samples were homogenized in TRizol until bones were completely dissolved. Total RNA was extracted using acid-phenol-chloroform using centrifugation (10,000g). The aqueous phase was isolated and transferred to a fresh tube, an equal volume of isopropanol was added, and the sample was incubated at room temperature for 10 minutes to precipitate the RNA. The RNA was pelleted by centrifugation (10,000g), washed with 70% ethanol, air dried, and dissolved in RNase-free water. Spectrophotometer readings were used to determine the concentration of each RNA sample, and the integrity of all samples was confirmed using 1% formaldehyde-agarose gels.

Gene expression for CTGF, runt-related transcription factor 2 (Runx-2), alkaline phosphatase (ALP), collagen, type I, osteocalcin (OC), transforming growth factor beta 1 (TGF- β ₁), and transforming growth factor beta receptors I and II (TGF β RI, TGF β RII), was determined by qPCR using Sybr Green Master Mix (Applied Biosystems, Foster City, CA) using 1 μ L cDNA, as described previously (Song et al., 2007). Reactions were run on a 7,500 Real-Time PCR system (Applied Biosystems). All samples were normalized to control GAPDH. At least three independent experiments were performed for each gene, and each experiment was conducted in triplicate. Primers are listed in Table 3-1. The cycling program was as follows 50°C, 2 min; 95°C, 10 min; 40 cycles of 95°C, 15 sec and 60°C, 1 min.

Statistical analysis

Statistical analyses for craniofacial landmark analyses were performed as described above. All other statistical analyses were performed using GraphPad Prism 5 (<http://www.graphpad.com>). Briefly, a two-tailed Student's *t*-test was used to determine statistically significant differences between group means for histomorphometric, micro-CT, and qPCR results. A *p*-value of less than 0.05 was considered statistically significant.

Table 2-1. Primer sequences used for quantitative real-time polymerase chain reaction (qPCR) analysis.

Gene Name	Primer	Sequence (5'-3')	PCR product (bp)	GenBank accession no.
GAPDH	Forward	ATCTTGGGCTACACTGAGGA	122	NM_008084
	Reverse	CAGGAAATGAGCTTGACAAAGT		
Runx2	Forward	CCGTGGCCTCAAGGTTG	118	NM_001146038
	Reverse	TTCATAACAGCGGAGGCATT		
ALP	Forward	TCCTGACCAAAAAACCTCAAAGG	101	NM_007431
	Reverse	TGCTTCATGCAGAGCCTGC		
OC	Forward	CTCACAGATGCCAAGCCCCA	98	NM_007541
	Reverse	CCAAGGTAGCGCCGGAGTCT		
Cyr61/CCN1	Forward	ATGAAGACAGCATTAAGGACTC	172	NM_010516
	Reverse	TGCAGAGGGTTGAAAAGAAC		
CTGF/CCN2	Forward	CCACCCGAGTTACCAATGAC	169	NM_010217
	Reverse	GTGCAGCCAGAAAGCCTCA		
Nov/CCN3	Forward	TGAAGTCTCTGACTCCAGCATT	230	NM_010930
	Reverse	TGGCTTCAGGGATTTCTTG		
TGF β -1	Forward	GCTAATGGTGGACCGCAACAACG	682	L42456
	Reverse	CTTGCTGTACTGTGTCCAGGC		
TGF β -RI	Forward	AGTGGTCTTGCACATCTTC	60	NM_009370
	Reverse	GGCAATAGCTGGTTTCCT		
TGF β -RII	Forward	AGATGGCTCGCTGAACACTACCAA	100	NM_009371
	Reverse	AGAACCTGCTGCCTCTGGCTTT		

Results

Multiple growth plate malformations occur in CTGF KO mice

We performed measurements in proximal tibial metaphyses of newborn (post natal day 0, P0) CTGF KO mice and WT littermates (Figure 2-1). Three distinct zones – proliferating, prehypertrophic, and hypertrophic – were determined based on previously established morphologic criteria (Farnum and Wilsman, 1987; Hunziker and Schenk, 1989; Hunziker et al., 1987; Kerkhofs et al., 2012). We demonstrated that the proliferating zone is significantly shorter in CTGF KO mice than their WT littermates. There was no significant difference between in the length of the prehypertrophic zone in CTGF KO tibia. However, CTGF KO mice did demonstrate a significant expansion in the hypertrophic zone length (Figure 2-1). An expansion in this zone has been noted in previous studies (Ivkovic et al., 2003; Kawaki et al., 2008a), however specific measurements were neither taken nor statistically analyzed.

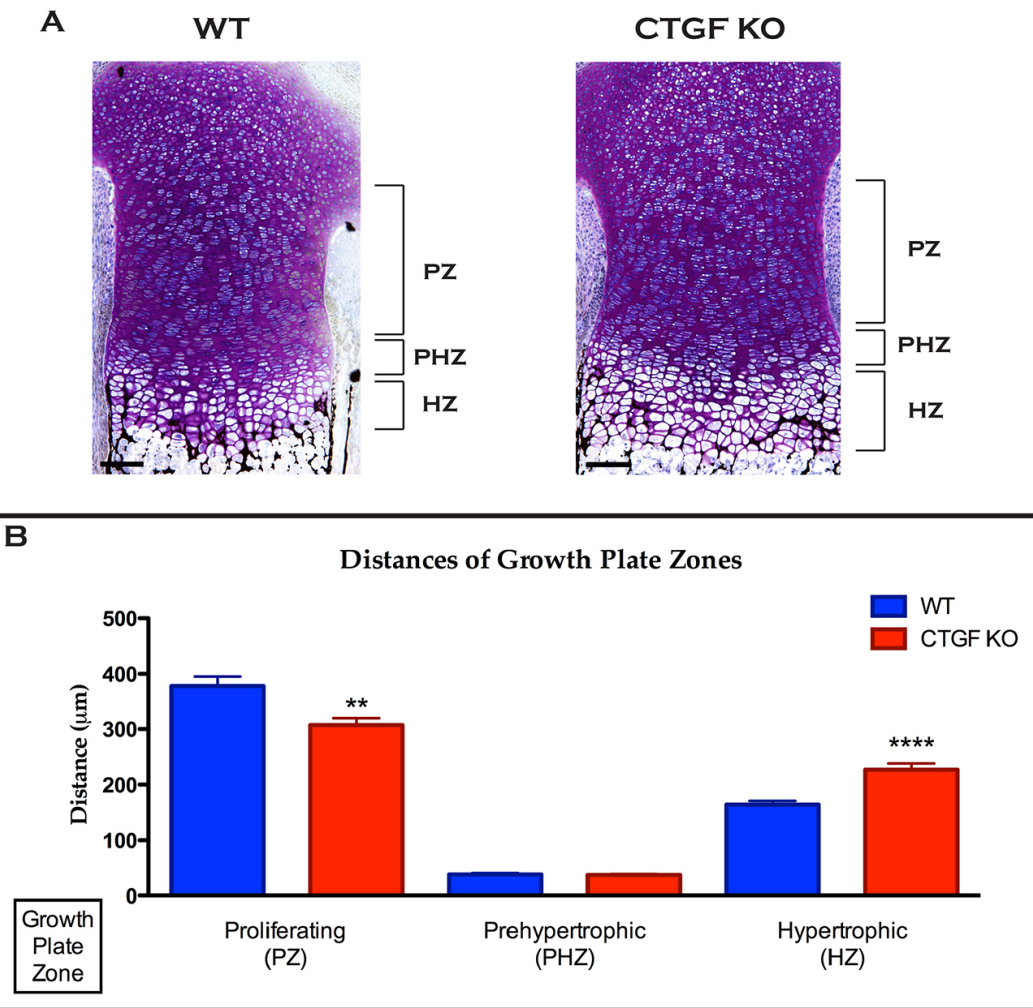


Figure 2-1. Growth plate malformations in CTGF KO mice.

(A) Sections through P0 wild-type (WT) and CTGF knockout (KO) proximal tibiae with brackets outlining the proliferating zone (PZ), prehypertrophic zone (PHZ), and hypertrophic zone (HZ). Scale bar: 100 μ m. (B) Quantification of growth plate zone thicknesses are shown in the graph. ** = $P < 0.01$ and *** = $P < 0.0001$.

CTGF KO mice have skeletal site-specific effects on bone formation

Using micro-CT, we performed a thorough analysis of the bone microarchitecture of multiple skeletal sites in CTGF KO mice; these included both appendicular (limbs) and axial skeletal divisions (vertebral bodies, craniofacial bones). Three-dimensional (3D) micro-CT reconstructions of hindlimbs demonstrated that femora in CTGF KO mice appeared phenotypically normal when compared to WT littermates (Figure 2-2 A-B). However, tibiae from CTGF KO mice were misshapen, displaying a bend or kink (Figure 2-2 G-H); while this kink was present in all CTGF KO tibiae, the exact proximal-distal position varied between mice (data not shown). We analyzed the trabecular bone of distal femora and proximal tibiae, as well as whole bone from femoral and tibial mid-diaphyses, from CTGF KO mice and WT littermates (Figure 2-2 and Table 2-2). Our results revealed a significant decrease in trabecular percent bone volume (BV/TV) in distal femoral and proximal tibial metaphyses in CTGF KO mice compared to WT littermates (Figure 2-2 E-F, I-J). Trabeculae were both less numerous and had increased separation in both bones. These changes are indicative of functionally defective endochondral bone formation (Table 1). We also assessed bone volume in the mid-diaphysis (Figure 2-2 C-D, K-L). Analysis of femoral diaphyses revealed modest reductions in total bone volume (BV) of CTGF KO mice compared to WT littermates; however, overall percent bone volume and periosteal perimeter (Ps.Pm) were not significantly affected. Analysis of tibial diaphysis (comprising the region of the kink) demonstrated that total tissue volume (TV), BV and Ps.Pm were markedly increased in CTGF KO mice. However, the percent bone volume was not significantly different when compared to WT littermates (Table 2-2).

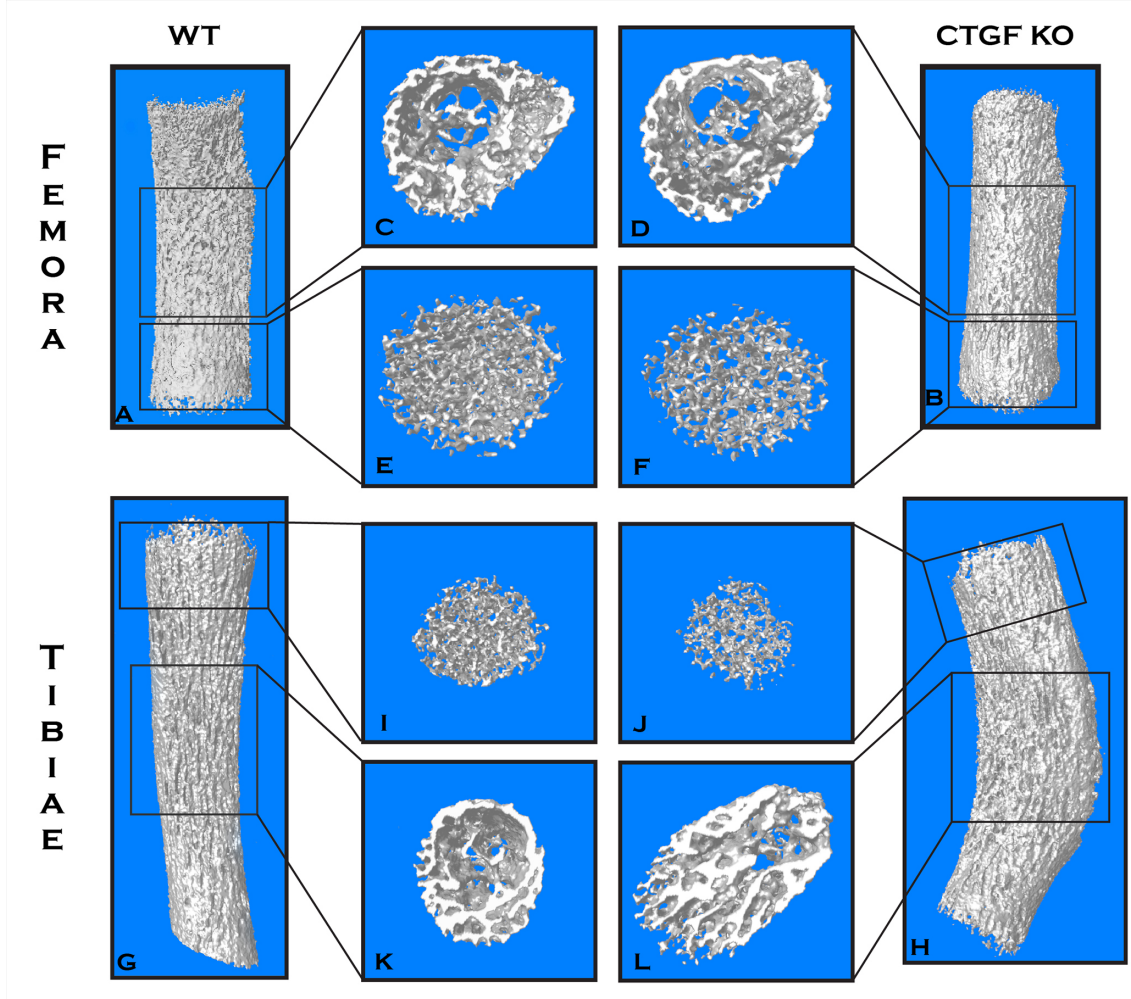


Figure 2-2. Skeletal site-specific effects on formed bone in CTGF KO appendicular skeleton.

Micro-CT reconstructions of P0 WT and CTGF KO femora (A,B) and tibiae (G,H) are shown, with isolation of mid-diaphyseal femoral bone (C,D), distal femoral trabecular bone (E,F), proximal tibial trabecular bone (I,J), and mid-diaphyseal tibial bone (K,L). Analysis of bone microarchitecture in these isolated regions is displayed in Table 2-2.

Femora			
Bone site and parameter	WT n = 10	KO n = 9	KO/WT ^b
Femoral Distal Metaphysis (trabecular bone)			%
Bone volume/tissue volume (BV/TV; %)	29.90 ± 2.017 ^a	21.25 ± 3.163 ^c	71.1
Trabecular Thickness (Tb.Th; mm)	0.025 ± 0.001	0.023 ± 0.001	
Trabecular Separation (Tb.Sp; mm)	0.037 ± 0.001	0.045 ± 0.003 ^c	121.6
Trabecular Number (Tb.N; mm ⁻¹)	11.94 ± 0.670	8.96 ± 1.243 ^c	75.0
Femoral Mid-Diaphysis (whole bone)			
Bone volume (BV; mm ³)	0.072 ± 0.003	0.060 ± 0.006 ^c	83.3
Tissue volume (TV, mm ³)	0.174 ± 0.005	0.160 ± 0.006	
Bone volume/tissue volume (BV/TV; %)	42.24 ± 1.354	36.66 ± 2.661	
Periosteal perimeter (Ps.Pm; mm)	2.25 ± 0.032	2.19 ± 0.032	
Tibiae			
Bone site and parameter	WT n = 9	KO n = 9	KO/WT
Tibial Proximal Metaphysis (trabecular bone)			%
Bone volume/tissue volume (BV/TV; %)	29.03 ± 2.486	17.60 ± 2.190 ^d	60.6
Trabecular Thickness (Tb.Th; mm)	0.026 ± 0.001	0.023 ± 0.0005 ^c	88.5
Trabecular Separation (Tb.Sp; mm)	0.039 ± 0.001	0.048 ± 0.003 ^d	123.1
Trabecular Number (Tb.N; mm ⁻¹)	11.28 ± 0.781	7.625 ± 0.909 ^d	67.6
Tibial Mid-Diaphysis (whole bone)			
Bone volume (BV; mm ³)	0.058 ± 0.003	0.073 ± 0.005 ^c	125.9
Tissue volume (TV, mm ³)	0.115 ± 0.003	0.159 ± 0.003 ^e	138.3
Bone volume/tissue volume (BV/TV; %)	50.55 ± 2.181	45.42 ± 2.277	
Periosteal perimeter (Ps.Pm; mm)	1.783 ± 0.024	2.235 ± 0.024 ^e	125.4

^a Values are shown as mean ± SEM

^b CTGF Knockout (KO) to Wild-type (WT) ratios (KO/WT; expressed as percentages) are displayed only for values with statistically significant differences.

^c $p < 0.05$

^d $p < 0.01$

^e $p < 0.0001$

Table 2-2. Micro-CT analysis of long bone microarchitecture in WT and CTGF KO femora and tibia.

In the axial skeleton, we studied two locations within the vertebral column – 8th thoracic (T8) and 1st lumbar (L1) – and also isolated bone from two sites in the craniofacial skeleton - parietal bone and mandible (Figure 2-3). Due to the small size of P0 mouse vertebral bodies, we assessed the percent bone volume of the entire vertebral body. Our micro-CT analysis demonstrated a significant decrease in the percent bone volume (BV/TV) of the more caudal (L1) vertebral body, where CTGF KO had 32.5% compared to 48.6% in WT mice ($p < 0.03$). However, the percent bone volume in the more cephalic (T8) vertebral body was similar in CTGF KO mice, with KO mice having 43.5% compared to 44.9% in WT mice ($p = 0.76$). We next assessed total bone volume of the parietal bones. Since at this age these flat bones have not yet developed a marrow cavity inside, total bone volume was measured. The bone volume in CTGF KO parietal bones was 0.165mm³ compared to 0.192mm³ in WT parietal bones ($p < 0.02$). Lastly, we analyzed the percent bone volume (BV/TV) of the mandible since the mandible develops around Meckel's cartilage, some of which persists in early postnatal development (Shimo et al., 2004). CTGF KO mice had 31.4% compared to 39.1% in WT mice ($p < 0.03$).

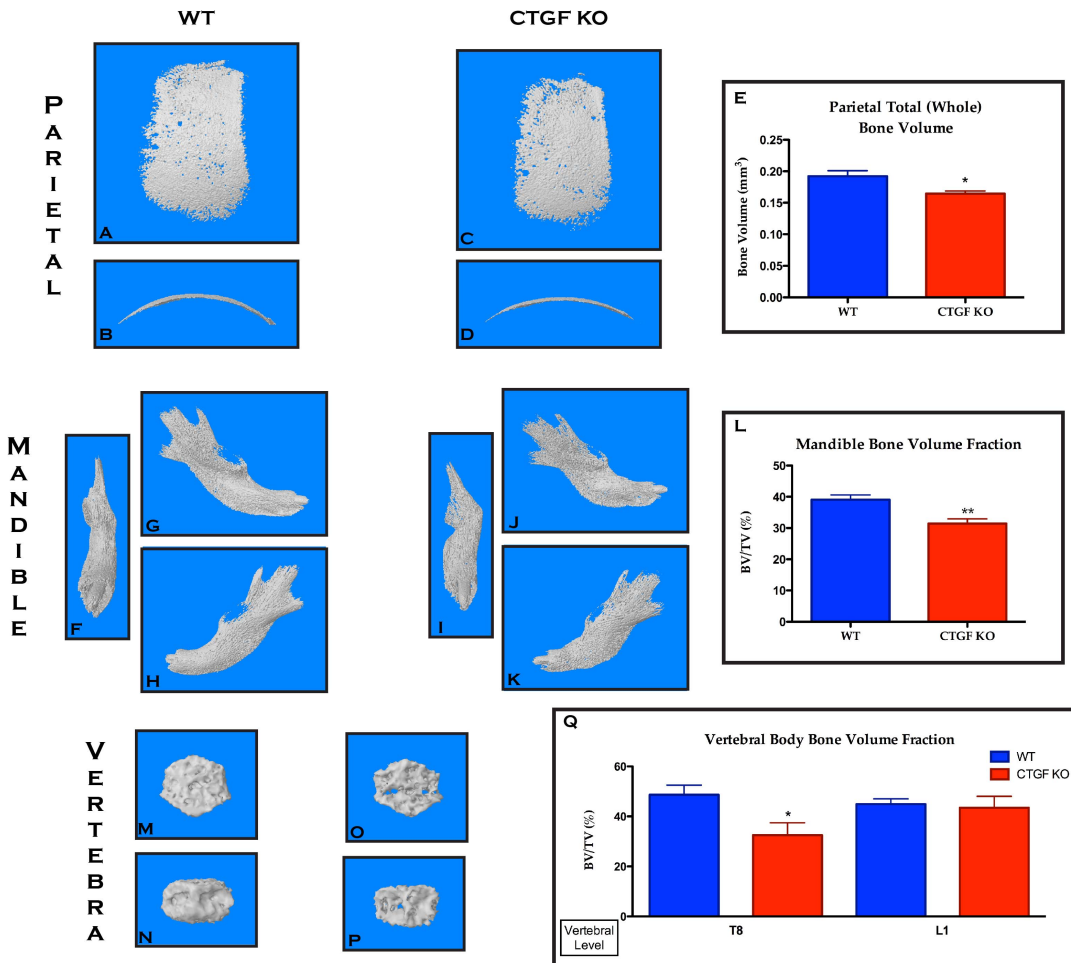


Figure 2-3. Skeletal site-specific effects on formed bone in CTGF KO axial skeleton.

Micro-CT reconstructions of P0 WT and CTGF KO parietal bones (A-D), mandibles (F-K), and L1 vertebral bodies (M-P) are shown. Superior (A,C) and anterior (B,D) views of the parietal bones are depicted. Total bone volume comparing WT and CTGF KO parietal bones is graphed (E). Mandibles are depicted with anterior (F,I), medial (G,J), and lateral (H,K) views. Bone volume fraction is graphed (L). L1 vertebral bones are shown from superior (M,O) and anterior (N,P) views. Both the T8 and L1 vertebral body data is graphed (Q). * = P < 0.05 and ** = P < 0.01.

Skull phenotypes of CTGF KO mice

Phenotypic differences of 10 WT and 11 CTGF KO skulls at P0 were compared using 3D morphometric methods to identify both overall variation in skulls and localized shape differences in the two samples of mice. Three-dimensional coordinates of 32 cranial landmarks were recorded on 3D micro-CT isosurfaces (Figure 2-4, Supplemental Table 1). The total landmark set was used to estimate a ‘global skull’ shape for each sample and used to statistically compare overall skull shape between KO and WT mice. We further defined subsets of landmarks to represent the shapes of the three skull regions: cranial vault (green), cranial base (yellow), and facial skeleton (blue) (Fig. 3); these are the three major developmentally and phylogenetically distinct divisions of the vertebrate skull. We performed a Generalized Procrustes analysis (GPA) of the global skull and of the three regions to determine the axes along which variation in these data sets were most profound and to explore the differences in shape variation between WT and KO mice. Localized differences in shape for the three landmark subsets were statistically evaluated using Euclidean Distance Matrix Analysis (EDMA) (Lele and Richtsmeier, 2001).

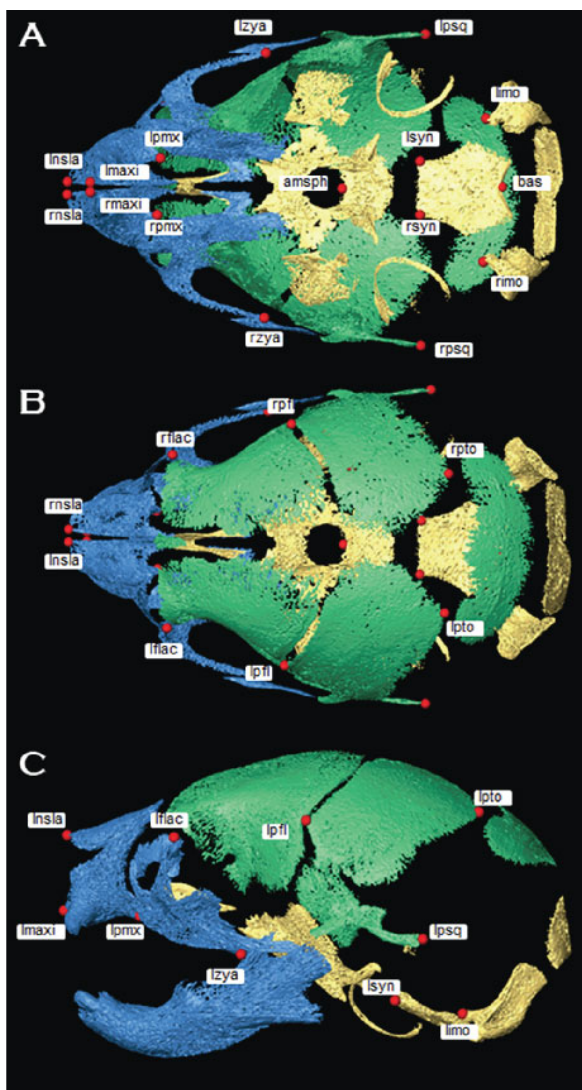


Figure 3-4. Landmarks collected from isosurfaces of micro-CT reconstructions of P0 murine skulls.

All landmarks used in the analysis of the global WT and CTKO KO skulls are shown from inferior (A), superoinferior (B), and lateral (C) views; depicted is a WT skull. Landmarks used in the analysis of the three landmarks subsets are shown on the facial skeleton (blue), cranial base (yellow), and cranial vault (green). Landmarks that define the subsets of regions are listed in Table 2-3 and defined on the laboratory website: <http://getahead.psu.edu>.

Table 2-3. Craniofacial landmark abbreviations and descriptions

Landmark Abbreviations	Description
lnsla	Most antero-medial point of the nasal bone, left side
lnslp	Most posterior-medial point of the nasal bone, left side
lfac	Intersection of the frontal process of the maxilla with frontal and lacrimal bones, taken on the maxilla, left side
lzya	Intersection of zygoma with zygomatic process of maxillary, taken on maxilla, left side
laalf	Most anterior point of the anterior palatine foramen, left side
lpmx	Most infero-lateral point of the premaxillary-maxillary suture, taken on premaxilla, left side
lpalf	Most posterior point of the anterior palatine foramen, left side
lptyp	Most posterior tip of the medial pterygoid process, left side
lsyn	Most antero-lateral point on the corner of the basioccipital, left side
lmaxi	Midline point on the premaxilla between the incisor and the nasal cavity just anterior of the incisive foramen, left side
lpppt	Most posterior projecting point on the turbinate, left side
lasph	Postero-medial point of the inferior portion of the left alisphenoid, left side
lamms	Most antero-medial point on the maxillary shelf, left side
lpmmss	Most postero-medial point on the maxillary shelf, left side
lpsq	Most posterior point on the posterior extension of the forming squamosal, left side
lpfl	Most lateral intersection of the frontal and parietal bones, taken on the parietal, left side
lpfm	Most medial intersection of the frontal and parietal bones, taken on the parietal, left side
lpto	Most postero-medial point on the parietal, left side
rnsla	Most antero-medial point of the nasal bone, right side
rnslp	Most posterior-medial point of the nasal bone, right side
rflac	Intersection of the frontal process of the maxilla with frontal and lacrimal bones, taken on the maxilla, right side
rzya	Intersection of zygoma with zygomatic process of maxillary, taken on maxilla, right side
raalf	Most anterior point of the anterior palatine foramen, right side
rpmx	Most infero-lateral point of the premaxillary-maxillary suture, taken on premaxilla, right side
rpalf	Most posterior point of the anterior palatine foramen, right side
rptyp	Most posterior tip of the medial pterygoid process, right side
rsyn	Most antero-lateral point on the corner of the basioccipital, right side
rmaxi	Midline point on the premaxilla between the incisor and the nasal cavity just anterior of the incisive foramen, right side
rpppt	Most posterior projecting point on the turbinate, right side
rasph	Postero-medial point of the inferior portion of the left alisphenoid, right side
ramms	Most antero-medial point on the maxillary shelf, right side
rpmmss	Most postero-medial point on the maxillary shelf, right side
rpsq	Most posterior point on the posterior extension of the forming squamosal, right side
rpfl	Most lateral intersection of the frontal and parietal bones, taken on the parietal, right side
rpfm	Most medial intersection of the frontal and parietal bones, taken on the parietal, right side
rpto	Most postero-medial point on the parietal, right side
ethma	Most anterior-superior point of the intersection of the left and right anterior turbinates
amsph	Most antero-medial point on the body of the sphenoid
bas	Mid-point on the posterior margin of the foramen magnum, taken on the basioccipital
limo	Most infero-medial point on the ectocranial surface of occipital lateralis, left side
rimo	Most infero-medial point on the ectocranial surface of occipital lateralis, right side
later	Most anterior tip of the ectotympanic ring, left side
lpter	Most posterior tip of the ectotympanic ring, left side
rater	Most anterior tip of the ectotympanic ring, right side
rpter	Most posterior tip of the ectotympanic ring, right side

Differences in cranial shape in CTGF KO mice

A GPA was used to superimpose coordinate data sets and to extract shape information from the data set for each skull region (Dryden and Mardia, 1998; Rohlf and Slice, 1990). A Principal Components Analysis (PCA) based on the Procrustes coordinates of the global skull configuration (Figure 2-5A) shows a clear separation between CTGF KO mice and their WT littermates along Principal Components axis 1 (PC1), which accounts for 69% of the total shape variation. While the skulls of CTGF KO mice show a wide range of variation along both PC1 and PC2 axes, the WT littermates are more tightly clustered, indicating less variation in skull morphology, especially along PC1. We also saw a separation between CTGF KO mice and their WT littermates along PC1 in the cranial base and face, with little to no separation between these groups in the cranial vault (Figure 2-5B-D).

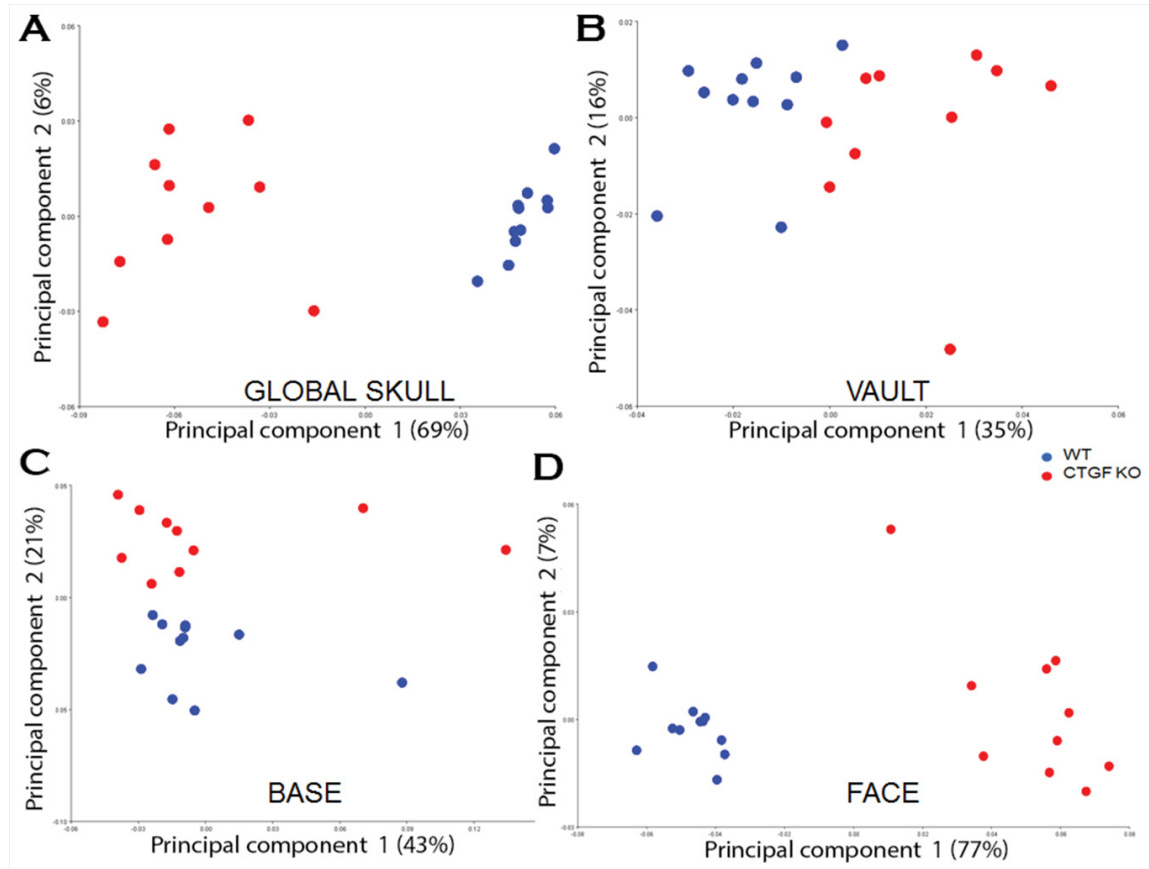


Figure 2-5. Differences in skull shape in CTGF KO mice.

Results of PCA analyses based on Procrustes coordinates from landmarks of the global skull (A), cranial vault (B), cranial base (C), and facial skeleton (D). In each figure, the shape of the cranial region of each mouse is represented as a single dot in the scatterplots of principal component 1 and principal component 2 scores before adjusting for the effects of allometry. The percentage of variation explained by each component is entered in parentheses after the axis label.

Procrustes superimposition reduces the effects of scale, but does not eliminate allometric shape variation that is related to size. We mathematically corrected for correlations among shape variables due to allometry (size related differences in shape) by computing a regression of shape on our chosen measure of size (centroid size) following the methods of Drake and Klingenberg (Drake and Klingenberg, 2008) (see Experimental Procedures for more details). The residuals for each specimen estimated from the regression analysis were then used to compute another PCA which did not include allometric effects. Though the distance between KO and WT mice along PC1 is reduced after this correction, the separation between the groups is maintained (data not shown). Additionally, the extent of variation of the WT mice is extended along PC1 after allometric correction indicating a greater variation in the non-allometric effects of shape variation in the WT mice. In summary, both allometric (those closely related to size) and non-allometric shape differences contribute to global differences in shape between the two samples of mice.

Localized differences in craniofacial shape in CTGF KO mice

We used the nonparametric bootstrap algorithm of EDMA to statistically test for differences in shape between the skulls of CTGF KO mice and WT littermates using landmark subsets that represented cranial vault, cranial base, and facial skeleton (Table 2-3). A test of the hypothesis of overall difference in shape for the cranial vault and facial skeleton revealed a statistical difference between the two samples ($p \leq 0.05$) but a test of difference in overall shape of the cranial base between the CTGF KO and WT mice did not reach statistical significance.

To identify localized differences in morphology, non-parametric confidence interval testing was used to identify those linear distances significantly different in the two groups. The results (Table 2-3 and Figure 2-6) indicate that many measures of the facial skeleton and anterior cranial vault are significantly increased along the mediolateral axis in the CTGF KO mice, while the rostro-caudal length of the cranial vault of CTGF KO mice is reduced relative to WT littermates. Although the overall shape of the cranial base subset was not shown to be statistically different between the two groups (Table 2-3), two distances demonstrate significant reduction in the rostro-caudal dimension of the basi occipital bone in the CTGF KO mice (Figure 2-6).

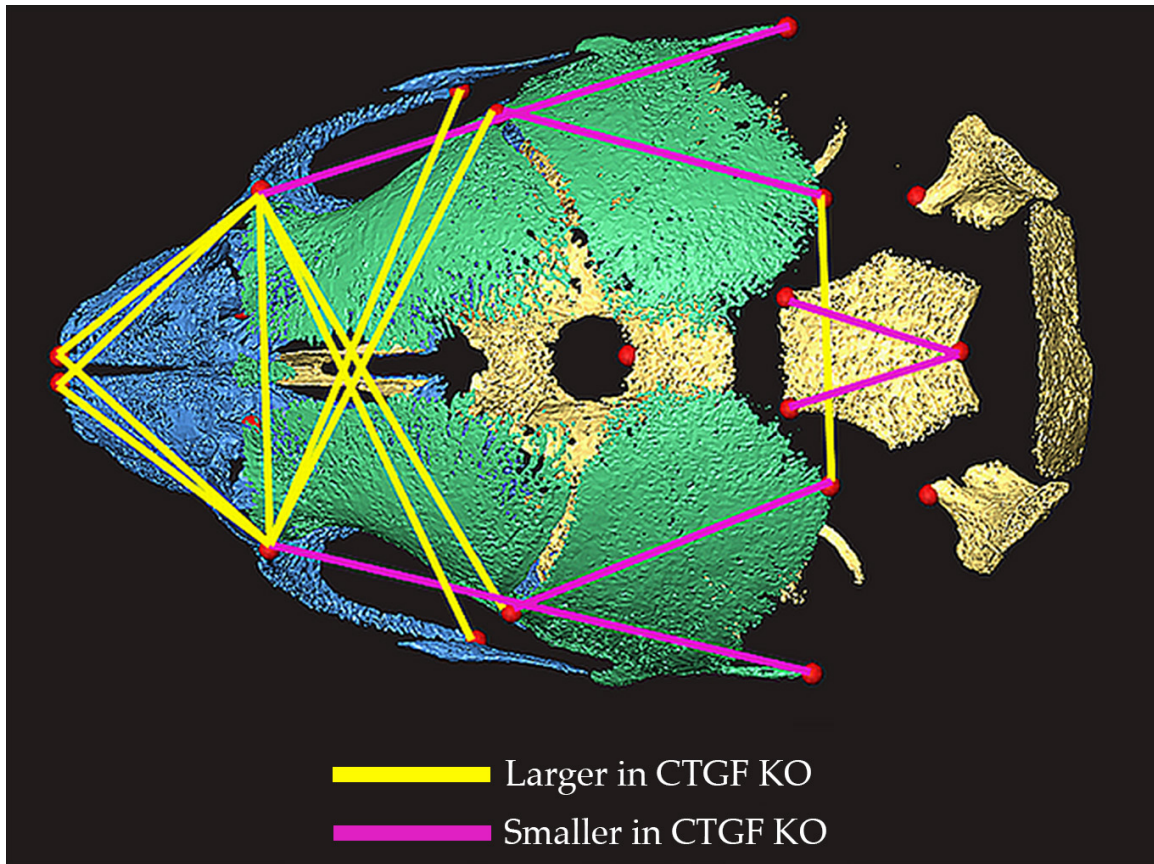


Figure 2-6. Localized differences in skull morphology in CTGF KO mice.

Distances between landmarks found to be significantly different when comparing WT and CTGF KO groups by EDMA are shown on a micro-CT reconstructed isosurface of a P0 WT mouse. The skull is seen from above with the rostral end to the left and caudal end to the right. Yellow lines indicate linear distances that are significantly larger in CTGF KO mice; magenta lines represent linear distances that are significantly smaller in CTGF KO mice.

Table 2-4. Results of EDMA testing for significant localized differences in CTGF KO skulls.

Landmark Subset	Landmarks included ^a	P-value ^b	Statistically Different Linear Differences ^c	
			Relatively larger in CTGF KO	Relatively smaller in CTGF KO
Cranial base	amsph bas limo lsyn rimo rsyn	0.173		bas- rsyn bas- lsyn
Face	lflac lmaxi lnsla lpmx lzya rflac rmaxi rnsla rpmx rzya	0.006	lpmx - rflac lflac - rpmx lpmx - rzya lzya - rzya rflac - rnsla lnsla - rflac lzya - rpmx lflac - lnsla lflac - rzya lzya - rflac lflac - rflac lflac - rnsla	rmaxi - rpmx lmaxi - lpmx lnsla - rnsla
Cranial Vault	lflac lpfl lpsq lpto rflac rpfl rpsq rpto	0.045	lflac - rflac lpto - rpto lpfl - rflac	lpfl - lpsq rpfl - rpto lflac - lpsq rflac - rpsq lpfl - lpto

^a See Figure 3-4 for landmark location

^b p-value for test of overall shape difference between CTGF KO and WT skulls for regions of study

^c Linear distances (identified by landmark endpoints) that show statistical difference between groups by confidence interval ($\alpha \leq 0.10$)

Morphologic traits unique to CTGF KO skulls

In addition to the aforementioned quantitative changes in the skull morphology of CTGF KO mice, we also found several unique, morphologic traits that are present in all CTGF KO mice (Figure 2-7). Not contained to a specific region of the skull, these dysmorphisms occur in the facial skeleton, mandibles, palate, and cranial base. The nasal bones in WT mice have a relatively straight superior surface (Figure 2-7A), while in CTGF KO mice they are curved (Figure 2-7B). CTGF KO mice also presented with defects in formation of the mandible resulting in a characteristic S-shaped bend of the mandibular body compared to WT littermates (Figure 2-7C-D).

It was previously reported that CTGF KO mice have a cleft palate at birth secondary to improper development of endochondrally-forming cranial bones. We found that in CTGF KO mice the maxillary and palatine processes failed to converge at the midline. Additionally, CTGF KO mice have a characteristic kink of the vomer (Figure 2-7C-D), although the side to which this bone kinks alters in fairly equal numbers. Lastly, the pterygoid plates in CTGF KO mice differ quite notably from their WT littermates. WT mice have nearly vertical pterygoid plates, while CTGF KO mice have much more horizontally oriented plates; these appear to be laterally displaced and flattened closer to the body of the sphenoid (Figure 2-7E-F). However, the actual body of the sphenoid is not severely affected in CTGF KO mice, although it appears more convex perhaps due to the lateral displacement of the pterygoid plates.

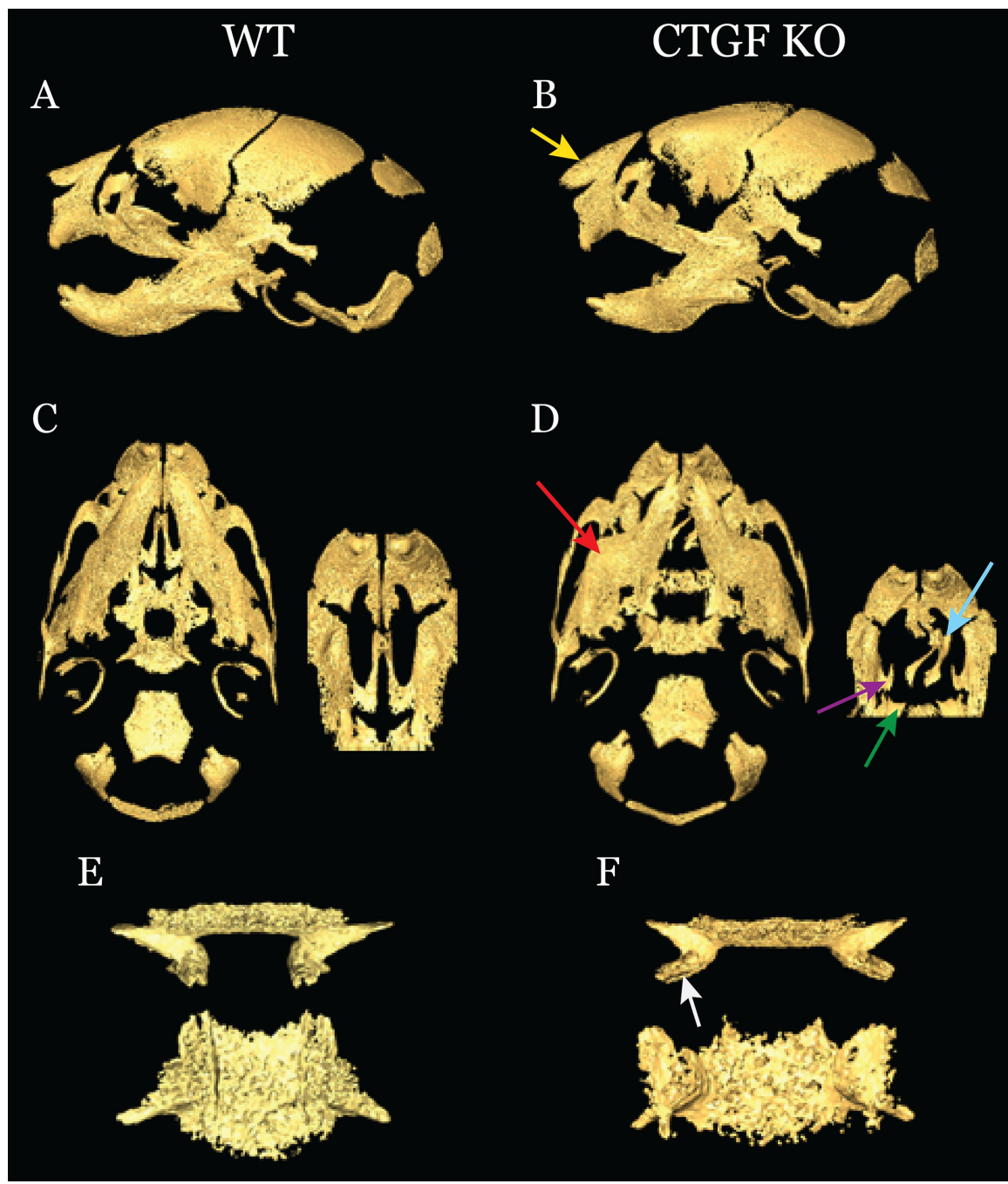


Figure 2-7: Morphologic traits seen in CTGF KO skulls.

Figure 2-7. Morphologic traits seen in CTGF KO skulls.

Micro-CT reconstructions of P0 WT and CTGF KO global skulls from lateral (A,B) and inferior views (C,D *left*) are shown, with isolation of the palate (C,D *right*) and sphenoid bones (E,F). Increased curvature of the nasal bones is seen in CTGF KO mice (B, *yellow arrow*) as well as an S-shaped bend in the mandibular body (D, *red arrow*). A close-up of the palate shows a characteristic kink in the CTGF KO vomer (D, *blue arrow*), as well as failed midline convergence of the maxillary (*purple arrow*) and palatine processes (*green arrow*). Isolation of the sphenoid bones demonstrates a difference in pterygoid plate morphology (*white arrow*) in CTGF KO mice. Sphenoid bones (E,F) are shown from a posterior view (*top row*) and inferior view (*bottom row*) with anterior directed upward.

In vivo gene expression patterns in CTGF KO skeletal sites

To examine the effect of CTGF ablation on key osteogenic markers in CTGF KO mice, we performed quantitative PCR (qPCR) analyses using mRNA derived from two skeletal sites in CTGF KO and WT: 1) the tibial midshaft, which includes the kinked region in the CTGF KO mice; and 2) the parietal bone. The patterns of expression of these osteogenic genes were opposite between the two sites. In the tibial midshaft of CTGF KO mice, *Runx-2*, alkaline phosphatase (*ALP*), and osteocalcin (*Oc*) were significantly upregulated compared to WT tibiae (Fig. 7A). In the parietal bone, expression of *Runx-2*, *ALP*, and *Oc* was significantly decreased compared to WT parietal bone (Fig. 7B). To determine whether decreased expression in the parietal osteogenic markers was due to altered cellular expression of these genes and not the result of fewer osteoblasts in CTGF KO bone, we performed histomorphometric analyses of the parietal bones using von Kossa stained sections counterstained with toluidine blue to measure the number of osteoblasts per bone perimeter (N.Ob/B.Pm). We demonstrated that CTGF KO parietal bones had 34.2 osteoblasts per 1mm of bone surface compared to 30.5 in WT mice ($p = 0.24$).

We also investigated the expression levels of CTGF along with two closely related CCN family members – Cyr61/CCN1 and Nov/CCN3 – at these two skeletal sites. Deletion of CTGF resulted in a significant increase in CCN3 levels in the tibial midshaft in CTGF KO mice, while CCN1 levels were not significantly different ($p=0.25$) (Figure 2-8A). CCN1 expression levels were significantly decreased in the parietal bone CTGF KO mice. While CCN3 levels were decreased relative to WT levels, they were not significantly different ($p=0.06$) (Figure 2-8B). To rule out the possibility that normal

variation in CTGF expression between skeletal sites could account for site-specific changes seen in the CTGF KO mice, we compared CTGF expression from the WT tibia, femur, parietal bone, and mandible. We found that there was no statistical difference between CTGF expression between these sites (Figure 2-8D).

Transforming growth factor beta (TGF- β) signaling is required for proper bone formation, and CTGF has been shown to functionally interact with components of this pathway (Abreu et al., 2002). We also noted unique morphologic traits in the CTGF KO skulls that closely resembled the craniofacial phenotype seen in *Tgfb2^{f/f};Wnt1-Cre* mice (see Discussion). Therefore, we examined the expression of TGF- β_1 , TGF- β receptor 2 (RII) (the ligand binding receptor), and TGF- β receptor 1 (RI) (the signaling receptor) in two sites of the craniofacial skeleton: the parietal bone and the mandible. Expression of TGF- β RI in both the parietal bone and mandible were significantly decreased in CTGF KO mice. Expression of the ligand, TGF- β_1 , was also decreased at both sites, with the mandible showing statistical significance and the parietal bone approaching significance ($p = 0.052$). Although levels of TGF- β RII were also lower in CTGF KO parietal bones and mandibles, the differences were not significantly different ($p=0.078$ and $p=0.068$, respectively) (Figure 2-8C). These findings are consistent with a dysregulation of the TGF- β_1 ligand/receptor interaction in the craniofacial skeleton in CTGF KO mice.

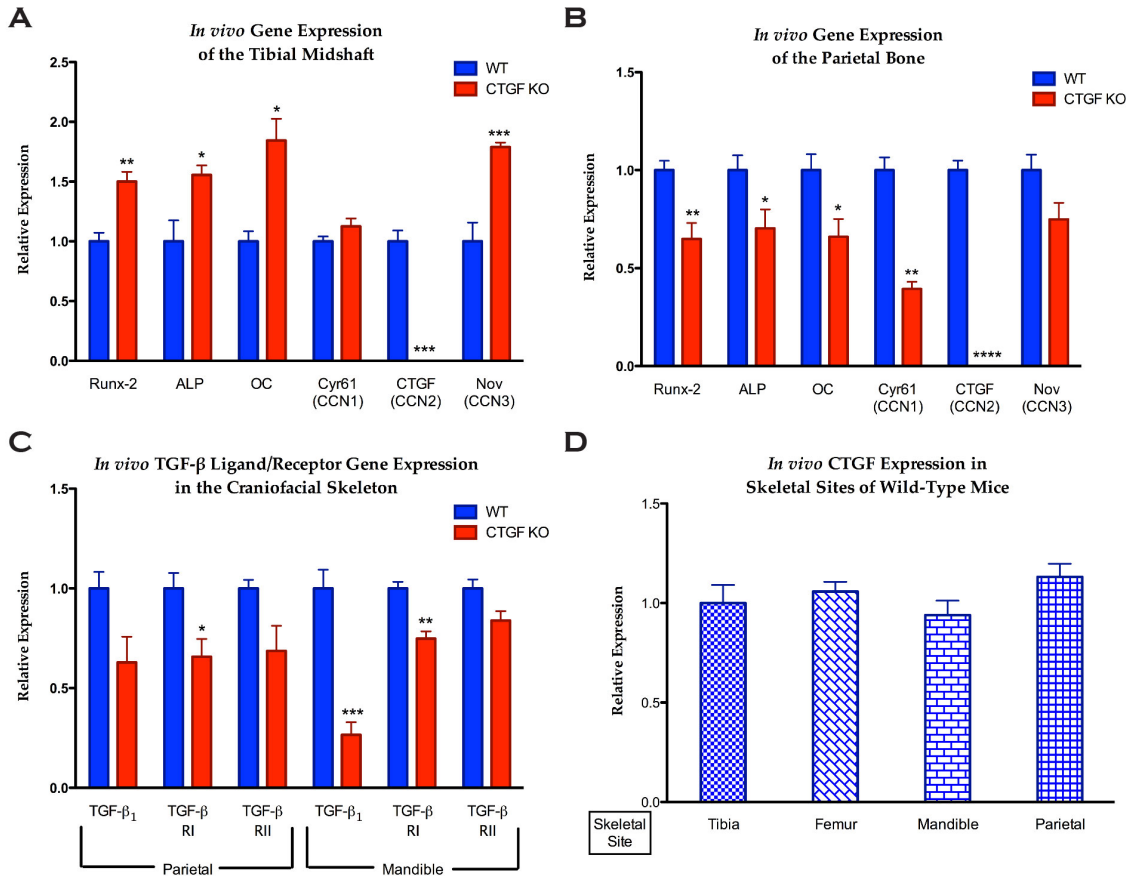


Figure 2-8. Gene expression patterns in CTGF KO skeletal sites.

In vivo mRNA gene expression from CTGF KO tibia (A) and parietal bone (B) is graphed relative to WT samples. *In vivo* expression of TGF- β ligand/receptor components from the craniofacial skeleton of CTGF KO mice is graphed relative to WT samples (C). *In vivo* mRNA expression of CTGF levels in WT mice as four skeletal sites. Abbreviations include: runt-related transcription factor 2 (Runx-2), alkaline phosphatase (ALP), osteocalcin (Oc), TGF- β_1 ligand and TGF- β receptors 1 and 2 (TGF- β RI and RII).

* = $P < 0.05$, ** = $P < 0.01$, *** = $P < 0.001$, and **** = $P < 0.0001$.

Discussion

Our morphometric results demonstrated a significant decrease in the length of the proliferating zone in CTGF KO mice. This zone is normally maintained by both adequate PTH-rP production in the resting zone as well as Ihh production in the prehypertrophic and hypertrophic zones (Chung et al., 2001). Our findings are consistent with the previous report of decreased PTH-rP and Ihh gene expression in the CTGF KO growth plate (Kawaki et al., 2008a). Furthermore, we found that while the hypertrophic zone length was increased, the prehypertrophic zone length was unaffected. This expansion is likely due to the previously reported decrease in Ihh production by these cells (Kawaki et al., 2008a). It has been shown that abrogation of PTH-rP signaling can still result in proper progression from proliferating through prehypertrophic to hypertrophic chondrocytes (Provot and Schipani, 2005). This could explain why the length of the prehypertrophic zone is unaffected in CTGF KO mice while hypertrophic zone expansion occurs.

Although bone forms through both endochondral (replacing a preexisting cartilage anlage) and intramembranous (*de novo*) ossification processes, individual bones may form from a combination of the two processes, as seen in the occipital bone of the skull (Rice, 2008). Furthermore, both chondrocytes and osteoblasts originate from precursor mesenchymal cells, the location of their condensations during prenatal skeletal development determines the embryonic cell lineage of the future bone – craniofacial bones from neural crest and paraxial mesoderm, the remaining axial skeleton from somatic mesoderm of the sclerotomes, and the appendicular skeleton from lateral and intermediate mesoderm (Karsenty, 1998). Taking this into account, we examined various

skeletal sites to determine if CTGF ablation produces global or site-specific changes in osteogenesis.

Our micro-CT and gene expression analyses demonstrated site-specific differences in bone formation within the appendicular skeleton. Using micro-CT, we found significant decreases in metaphyseal trabecular bone in both the phenotypically abnormal (kinked) tibiae and phenotypically normal (straight) femora in CTGF KO mice compared to WT littermates. These differences indicate defective endochondral ossification, as the trabeculae in this region form through this process. Nonetheless, we cannot discount that altered chondrogenesis could be contributing to these changes in bone mass as we and others have demonstrated dysregulation of the growth plate zones as well as production of crucial cartilage ECM components, such as aggrecan and collagen type X (Ivkovic et al., 2003; Kawaki et al., 2008a). However, it is less likely that aberrant osteoclast function is solely responsible for the bone phenotype presented herein. As it was previously demonstrated that CTGF KO mice have fewer osteoclasts in the metaphyseal region (Ivkovic et al., 2003), this decrease in resorption would be expected to cause a resultant increase in trabecular bone; this is not the case in the CTGF KO mice.

Our analyses of the midshaft of these same bones demonstrated different trends in bone formation, such that it was normal in the femur and increased in the tibia. In the phenotypically normal femur, the percent of bone at the midshaft was not significantly different in CTGF KO mice compared to WT littermates. On the contrary, in the phenotypically abnormal tibia, the midshaft showed a dramatic increase in total bone volume in CTGF KO mice compared to WT littermates. These results demonstrate specific differences in the bone volume at these various sites. To confirm if this was due

to an increase in osteoblast function, we analyzed the gene expression of *Runx-2* (marker of early osteoblast commitment), *ALP* (marker of osteoblast maturation), and *Oc* (marker for terminal osteoblast differentiation). Our qPCR analyses demonstrated increased expression of all three osteoblast markers, consistent with increased bone formation at the cellular level. We also found a significant increase in *Nov/CCN3* expression, which has previously been shown in the growth plate of CTGF KO mice (Kawaki et al., 2008a). These results demonstrate that not only is bone formation variably affected depending on the skeletal site, and in this case the site within an individual bone, but also that CTGF ablation does not result in a global decrease in bone formation.

An interesting point worth noting is the specificity and reproducibility of the abnormal bones in the CTGF KO skeleton. The CTGF KO phenotype involves distinct kinks in appendicular long bones, specifically bones of the embryonic *zeugopod* region, which comprises the radius and ulna in the forelimb (FL) and the tibia and fibula of the hindlimb (HL). However, the bones of the *stylopod* – humerus (FL) and femur (HL) – and *autopod* – carpus (FL), tarsus (HL), and digits (FL&HL) – remain unchanged. Why CTGF ablation only affects the *zeugopod* region could be due to changes in skeletal patterning, mechanobiological alterations, or a combination of the two. One of the key classes of genes involved in limb development includes the Hox genes, and it has been shown that specific mutations in *Hoxa11*, *Hoxc11*, and *Hoxd11* deleteriously affect normal development of the *zeugopod* (Koyama et al., 2010; Wellik and Capecchi, 2003; Zakany and Duboule, 2007). Mechanobiological cues are also important in proper limb development, where muscle-induced mechanical load is necessary for proper bone

formation *in utero* (Nowlan et al., 2012; Nowlan et al., 2007, 2008; Nowlan et al., 2010; Sharir et al., 2011).

The craniofacial skeleton is unique in terms of skeletal development in that it derives from multiple cell types and involves both forms of ossification (Noden and Trainor, 2005; Sperber et al., 2010). Crania are historically analyzed by subdividing them into three regions— the cranial vault or calvaria, the cranial base, and the facial skeleton. During development, a dual-layered capsular membrane known as the *ectomeninx* surrounds the developing brain. This *ectomeninx*, of both paraxial mesoderm and neural crest origin, forms the dura mater, which has an outer layer with chondro-/osteogenic properties. In the region of the future calvarium, this membrane will undergo intramembranous ossification, while in the area of the future cranial base this membrane will undergo endochondral ossification. The facial skeleton is of solely neural crest origin and forms through only intramembranous ossification (Sperber et al., 2010). Therefore, generally speaking, global aberrations in endochondral ossification are seen only in the cranial base, while effects on intramembranous ossification present as defects in cranial vault or facial bones, the differences between which can result from their different ossification processes.

Micro-CT, gene expression, and landmark analyses of the axial skeleton of CTGF KO mice demonstrated multiple aberrations in the bone formation of these mice. It has been previously shown that the ribcage of CTGF KO mice presents with characteristic kinks in the bone (Ivkovic et al., 2003). When assessing bony elements in the axial skeleton of CTGF KO and WT mice, we analyzed the amount of bone at two sites within the craniofacial skeleton and two locations within the vertebral column. We saw a

dramatic difference within the vertebral column, such that the more caudal vertebral bodies (L1) had decreased bone while the more rostral (T8) were not significantly affected. Ossification of the vertebral column at birth is most prominent in the thoracic region of normal newborn mice while other more rostral and caudal sites fully ossify perinatally (Theiler, 1989). Therefore, the decreased ossification found at L1 and not T8 could have resulted from a delay in ossification in CTGF KO mice.

We also analyzed the parietal bones, which form solely from intramembranous ossification. These bones demonstrated decreased ossification in CTGF KO compared to WT mice. This coincides with our findings of decreased expression osteogenic markers in CTGF KO parietal bones (Fig. 7B). These results are in agreement with a previous study that showed a reduction in the expression of some of these markers during osteogenic differentiation of primary osteoblast cultures derived from CTGF KO mice compared to WT littermates (Kawaki et al., 2008b). Furthermore, we demonstrated through histomorphometric analyses that the number of osteoblasts in CTGF KO parietal bones is similar to that in WT parietal bones. Therefore, the decreased expression in osteoblast markers was not due to a decrease in osteoblast numbers but rather a decrease in gene expression on a per cell basis. We also demonstrated a decrease in expression of closely related CCN family member, Cyr61/CCN1 in CTGF KO parietal bones. Since it has been demonstrated that CCN1 can stimulate osteogenesis *in vitro* (Su et al., 2010), the absence of CTGF coupled with decreased CCN1 expression is consistent with the aforementioned reduction in the expression of osteogenic markers.

We determined phenotypic differences between CTGF KO and WT skulls using 3D coordinates of cranial landmarks for the entire skull, and then analyzed landmarks

representing regions of the skull separately. Our PCA analysis of the global skull landmark set demonstrated a clear separation between CTGF KO and WT littermates with both allometric and non-allometric skull shape differences contributing to the changes seen in the skulls of CTGF KO mice. PCA analyses of the landmark subsets representing the three cranial regions also revealed separation between groups.

We further computed localized differences in craniofacial shape using the non-parametric bootstrap algorithm of EDMA (Lele and Richtsmeier, 2001). Overall differences in craniofacial shape were significant in CTGF KO cranial vault and facial skeleton regions, but not so for the cranial base. Confidence interval tests for each linear distance demonstrated relative increases along the medio-lateral axis for the facial skeleton and anterior cranial vault and relative decreases in distances along the rostro-caudal axes of the cranial vault.

In addition to our landmark analyses, we also noted several obvious morphologic differences in CTGF KO skulls; these included changes in the nasal bones, mandibles, palate and vomer, and pterygoid plates of the sphenoid bone. These abnormal phenotypic traits were conserved in all CTGF KO mice studied. In order to relate the site specificity of these changes to any potential underlying mechanisms, we need to take into account; 1) the embryonic cell origins of these bones, and 2) the signaling pathways known to involve CTGF in craniofacial development. The nasal bones, mandibles, palate, and vomer derive entirely from the cranial neural crest population, while the sphenoid has a dichotomous embryonic cell origin such that the sphenoid body is derived from paraxial mesoderm, while the pterygoid plates are derived from neural crest cells (Noden and Trainor, 2005).

The mandibles of CTGF KO mice, while aberrant in phenotype (Fig. 6D), displayed decreased percent bone volume compared to WT mice. The mandible has a complex process of bone formation involving both intramembranous and endochondral ossification, as it forms around Meckel's cartilage (Lee et al., 2001; Shimo et al., 2004). Additionally, it has been shown that CTGF is required for Meckel's cartilage development (Shimo et al., 2004). Therefore, this decrease in bone could be due to a combination of alterations in the preexisting Meckel's cartilage, decreased ossification at this site, or both.

The TGF- β signaling family has been shown to be involved in CTGF expression and signaling in bone development (Arnott et al., 2011). A role for CTGF in TGF- β signaling-mediated craniofacial development was shown by the Chai laboratory using a cranial neural crest-specific knockout of the TGF- β receptor II (*Tgfb2^{fl/fl};Wnt1-Cre*) (Ito et al., 2003; Iwata et al., 2010; Oka et al., 2007). These mice demonstrated decreased CTGF expression in developing Meckel's cartilage, concomitant with a mandibular phenotype similar to that of the CTGF KO mice (Oka et al., 2007). Analysis of the craniofacial phenotype in the *Tgfb2^{fl/fl};Wnt1-Cre* mice also demonstrated similarities with the CTGF KO mice in the development of their nasal bones, vomer, and palate (Ito et al., 2003; Iwata et al., 2010). Bones formed by endochondral ossification were targeted in mice in which the TGF- β receptor II was conditionally inactivated in chondrocytes under the type II collagen, alpha 1 (Col2a1) promoter (Col2acre^{+/+}; *Tgfb2^{loxP/loxP}*). These mice demonstrated changes in the sphenoid body (Baffi et al., 2006; Baffi et al., 2004), which were not observed in our analysis of CTGF KO skulls. Therefore, the effects of

CTGF ablation on TGF- β RII signaling in neural crest cells may provide an explanation for the craniofacial phenotype seen in our analyses.

We found aberrations in the TGF- β signaling pathway at both the receptor and ligand levels in CTGF KO parietal bones and mandibles. We demonstrated reductions in the expression of both TGF- β RI and RII; TGF- β RI is responsible for propagating the TGF- β signal through phosphorylation of Smads 2 and 3 (Hendy et al., 2005). It is interesting to note that in *Tgfb2^{fl/fl};Wnt1-Cre* mice (discussed above), the expression of CTGF was decreased in developing Meckel's cartilage, and that the abnormal craniofacial phenotype was partially rescued by adding back exogenous CTGF (Oka et al., 2007). These results demonstrate the importance of CTGF as a necessary downstream player in TGF- β -mediated craniofacial development. A comparison of phenotypic changes seen in CTGF KO skulls with those in the skulls of *Tgfb2^{fl/fl};Wnt1-Cre* mice highlights a potentially crucial role of the TGF- β -CTGF signaling loop in craniofacial development. We postulate that the absence of CTGF in mice results in a dysregulation of TGF- β signaling, thus providing a possible mechanistic explanation for the abnormal skull phenotype.

CHAPTER 3: AN ANALYSIS OF BONE CELL ULTRASTRUCTURE AND MATRIX COMPOSITION IN CONNECTIVE TISSUE GROWTH FACTOR KNOCKOUT (CTGF KO) MICE

Lambi, A.G., McGoverin, C.M., Gannon, M., Pleshko, N., and Popoff, S.N.

Introduction

Connective tissue growth factor (CTGF) is a 38kDa secreted protein involved in multiple normal and pathologic scenarios. Its varied roles are made possible by the multi-modular structure of CTGF. As such, it was grouped with other proteins into the CCN family of proteins. Named for first three members identified in the literature – Cysteine-rich 61 (Cyr61/CCN1), CTGF (CCN2), and Nephroblastoma overexpressed protein (Nov/CCN3) – the CCN family has also come to include the Wnt-induced secreted proteins -1 (Wisp-1/CCN4), -2 (Wisp-2/CCN5), and -3 (Wisp-3/CCN6) (Brigstock et al., 2003). CCN proteins are 30-40kDa proteins, rich in cysteine residues, and primarily composed of four conserved modules: 1) an insulin-like growth factor (IGF)-binding domain; 2) a von Willebrand type C domain; 3) a thrombospondin-1 domain; and 4) a C-terminal domain containing a putative cysteine knot (Figure 1-3) (Bork, 1993; Brigstock, 1999; Lau and Lam, 1999; Perbal, 2001). The mosaic structure of these proteins allows for their involvement in many normal cellular events that contribute to key physiologic processes necessary for skeletogenesis.

A role for CTGF in skeletal tissues first emerged from studies demonstrating its expression in developing cartilage, bone, and teeth (Friedrichsen et al., 2003; Ivkovic et al., 2003; Safadi et al., 2003; Yamashiro et al., 2001). However, the key finding for the indispensability of CTGF in skeletogenesis came with the generation of CTGF knockout (KO) mice. These mice are born with defects in growth plate chondrogenesis,

angiogenesis, endochondral bone formation, and ECM production (Ivkovic et al., 2003). In addition to aberrations in growth plate formation and zone organization, newborn CTGF KO mice also have chondrodysplasia in limb and rib cartilage and Meckel's cartilage. Interestingly, the gross skeletal defects seen in CTGF KO mice consistently involve kinking of the ribs, tibiae, fibulae, radii, and ulnae, as well as craniofacial abnormalities. It has been presumed due to the severe rib cage dysmorphology, as well as pulmonary hypoplasia, results in respiratory failure shortly after birth (Baguma-Nibasheka and Kablar, 2008; Ivkovic et al., 2003). The resulting neonatal lethality of CTGF KO mice constitutes the chief difficulty in studying the role of CTGF in bone development, formation and function. We extended the previously reported analyses of the CTGF KO skeletal phenotype in Chapter 2 by performing an in depth, quantitative analysis utilizing multiple *in vivo* and *in vitro* techniques. Using this approach, we determined that newborn CTGF KO mice have skeletal site-specific changes in bone formation (Lambi et al., 2012).

CTGF belongs to a subset of proteins secreted into the extracellular matrix (ECM) known as matricellular proteins (Chen and Lau, 2009). Originally described in the literature in the context of thrombospondin 1 (TSP-1), the category of matricellular proteins arose from the diversity of functions individual ECM molecules could have resulting in, at times, seemingly conflicting results when studied (Bornstein, 1995). Additional members in this category included secreted protein acidic and rich in cysteine (SPARC, or osteonectin), tenascin-C, and has more recently included thrombospondin 2, osteopontin (OPN), tenascin X, and the CCN protein family members (Bornstein, 1995; Bornstein and Sage, 2002; Sage and Bornstein, 1991). Unlike structural proteins of the

ECM, matricellular proteins act contextually to effect cell responses through modulation of cell-matrix interactions. The diversity of their function relies on the specific cell-surface receptors, cytokines, growth factors, and/or proteases with which they interact in the local ECM milieu (Bornstein, 2001). Interestingly, other characteristics shared by this subset of proteins include high expression during development, growth, injury response, and in normal tissues with continued turnover, such as bone.

Due to the intricate role of CTGF in cell-matrix interactions, we conducted studies to determine the effects of global CTGF ablation on bone cell ultrastructure and biochemical composition. We hypothesized that the loss of CTGF would result in ultrastructural changes in bone consistent with findings of decreased trabecular and increased diaphyseal bone in CTGF KO. We also hypothesized that biochemical alterations in CTGF KO bone composition resulted in impaired structural integrity. Based on these hypotheses, we isolated tibiae from newborn wild-type and CTGF KO mice. Techniques utilized included transmission electron microscopy (TEM) and Fourier transform infrared spectroscopy (FT-IR). The studies herein present predominantly preliminary data, the ongoing studies of which are expected to yield novel information regarding the role of CTGF in bone ultrastructure and composition.

Materials and Methods

Animals

CTGF KO (CTGF^{LacZ/LacZ}) mice were obtained from breeding CTGF heterozygous (CTGF^{+/LacZ}) mice as previously described ((Crawford et al., 2009)). Animals used for the analyses of this study were sacrificed at birth (P0). Genotype was

determined as previously described (Crawford et al., 2009). Briefly, CTGF KO mice were distinguished from their wild-type ($\text{CTGF}^{+/+}$) and heterozygous littermates based on the appearance of ribcage dysmorphology seen in all CTGF KO mice (Ivkovic et al., 2003; Lambi et al., 2012) and a positive X-gal staining result (Quiagen, Valencia, CA). Heterozygous mice were distinguished from wild-type littermates as those with normal ribcage morphology and a positive X-gal staining result. All animals were maintained and used according to the principles in the NIH Guide for the Care and Use of Laboratory Animals (U.S. Department of Health and Human Services, Publ NO. 86-23, 1985) and guidelines established by the IACUC of Temple University.

Electron Microscopy Tissue Preparation

Animals used for this study were euthanized at birth (P0) by decapitation. Subsequently, tails were removed and used for genotype analysis (described above). For EM studies, hindlimbs were dissected in PBS and fixed immediately in a fixative solution of 2.5% glutaraldehyde (Electron Microscopy Sciences, Fort Washington, PA) and 2% paraformaldehyde (PFA) (Affymetrix Microarray Solutions, Santa Clara, CA) diluted in PBS; these were then placed at 4°C for 24h. Subsequently, tibiae were carefully dissected free of all surrounding tissues, including removal of the fibulae, and replaced with fresh fixative solution for 24h at 4°C. Samples were then subject to two 15 minute washes in PBS at room temperature (RT) after which the samples were decalcified using Formical-2000 (Decal Chemical, Tallman, NY). Solution was replaced at 24h. At 48h, samples were again subject to washes at RT with PBS, after which they were placed in fixative solution at 4°C and transported to the Electron Microscopy Resource Lab at the University of Pennsylvania. The samples were post-fixed in 2.0% osmium tetroxide for

1h at RT, and rinsed in deionized water prior to *en bloc* staining with 2% uranyl acetate. After dehydration through a graded ethanol series, the tissue was infiltrated and embedded in EMbed-812 (Electron Microscopy Sciences, Fort Washington, PA). Thin sections (60-70 µm) were cut using a Reichert-Jung Ultracut E ultramicrotome (Leica Microsystems, Wetzlar, Germany) and were picked up on formvar-coated copper slot grids. Thin sections were then stained with uranyl acetate and lead citrate and examined with a JEOL 1010 electron microscope fitted with a Hamamatsu digital camera and AMT Advantage image capture software.

FT-IRIS Tissue and Section Preparation

Animals used for this study were euthanized at birth (P0) by decapitation. Subsequently, tails were removed and used for genotype analysis (described above). For FT-IRIS studies, hindlimbs were dissected in PBS and fixed immediately in 4% PFA (buffered in PBS) for 24h at 4°C. Subsequently, tibiae were dissected free of all surrounding tissues while the fibulae were left intact; this aided in proper orientation during embedding. Samples again were placed in PFA for 24h at 4°C, after which they underwent two 15 minute washes in PBS. Specimens were then dehydrated and cleared, followed by infiltration with and embedding in methylmethacrylate resin (Osteo-Bed Bone Embedding Kit, Polysciences, Warrington, PA). Five µm sections were obtained from the polymerized resin blocks, then de-plasticized and stained with von Koss staining technique, for mineralization, and counterstained with toluidine blue ((Abdelmagid et al., 2010; Ivkovic et al., 2003; Lambi et al., 2012; Zhou et al., 2010). These stained sections were used to determine appropriate section level for subsequent FT-IRIS analysis. For FT-IRIS analysis, 9 µm of embedded tissue were mounted on low-e reflective-coated

infrared microscope slides (MirrIR slides, Kevley Technologies, Chesterland, OH). Sections were air-dried at RT for 30 min, followed by dissolving embedding medium in deionized water, fixation in 10% formalin, and air-drying.

FT-IRIS Data Acquisition and Analysis

FT-IRIS images of the entire (newborn) tibiae were acquired at 25 μm pixel resolution and 8cm^{-1} spectral resolution with two co-added scans using a Perkin Elmer Spotlight 400 spectrometer (Shelton, CT) as previously described (Boskey and Pleshko Camacho, 2007; Cheheltani et al., 2012; Hanifi et al., 2012). The spectrometer source is an electrically heated silicon carbide light source with high emissivity and a quasi-blackbody emission spectrum with an effective temperature of \sim 1300 K. Data were analyzed with Isys 5.0 software (Spectral Dimensions Inc., Olney, MD). The integrated area of the phosphate absorbance band, centered near 1050 cm^{-1} (Boskey and Pleshko Camacho, 2007), was used to mask each sample such that only bone regions of the image were included in analyses. Four specific parameters measuring particular bone properties were analyzed using previously established spectral regions are listed in Table 3-1 (Boskey and Pleshko Camacho, 2007).

Table 3-1. Bone Properties Measured by FT-IR Spectroscopy.

This table was adapted from (Boskey and Pleshko Camacho, 2007).

Parameter	Definition	Validation	Variation with Age
Mineral-to-Matrix Ratio	Area of phosphate band ($900\text{-}1200\text{ cm}^{-1}$) / Area of amide I band ($1585\text{-}1720\text{ cm}^{-1}$)	Linearly related to ash content of synthetic collagen and apatite mixtures	Increases
Carbonate-to-Phosphate Ratio	Area of carbonate band ($850\text{-}890\text{ cm}^{-1}$) / Area of phosphate band ($900\text{-}1200\text{ cm}^{-1}$)	Related to tissue carbonate content as determined by elemental analyses	Increases
Crystallinity	Peak area or intensity ratio of subbands at 1030 and 1020 cm^{-1}	Related to crystal size in <i>c</i> -axis dimension as determined by X-ray diffraction line broadening	Increases
XLR	Peak area or intensity ratio of subbands at 1660 and 1690 cm^{-1}	Related to collagen maturity where ratio changes with photolysis of collagen cross-links	Increases

Statistical Data Analysis

Statistical analyses for FT-IRIS were performed using GraphPad Prism 5 (<http://www.graphpad.com>). Briefly, a two-tailed Student's *t*-test was used to determine statistically significant differences between WT and CTGF KO group means for FT-IR analyses. A *p*-value of less than 0.05 was considered statistically significant.

Results

Ultrastructure of Osteoblasts and Osteocytes in WT and CTGF KO Tibiae

As we have already demonstrated that markers of osteoblast differentiation and function are decreased at certain skeletal sites in CTGF KO mice (Lambi et al., 2012), we next chose to study if the osteoblasts present in these mice appeared normal at the ultrastructure level. Using transmission electron microscopy (TEM), we visualized

osteoblasts within multiple regions within the bone, including the newly synthesized trabeculae of the metaphysis, the periosteal collar, and diaphysis (encompassing the kink in the CTGF KO tibiae). In the metaphyseal region, osteoblasts of both WT and CTGF KO mice had similar ultrastructural appearances (Figure 3-1). At lower magnification, osteoblasts line the surface of newly formed trabecular bone² in close apposition to one another (Fig. 3-1A-D). It is common for these cells, under the electron microscope, to demonstrate an irregular border with the newly formed osteoid due to the long, branched processes the cells send out into the unmineralized matrix (Scherft and Groot, 1990). At higher magnification, additional features of mature osteoblasts were noted in both WT and CTGF KO mice; these include heterochromatic nuclei, abundant mitochondria, extensive rough endoplasmic reticulum (RER), as well as collagen deposition into the unmineralized osteoid (Fig. 3-1E-F). The aforementioned features are all indicative of metabolically active osteoblasts concomitant with bone formation.

Osteoblasts of the diaphyseal region of the CTGF KO tibiae, which includes the phenotypic kink, demonstrated ultrastructural characteristics that differed from those under the growth plate (Figure 3-2). The border between these osteoblasts was difficult to demarcate due to extensive intracellular inclusions (Figure 3-2A), which higher magnification revealed to be predominantly dilated RER (Fig. 3-2C-D). In WT tibiae, these ultrastructural features were only apparent in osteoblasts of the periosteal collar, and yet the magnitude of RER dilation was not as great as that observed in CTGF KO tibiae.

² For ultrastructure studies, trabecular bone (Tb) under the growth plate comprises newly mineralized cancellous bone formed on a cartilaginous core.

Comparison of osteocyte ultrastructure revealed ultrastructural differences between WT and CTGF KO tibiae. We chose to compare osteocytes that had either just become encased in bone matrix or those fully enveloped by matrix and further from the trabecular margins. In WT tibiae, osteocytes just becoming encased in matrix continue to demonstrate an abundance of RER and mitochondria, indicative of a metabolically active cell that is still synthesizing matrix proteins (Figure 3-3A). However, CTGF KO osteocytes of a similar stage of matrix envelopment have a more extensive, dilated RER (Figures 3-2A, 3-3B). WT osteocytes that are further from the trabecular margin appear to be quiescent cells, while those in CTGF KO tibiae still appear to be actively synthesizing proteins (Figure 3-3C-D).

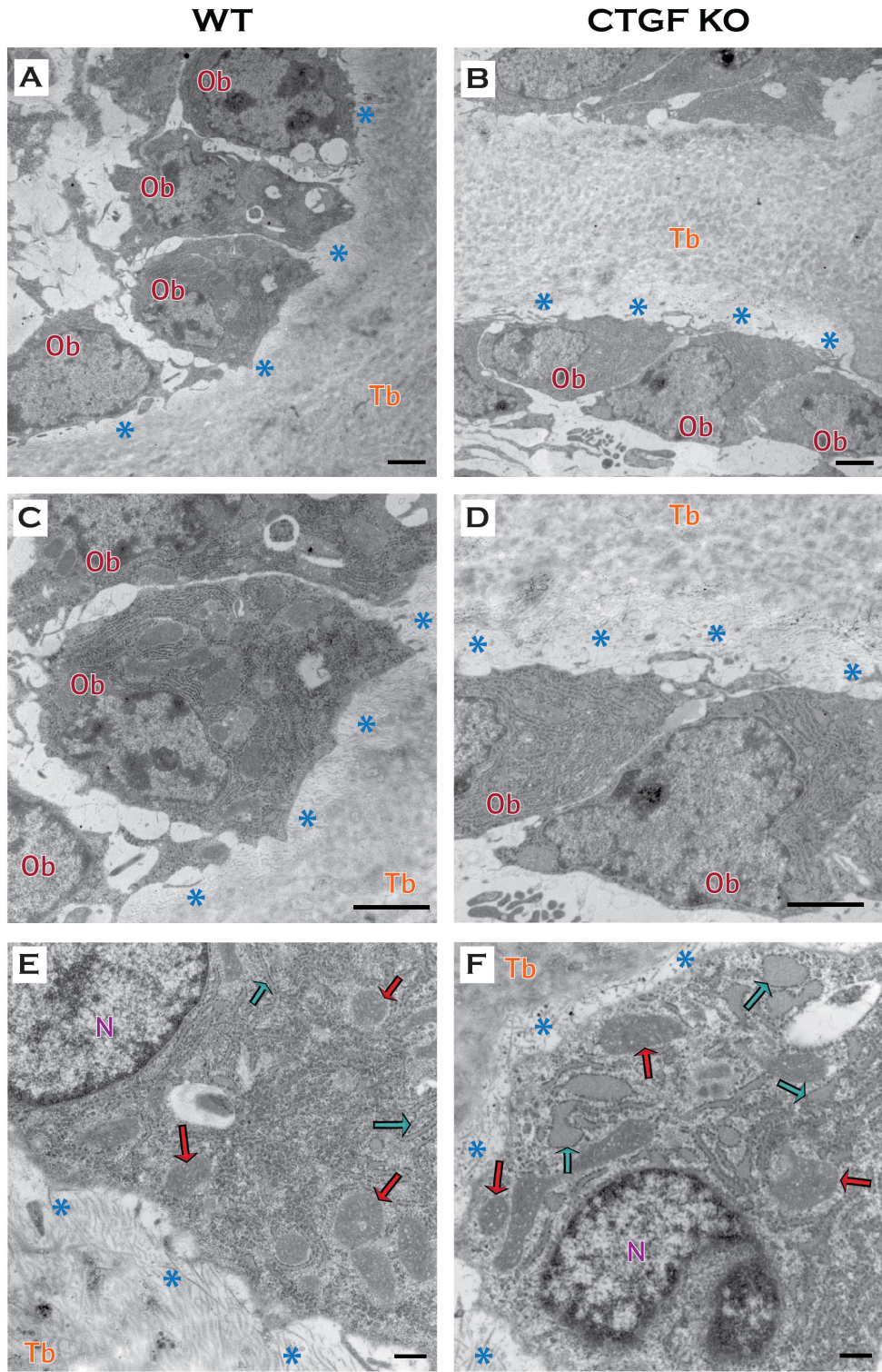


Figure 3-1. Comparison of WT and CTGF KO Metaphyseal Osteoblast Ultrastructure

Figure 3-1. Comparison of WT and CTGF KO Metaphyseal Osteoblast

Ultrastructure

Electron microscopy of tibial proximal metaphyses comparing osteoblast ultrastructure from WT (A,C,E) and CTGF KO (B,D,F) bones. At lower magnifications (A-D), individual osteoblasts (Ob) can be visualized, as well as newly formed, unmineralized osteoid (*blue asterisks*), and trabecular bone (Tb). Additionally, at higher magnifications (E-F), heterochromaticity of nuclei (N) is appreciated, as well as abundant mitochondria (*red arrows*) and rough endoplasmic reticulum (*cyan arrows*). Scale bar: 2 μ m (A-D) and 500nm (E-F).

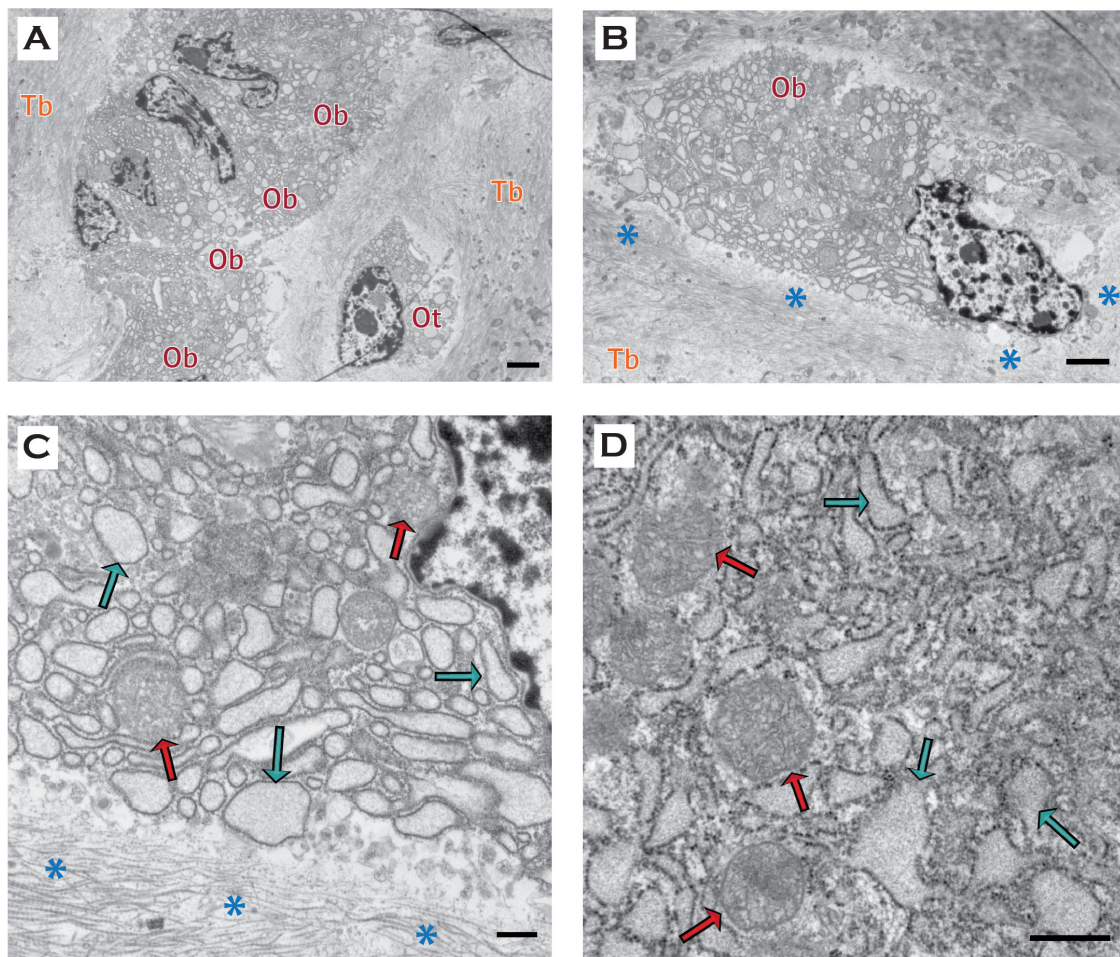


Figure 3-2. Ultrastructural Features of CTGF KO Diaphyseal Osteoblasts

Electron microscopy of CTGF KO tibial diaphyses demonstrates characteristics of actively synthesizing cells. (A) The borders between individual osteoblasts (Ob) are difficult to distinguish due to heavily distended rough endoplasmic reticulum (RER). A newly formed osteocyte (Ot) still appears very active in producing matrix components. (B) These cells continue producing collagen-rich osteoid (*blue asterisks*) on trabecular bone (Tb). Higher magnification (C-D) demonstrates abundant mitochondria (*red arrows*) and RER (*cyan arrows*). Scale bar: 2 μ m (A-B) and 500nm (C-D).

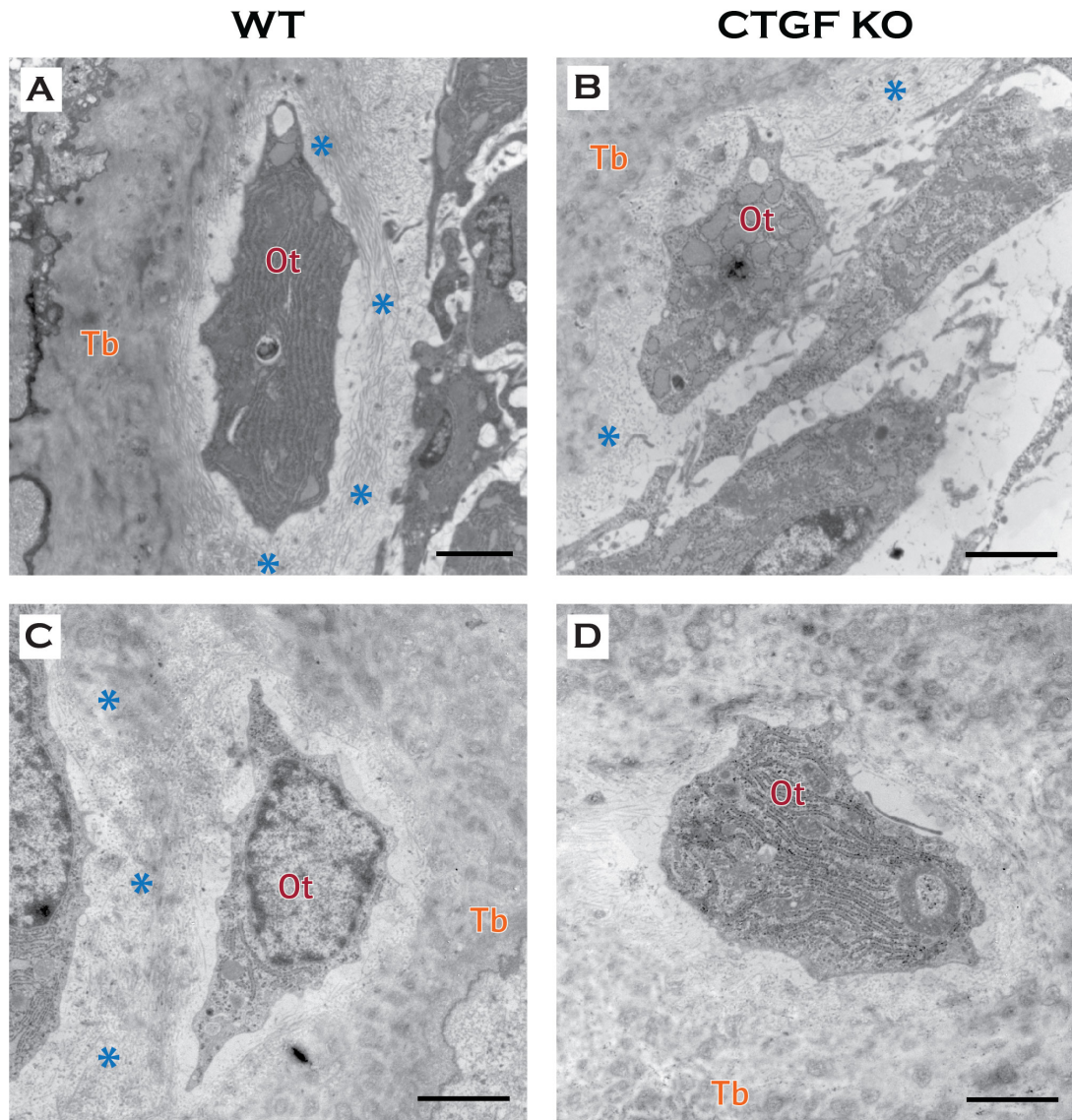


Figure 3-3. Comparison of Wild-type and CTGF KO Osteocyte Ultrastructure

Electron microscopy of tibiae comparing osteocyte (Ot) ultrastructure from WT (A,C) and CTGF KO (B,D) bones demonstrates greater abundance and/or dilation of rough endoplasmic reticulum (RER) in CTGF KO compared to WT tibiae. This is visible in osteocytes just becoming encased in matrix as well as those fully encased in trabecular bone (Tb.) Scale bar: 500nm.

Ultrastructure of Osteoclasts in WT and CTGF KO Tibiae

We also examined the ultrastructure of osteoclasts in WT and CTGF KO tibiae; this encompassed multiple regions within the bone, including the newly synthesized trabeculae of the metaphysis, the periosteal collar, and diaphysis (including the kink in the CTGF KO tibiae). The ultrastructure of mature, functional osteoclasts has been well characterized (Marks and Popoff, 1990), and includes the following prominent features: 1) multiple, typically heterochromatic, nuclei; 2) a sealing zone, in which (predominantly $\alpha_v\beta_3$) integrins facilitate osteoclast attachment to underlying bone and/or calcified cartilage; 3) a clear zone, adjacent to the sealing zone, which is devoid of organelles; 4) a ruffled border, an area bounded by the clear zone, in which bone resorption occurs; and 5) prominent vacuolization of the cytoplasm. Electron microscopy of WT tibiae demonstrated the aforementioned features of normal osteoclast ultrastructure (Figure 3-4). CTGF KO osteoclasts also demonstrated features of actively resorbing, mature cells (Figure 3-5).

Throughout the analysis of CTGF KO osteoclasts, multiple ultrastructural dysmorphologies were seen that, while not necessarily unique to CTGF KO tibiae, were more prevalent than in WT tibiae (Figure 3-6). Osteoclasts were more abundant in sections of CTGF KO compared to WT tibiae (Figure 3-6A-B). Although these cells exhibited ultrastructural features typical of normal, functional osteoclasts, there were also several distinct dysmorphologies observed in CTGF KO osteoclasts. One dysmorphism seen in CTGF KO osteoclasts was a multi-layered structure that appears to be composed of infolded rings of membrane (Figure 3-6C). These are typically present immediately adjacent to the ruffled border and could represent a remnant from ruffled border

formation. We also noticed a disproportionate amount of clear zone compared to the extent of ruffled border formation in many CTGF KO osteoclasts (Figure 3-6D-F). Lastly, many of the CTGF KO osteoclasts demonstrated a less extensive cytoplasmic vacuolization compared to WT.

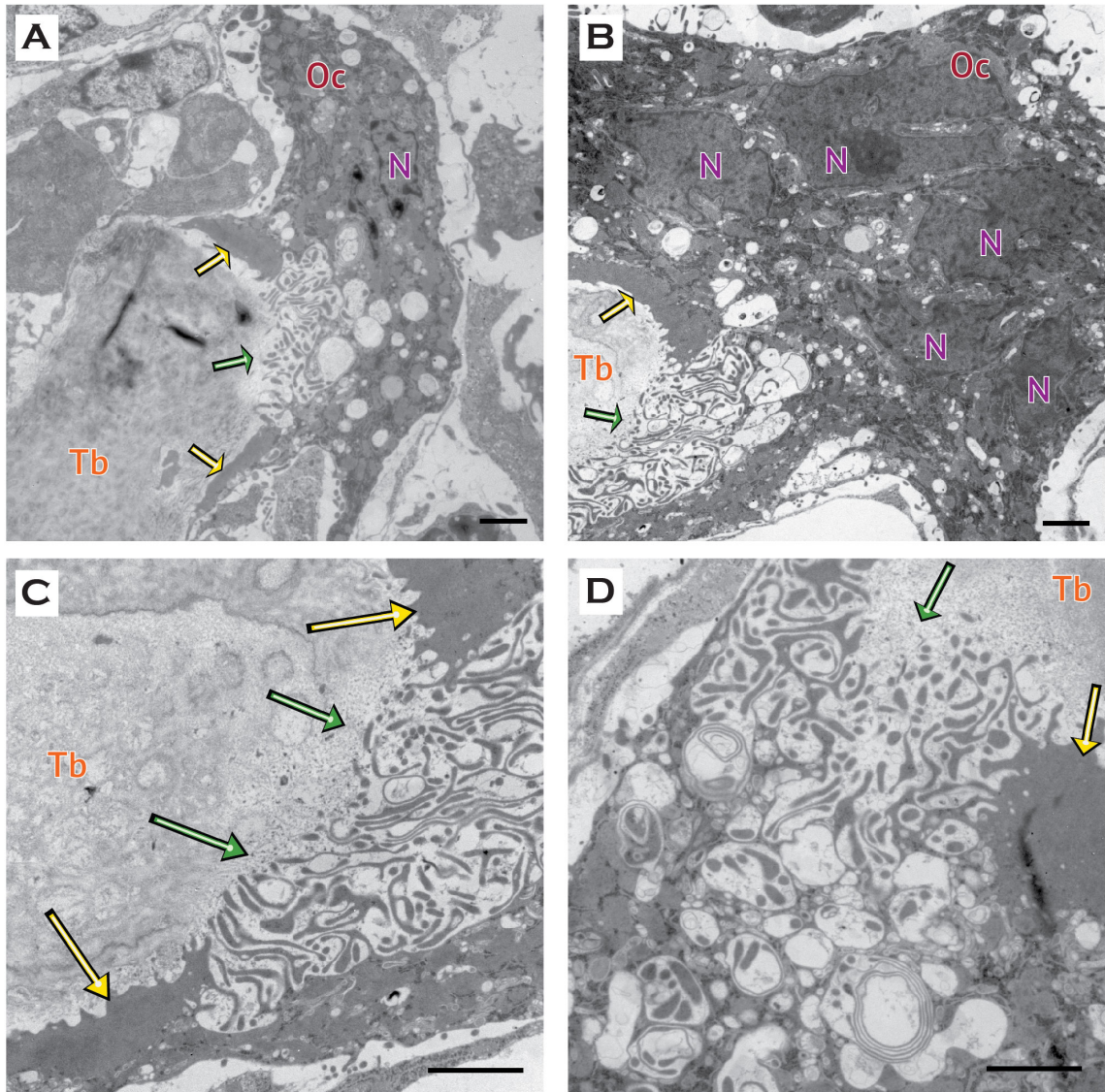


Figure 3-4. Analysis of WT Osteoclast Ultrastructure

Electron microscopy of WT tibiae demonstrates normal osteoclast (Oc) ultrastructure. Hallmarks of normal osteoclast ultrastructure are appreciated at lower (A-B) and higher magnification (C-D), such as extensive vacuolization (A,D) and ruffled border formation (B-C). Clear zones (*yellow arrows*) are identified at the periphery of ruffled borders (*green arrows*). Scale bar: 2 μ m (A-B) and 500nm (C-D).

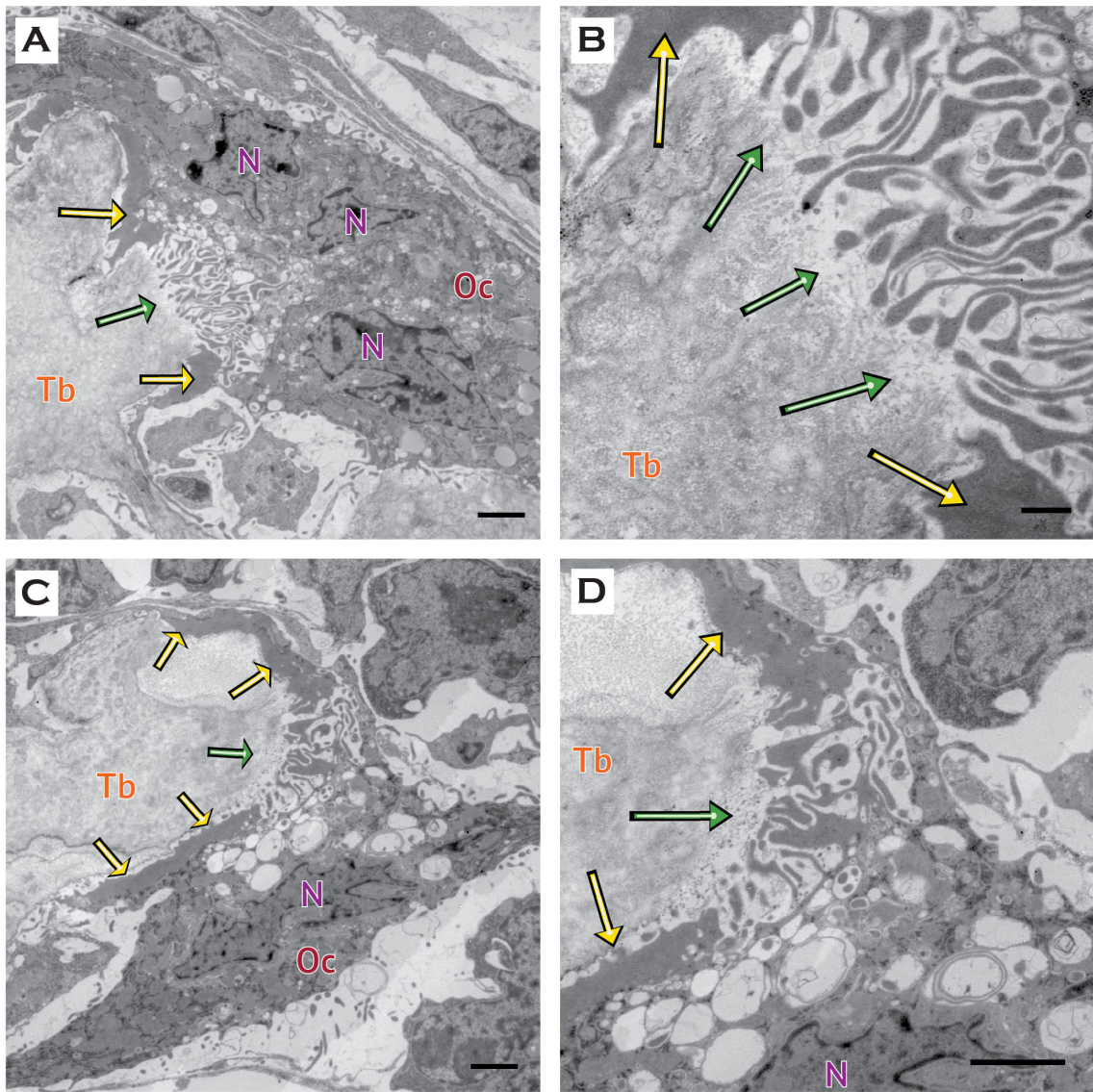


Figure 3-5. Analysis of CTGF KO Osteoclast Ultrastructure

Electron microscopy of CTGF KO tibiae demonstrates features of normal osteoclast (Oc) ultrastructure; these include multiple nuclei (N), vacuolization (C-D), and ruffled border formation (A-D). Clear zones (*yellow arrows*) are identified at the periphery of ruffled borders (*green arrows*). Scale bar: 2 μ m (A-C) and 500nm (D).

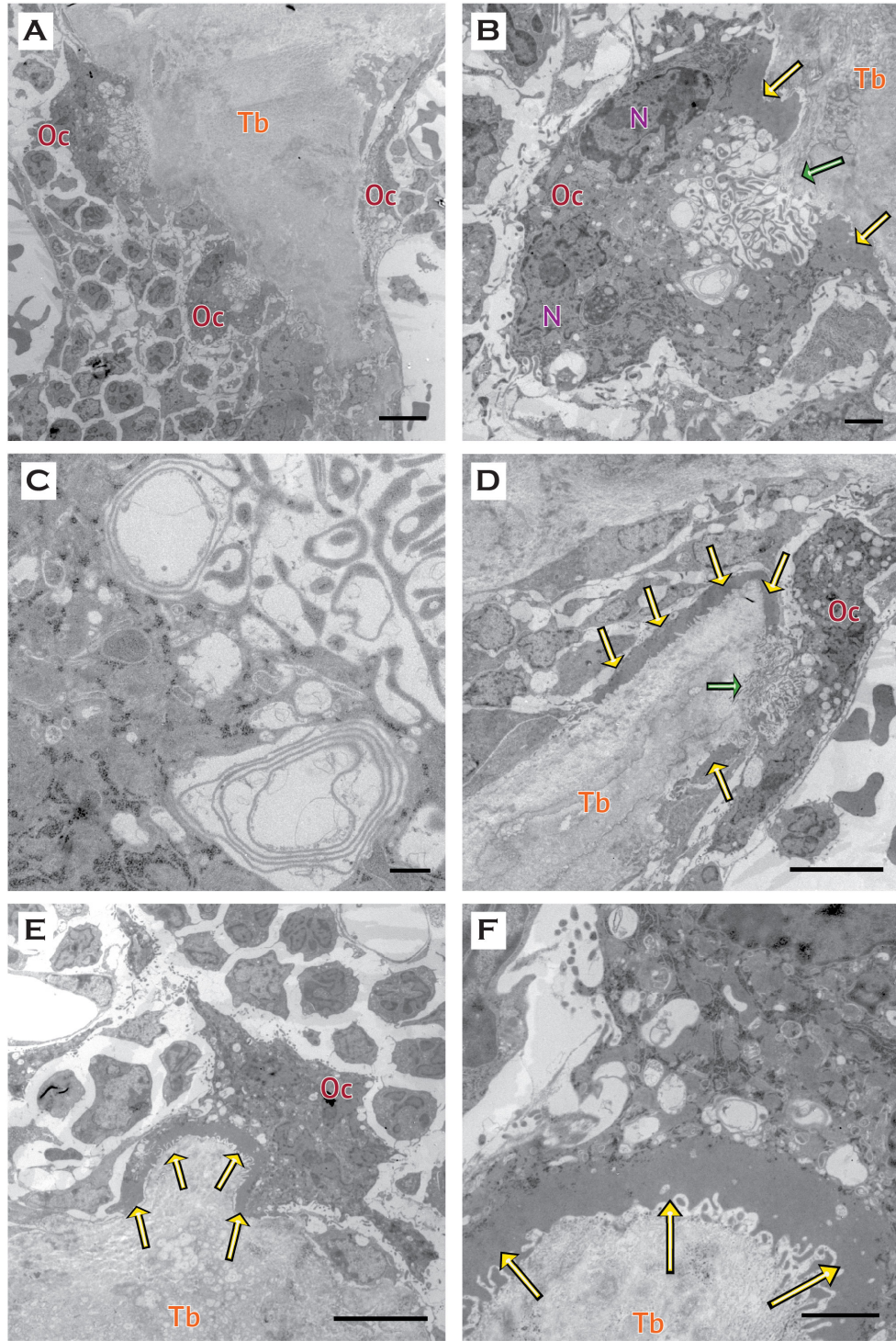


Figure 3-6. Ultrastructural Dysmorphologies Prevalent in CTGF KO Osteoclasts

Figure 3-6. Ultrastructural Dysmorphologies Prevalent in CTGF KO Osteoclasts

Electron microscopy of CTGF KO tibiae demonstrated ultrastructural dysmorphologies prevalent in CTGF KO osteoclasts. (A) Osteoclasts (Oc) were frequently observed in CTGF KO tibiae, as demonstrated by the appearance of three closely adjacent osteoclasts capping the end of a single trabecular. (B) Higher magnification of an osteoclast from panel A is shown. (C) CTGF KO osteoclasts also frequently exhibited multi-layered structures that appear to be composed of infolded rings of membrane (C). Many osteoclasts also had a disproportionately large amount of clear zone (*yellow arrows*) compared to the extent of ruffled border (*green arrow*). Scale bar: 2 μ m (A-C) and 500nm (D-F).

FT-IR Spectroscopy of Bone Matrix Properties in CTGF KO and WT Tibiae

We also conducted studies on the biochemical composition of the bone matrix in CTGF KO tibiae compared to WT samples using Fourier transform infrared (FT-IR) spectroscopy. This technique measures four key parameters of bone formation and/or maturation all of which increase with normal age; they included the mineral-to-matrix ratio, carbonate-to-phosphate ratio, crystallinity, and XLR. Definitions and validations of these parameters are listed in Table 3-1. Although statistical differences were not observed between WT and CTGF KO tibiae in whole bone and mid-shaft analyses (Figure 3-7), CTGF KO samples demonstrated a wider range of values suggesting a greater heterogeneity in the maturation of bone matrix present.

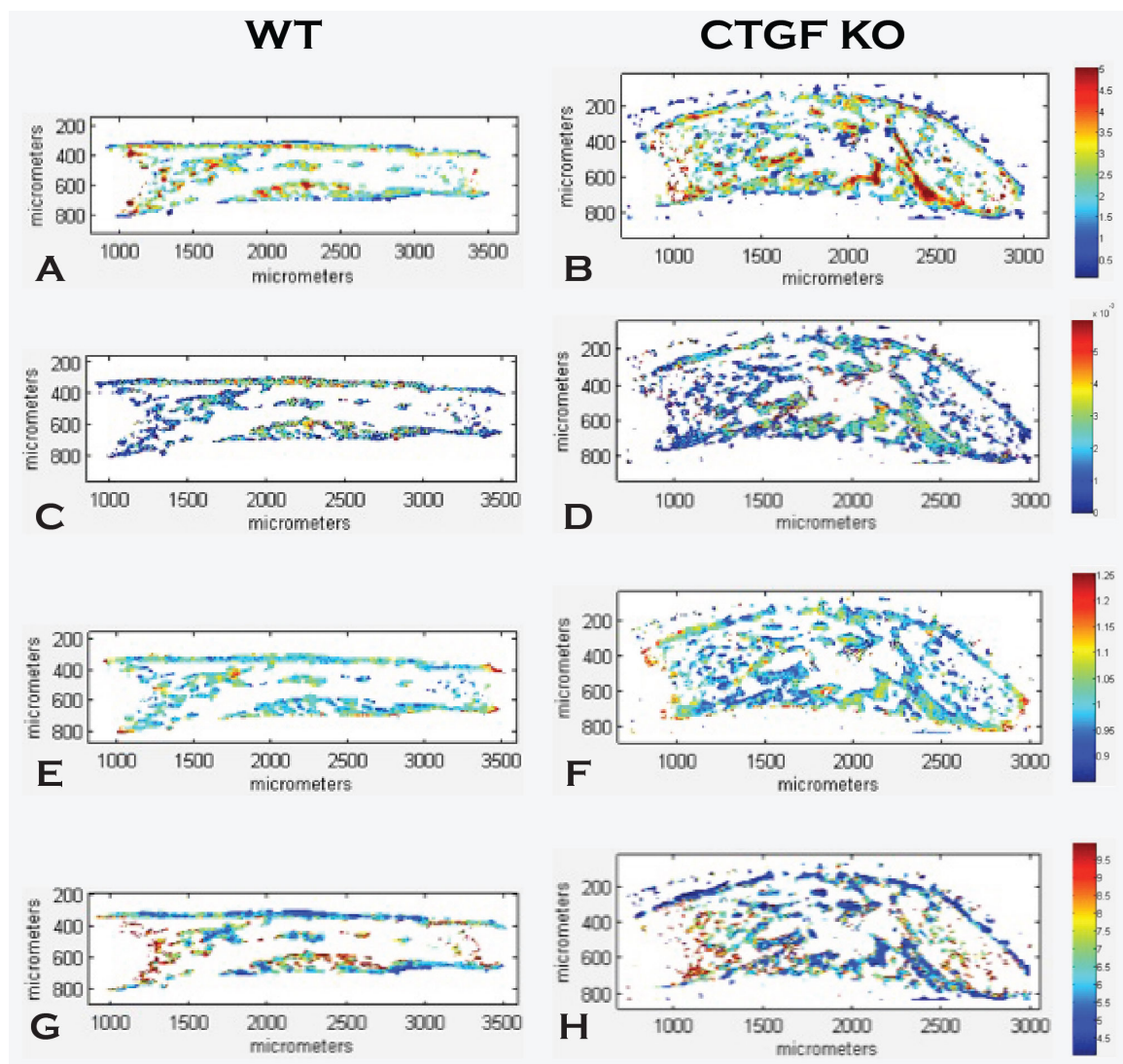


Figure 3-7. FT-IR Spectroscopy of Bone Matrix Properties in WT and CTGF KO

Tibiae

FT-IR spectroscopy measured four key properties of bone matrix composition and/or maturity in WT and CTGF KO tibiae; these included mineral-to-matrix ratio (A-B), Carbonate-to-phosphate ratio (C-D), crystallinity (E-F), and XLR (G-H). See table 3-1 for definitions of these terms.

Discussion

The analyses of CTGF KO bone cell ultrastructure demonstrated that CTGF is not requisite for the complete morphologic maturation of bone cells, but that its absence does lead to features at the ultrastructure level not commonly seen in WT bones. Osteoblasts in both WT and CTGF metaphyseal regions of the proximal tibiae demonstrated normal formation, proximity to trabecular bone surface and hallmark features of metabolically active cells. Osteoblasts in the diaphyseal region of CTGF KO tibiae, however, demonstrated drastically extended rough endoplasmic reticulum (RER) the degree of which obscured the demarcation between adjacent cells. Only in the periosteal collar of WT tibiae were osteoblasts with severely distended RER seen, and yet not to this degree. This ultrastructural characteristic could be due to defects in protein synthesis, processing, and/or secretion caused by the absence of CTGF. This highlights the need for further studies to examine whether defects in these processes are occurring in CTGF KO osteoblasts.

Osteoclasts in both WT and CTGF KO tibiae also demonstrated ultrastructural characteristics indicative of normal, functional osteoclast maturation. It was noted when the CTGF KO mouse model was first described in the literature that bones from these mice have decreased osteoclastogenesis as determined by tartrate-resistant acid phosphatase (TRAP) staining (Ivkovic et al., 2003). However, our TEM analysis demonstrated an abundance of osteoclasts in CTGF KO tibiae compared to WT tibiae. This discrepancy could be due to the fact that TRAP staining may not have conclusively identified functional osteoclasts in CTGF KO tibiae; this could have been due to decreased levels of TRAP production compared to WT osteoclasts as well as the young

age of these (newborn) bones. Furthermore, we found several ultrastructural dysmorphologies more prevalent in CTGF KO osteoclasts; these included multi-layered structures that appear to be composed of infolded rings of membrane, and a disproportionate amount of clear zone compared to the extent of ruffled border. Expansion of clear zones in CTGF KO osteoclasts would suggest a defect in cell attachment. Integrins (especially $\alpha_v\beta_3$) are required for formation of the sealing and clear zones in maturing osteoclasts. It is well established that CTGF modulates cell-matrix interactions through direct binding with integrins as well as indirect mechanisms of modulating molecules in the extracellular matrix (Arnott et al., 2011). Therefore, the absence of CTGF in these tibiae could result in impaired osteoclast attachment to the bone matrix, which could lead to subsequent (compensatory) clear zone expansion decreased ruffled border formation and ultimately defective bone resorption concomitant with decreased cytoplasmic vacuolization. This underlying intrinsic defect could contribute to the increased bone we have shown in the diaphysis (phenotypic kink) of CTGF KO tibiae.

Lastly, we conducted FT-IR spectroscopy analyses of CTGF KO and WT tibiae to determine if differences in the bone matrix composition resulted from global ablation of CTGF. It was previously reported that growth plates in CTGF KO long bones contain reduced levels aggrecan and link protein, the latter of which is necessary for the structural integrity of cartilage and deficiency of which results in phenotypic changes in the same subset of long bones as seen in the CTGF KO mouse (Ivkovic et al., 2003; Morgelin et al., 1994; Watanabe and Yamada, 1999). Although the means of these measures did not show statistical differences between the WT and CTGF KO tibiae, there was a greater

heterogeneity of data in CTGF KO tibiae. This warrants an expansion in the sample size pool.

Taking into account findings presented in Chapter 2 where we demonstrated increased amounts of total bone volume in the mid-diaphyses of CTGF KO tibiae, these FT-IR results suggest that while more bone is present in this region, its biochemical composition is normal. Therefore, the bone being produced in excess in CTGF KO tibial diaphyses is the result of a dysregulation leading to more (normal) bone in that specific region. To that effect, we have produced sections of WT and CTGF KO tibiae stained with Safranin-O and fast green, which allows visualization of cartilage and bone, respectively (images not shown). In newborn bone samples, a cartilaginous core of trabecular bone is visible as these cartilage spicules, produced in the growth plate, act as the template (*anlagen*) for future bone to be deposited during development and long bone growth. When studying the Safranin-O sections of CTGF KO tibiae, while the trabecular bone under the growth plate contains cartilaginous cores, the bone of the kinked region does not; this suggests that this bone formed directly through intramembranous ossification, likely through an expansion of the periosteal collar. Future analyses using FT-IR to distinguish trabecular composition of type I versus type II collagen will allow a comparison of trabecular and periosteal collar bone in WT and CTGF KO tibiae with bone of the diaphyseal kink in CTGF KO tibiae. This will provide necessary data to conclude whether the abnormal bone deposition in certain CTGF KO bones is the result of dysregulated endochondral or intramembranous ossification.

CHAPTER 4: SUMMARY

Although a score has passed since the discovery and identification of connective tissue growth factor (CTGF) in the literature, much of its signaling, mechanism(s) of action, and exact role(s) in normal and pathologic processes remains unclear. A role for CTGF in skeletal tissues first emerged from studies demonstrating its expression in developing cartilage, bone, and teeth (Friedrichsen et al., 2003; Ivkovic et al., 2003; Safadi et al., 2003; Xu et al., 2000; Yamashiro et al., 2001). However, the key finding for the indispensability of CTGF in skeletogenesis came with the generation of genetically engineered mice lacking CTGF production (Crawford et al., 2009; Ivkovic et al., 2003). These CTGF knockout (KO) mice have provided great insight into the importance of CTGF in normal skeletal development. The initial study demonstrated that CTGF KO mice are born with multiple skeletal dysmorphisms, including bends (or kinks) in specific long bones, craniofacial abnormalities, and misshapen ribs (Ivkovic et al., 2003). Defects were also found in chondrogenesis and angiogenesis of the growth plate, two critical processes involved in endochondral ossification (Ivkovic et al., 2003; Kawaki et al., 2008a). A subsequent study revealed a lack of ossification in specific flat bones of the skull, which would indicate defective intramembranous ossification. Therefore, from these studies, it was concluded and established as dogma of the CCN protein family field that a lack of CTGF results in global deficiencies in bone formation.

We believe that this dogma constitutes an oversimplification of the role of CTGF in osteogenesis, as systemic deficiencies in bone formation would simply not account for the unique skeletal phenotype seen in CTGF KO mice. A global decrease in bone formation would in all likelihood result in systemic osteopenia, and not the distinct

phenotype of CTGF KO skeletons, where phenotypically normal and abnormal bones are juxtaposed in a highly reproducible fashion. To that end, we performed a comprehensive characterization of the skeletal phenotype in this model, choosing sites within the axial and appendicular skeleton, as well as various *in vivo* techniques to elucidate differences in CTGF KO bones (Figure 1-5).

The results of this dissertation unequivocally demonstrate that global ablation of CTGF results in skeletal site-specific changes in prenatal osteogenesis. In Chapter 2, we reported site-specific changes in growth plate organization, bone microarchitecture, and shape and gene expression levels in CTGF KO compared to WT mice. Malformations of the growth plate included increased hypertrophic zone and decreased proliferative zone lengths. Sites within the appendicular skeleton of CTGF KO mice – metaphyses and diaphysis of femora and tibiae – demonstrated less metaphyseal trabecular bone, while having increased mid-diaphyseal bone in CTGF KO tibiae; this region comprises the phenotypic kink. The increase in tibial diaphyseal bone in CTGF KO mice was concomitant with increased osteogenic expression markers. Similar analyses in several sites of the axial skeleton – vertebral bodies, parietal bones and mandibles – also demonstrated decreased bone coupled with decreased osteogenic markers. Our craniofacial landmark analyses highlighted changes in CTGF KO skull size and shape, as well as unique dysmorphologies found therein. Our analysis of bone cell ultrastructure and composition in the studies of Chapter 3 demonstrated that while CTGF is not requisite for the complete ultrastructural maturation of bone cells, its absence leads to unique ultrastructural dysmorphologies not seen in WT bones. Change in osteoblast ultrastructural of CTGF KO tibiae were seen in a site-specific manner within tibiae,

where metaphyseal trabecular osteoblasts appeared normal or slightly more active, diaphyseal osteoblasts had characteristics that could be due to defects in protein synthesis. Furthermore, composition analysis of CTGF KO tibia demonstrated that, while the means of particular properties were not significantly different from WT tibiae, heterogeneity in data was present. Lastly, ultrastructure of CTGF KO osteoclasts revealed an abundance of morphologically mature cells, despite prior reports (Ivkovic et al., 2003), but these cells often presented with ultrastructural dysmorphologies such as decreased vacuolization, ruffled border, and disproportionately large amounts of clear zone. Taken together, this could suggest an intrinsic defect in the maturation and/or function of osteoclasts when CTGF is absent *in vivo*.

The studies of this dissertation have shown that the role of CTGF in osteogenesis is more complicated than previously purported. Our reports have not only demonstrated quantitative differences in the microarchitecture, structure, ultrastructure and expression patterns in CTGF KO compared to WT bones, but we showed that these occur in a skeletal site-specific pattern. Therefore, with all due deference to the great orator Sir Winston Churchill, out of intense complexities intense simplicities do NOT always emerge. Notwithstanding the apparently more complex picture of CTGF in prenatal osteogenesis, our studies have identified several areas of interest for future studies.

TGF- β -CTGF Axis: A potential Mechanistic Explanation for the CTGF KO Craniofacial Phenotype

Results of skull phenotype analysis and expression patterns revealed a potential explanation for the CTGF KO craniofacial phenotype: the TGF- β -CTGF axis. It is well

established that the TGF- β signaling family is involved in CTGF expression during osteogenesis (reviewed in (Arnott et al., 2011). Furthermore, mice that lack the TGF- β receptor II specifically in neural crest cells ($Tgfb2^{fl/fl};Wnt-Cre$) present with some strikingly similar craniofacial dysmorphologies; these include a kinked vomer, curved nasal bones, shortened mandibles, and failed midline convergence of the palate (Ito et al., 2003; Iwata et al., 2010; Oka et al., 2007). A cartoon of the palate from CTGF KO and $Tgfb2^{fl/fl};Wnt-Cre$ mice demonstrates the degree of similarity found between these two models, with particular emphasis on the dysmorphology of the vomer, a phenotype not found in any other model, to our knowledge (Figure 4-1A). Taking into account this common traits between the two mouse models, as well as our reported dysregulation of TGF- β 1 ligand/receptor interaction in the CTGF KO skull, we propose the TGF- β -CTGF axis as a mechanism for the craniofacial changes seen (Figure 4-1B). This axis must be further explored through a complete comparison of CTGF KO and $Tgfb2^{fl/fl};Wnt-Cre$ skulls, as well as the development of a cranial neural crest specific CTGF knockout model.

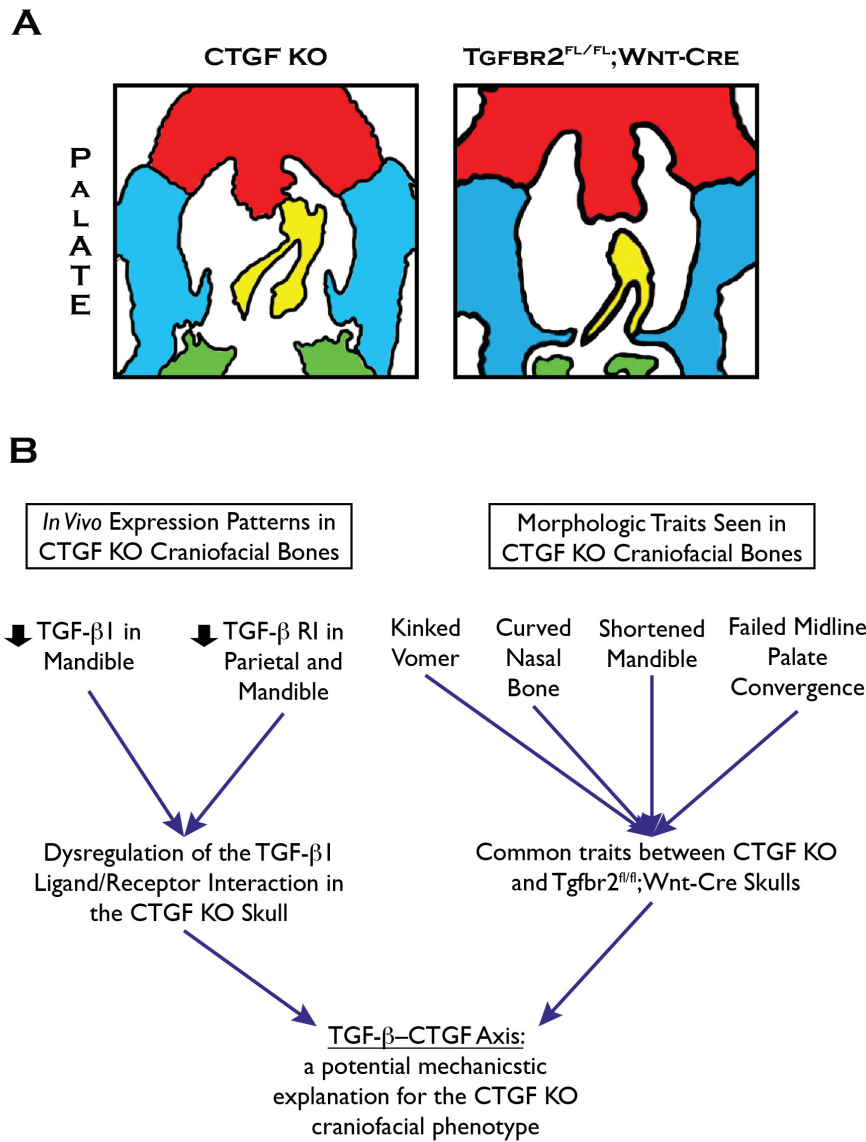


Figure 4-1: The TGF-β-CTGF Axis: a potential mechanistic explanation for CTGF KO craniofacial phenotype

(A) A cartoon comparing the inferior aspect of the palate of CTGF KO and Tgfb2^{fl/fl};Wnt-Cre mice, including premaxillae (red), maxillae (blue), palatine (green), and vomer (yellow). (B) Flowchart demonstrating the evidence supporting the TGF-β-CTGF axis as a potential mechanistic explanation for the craniofacial phenotype seen in CTGF KO mice.

Solving the Riddle of the Kinks

Having established the location and degree of bone abnormalities in CTGF KO mice, the next step in elucidating the developmental role of CTGF in bone formation is answering why these defects always and only occur in specific bones in these mice. It is well established that proper skeletal development requires both the influence of key skeletal patterning factors, such as the *Hox* genes, as well as muscle-generated mechanical forces to guide bone shaping during development (reviewed in (Nowlan et al., 2010; Sharir et al., 2011; Zakany and Duboule, 2007)). In addition to the high reproducibility of the bone defects seen in CTGF KO mice, suggesting an effect on skeletal patterning, it has previously been shown that the cartilage anlagen of future limb bones are bent at embryonic day (E) 14.5 in concert with future bone kinks (Ivkovic et al., 2003). Therefore, the loss of CTGF affects could affect local skeletal patterning and/or mechanobiological cues during bone development, rendering specific skeletal sites susceptible to future bone defects, and ultimately resulting in the unique phenotype seen in CTGF KO mice. To determine which of these processes is affected in CTGF KO mice, the exact timing of limb bone abnormalities during development must be determined. This involves studying several prenatal time points that represent the developmental stages of these bones: E12.5, where developing bones still include mesenchymal stem cell (MSC) condensations, particularly in the hind limb and all digits; E14.5, at which point limb bones of the *stylopod* and *zeugopod* regions comprise cartilage anlagen; and E16.5, when the periosteal collars for the bones of the aforementioned regions are present and trabecular bone is beginning to form (Taher et al., 2011; Theiler, 1989). These

studies would yield novel information regarding both the temporal role of CTGF in bone development as well as mechanisms through which it accomplishes this.

The Clinical Quagmire of CTGF in Bone

The utility of targeting CTGF clinically to treat conditions of insufficient bone formation, while ripe with potential, is still far from being a complete picture. As mentioned in Chapter 1, studies in which rCTGF was injected into the marrow cavity of rat femurs demonstrated an anabolic response to CTGF in bone formation (Safadi et al., 2003; Xu et al., 2000). However, since 1) the functional diversity of CTGF largely depends on the matricellular molecules with which it interacts and 2) we have shown that CTGF exerts roles on osteogenesis in a site-specific fashion (Lambi et al., 2012), the anabolic nature of CTGF in bone is likely contingent upon the presence and/or absence of specific molecules at a target skeletal site. Therefore, the effect of CTGF on bone would be variable from site to site. To illustrate this, consider the interaction of CTGF with the TGF- β and bone morphogenetic proteins (BMP) pathways. While both of these pathways are critical in bone formation, it has been shown that CTGF can positively enhance TGF- β signaling through interactions with TGF- β_1 while inhibiting BMP receptor signaling through interaction with BMP-4 (Abreu et al., 2002). Furthermore, we have demonstrated that treatment of primary osteoblasts that lack CTGF (isolated from CTGF KO mice) with rBMP-2 causes enhanced differentiation and signaling when compared to WT osteoblasts (Mundy and Popoff, unpublished data). These data suggest that CTGF acts to inhibit the anabolic effect of BMP-2 on bone formation.

Herein lies the current paradox of targeting CTGF clinically in bone: how is it that CTGF alone produces osteoinductive effects, while also potentially countering the well-established osteoinductive effects of BMP-2? While there is insufficient research evidence to currently tease apart this discrepancy, both have current clinical implications. As CTGF expression normally increases during fracture repair, one could postulate that abrogation of CTGF signaling through FG-3019-mediated blockade would negatively affect fracture healing and potentially hasten development of age-related osteoporosis (Kadota et al., 2004; Nakata et al., 2002; Safadi et al., 2003; Yamashiro et al., 2001). This would present a serious detractor to FG-3019 therapy, particularly in post-menopausal women. Additionally, knowledge of the CTGF-BMP interaction could identify a potential use for the addition (or blockade) of CTGF in concert with recombinant BMP2 (rBMP-2) administration in treatment of bony defects and malunions. To fully understand the therapeutic potential of CTGF in bone formation, studies must utilize the following: 1) animal models simulating various clinical scenarios, such as fracture repair and osteoporosis; and 2) local or global treatment using rCTGF or FG-3019 with or without rBMP-2. Once results from these *in vivo* models are obtained, only then can we understand the clinical applications of CTGF for treatment of patients with bone disorders.

REFERENCES CITED

- Abdelmagid, S.M., Barbe, M.F., Hadjiaargyrou, M., Owen, T.A., Razmpour, R., Rehman, S., Popoff, S.N., and Safadi, F.F. (2010). Temporal and spatial expression of osteoactivin during fracture repair. *J Cell Biochem 111*, 295-309.
- Abreu, J.G., Ketpura, N.I., Reversade, B., and De Robertis, E.M. (2002). Connective-tissue growth factor (CTGF) modulates cell signalling by BMP and TGF-beta. *Nat Cell Biol 4*, 599-604.
- Aldridge, K., Boyadjiew, S., Capone, G., DeLeon, V., and Richtsmeier, J.T. (2005). Precision and error of three-dimensional phenotypic measures acquired from 3dMD photogrammetric images. *Amer J Med Genet 138*, 247-253.
- Allen, M.R., Hock, J.M., and Burr, D.B. (2004). Periosteum: biology, regulation, and response to osteoporosis therapies. *Bone 35*, 1003-1012.
- Arnott, J.A., Lambi, A.G., Mundy, C., Hendesi, H., Pixley, R.A., Owen, T.A., Safadi, F.F., and Popoff, S.N. (2011). The role of connective tissue growth factor (CTGF/CCN2) in skeletogenesis. *Crit Rev Eukaryot Gene Expr 21*, 43-69.
- Arnott, J.A., Nuglozeh, E., Rico, M.C., Arango-Hisijara, I., Odgren, P.R., Safadi, F.F., and Popoff, S.N. (2007). Connective tissue growth factor (CTGF/CCN2) is a downstream mediator for TGF-beta1-induced extracellular matrix production in osteoblasts. *J Cell Physiol 210*, 843-852.
- Arosarena, O.A. (2007). Cleft lip and palate. *Otolaryngol Clin North Am 40*, 27-60, vi.
- Baffi, M.O., Moran, M.A., and Serra, R. (2006). Tgfbr2 regulates the maintenance of boundaries in the axial skeleton. *Dev Biol 296*, 363-374.
- Baffi, M.O., Slattery, E., Sohn, P., Moses, H.L., Chytil, A., and Serra, R. (2004). Conditional deletion of the TGF-beta type II receptor in Col2a expressing cells results in defects in the axial skeleton without alterations in chondrocyte differentiation or embryonic development of long bones. *Dev Biol 276*, 124-142.
- Baguma-Nibasheka, M., and Kablar, B. (2008). Pulmonary hypoplasia in the connective tissue growth factor (Ctgf) null mouse. *Dev Dyn 237*, 485-493.

Bang, O.S., Kim, E.J., Chung, J.G., Lee, S.R., Park, T.K., and Kang, S.S. (2000). Association of focal adhesion kinase with fibronectin and paxillin is required for precartilage condensation of chick mesenchymal cells. *Biochem Biophys Res Commun* 278, 522-529.

Bork, P. (1993). The modular architecture of a new family of growth regulators related to connective tissue growth factor. *FEBS Lett* 327, 125-130.

Bornstein, P. (1995). Diversity of function is inherent in matricellular proteins: an appraisal of thrombospondin 1. *J Cell Biol* 130, 503-506.

Bornstein, P. (2001). Thrombospondins as matricellular modulators of cell function. *J Clin Invest* 107, 929-934.

Bornstein, P., and Sage, E.H. (2002). Matricellular proteins: extracellular modulators of cell function. *Curr Opin Cell Biol* 14, 608-616.

Boskey, A., and Pleshko Camacho, N. (2007). FT-IR imaging of native and tissue-engineered bone and cartilage. *Biomaterials* 28, 2465-2478.

Bove, G.M., Weissner, W., and Barbe, M.F. (2009). Long lasting recruitment of immune cells and altered epi-perineurial thickness in focal nerve inflammation induced by complete Freund's adjuvant. *J Neuroimmunol* 213, 26-30.

Bradham, D.M., Igarashi, A., Potter, R.L., and Grotendorst, G.R. (1991). Connective tissue growth factor: a cysteine-rich mitogen secreted by human vascular endothelial cells is related to the SRC-induced immediate early gene product CEF-10. *J Cell Biol* 114, 1285-1294.

Brigstock, D.R. (1999). The connective tissue growth factor/cysteine-rich 61/nephroblastoma overexpressed (CCN) family. *Endocr Rev* 20, 189-206.

Brigstock, D.R. (2003). The CCN family: a new stimulus package. *J Endocrinol* 178, 169-175.

Brigstock, D.R., Goldschmeding, R., Katsume, K.I., Lam, S.C., Lau, L.F., Lyons, K., Naus, C., Perbal, B., Riser, B., Takigawa, M., *et al.* (2003). Proposal for a unified CCN nomenclature. *Mol Pathol* 56, 127-128.

Burkus, J.K., Ganey, T.M., and Ogden, J.A. (1993). Development of the cartilage canals and the secondary center of ossification in the distal chondroepiphysis of the prenatal human femur. *Yale J Biol Med* 66, 193-202.

Canalis, E., Zanotti, S., Beamer, W.G., Economides, A.N., and Smerdel-Ramoya, A. (2010). Connective tissue growth factor is required for skeletal development and postnatal skeletal homeostasis in male mice. *Endocrinology* 151, 3490-3501.

Caplan, A.I., and Bruder, S.P. (2001). Mesenchymal stem cells: building blocks for molecular medicine in the 21st century. *Trends Mol Med* 7, 259-264.

Cheheltani, R., Rosano, J.M., Wang, B., Sabri, A.K., Pleshko, N., and Kiani, M.F. (2012). Fourier transform infrared spectroscopic imaging of cardiac tissue to detect collagen deposition after myocardial infarction. *J Biomed Opt* 17, 056014.

Chen, C.C., Chen, N., and Lau, L.F. (2001). The angiogenic factors Cyr61 and connective tissue growth factor induce adhesive signaling in primary human skin fibroblasts. *J Biol Chem* 276, 10443-10452.

Chen, C.C., and Lau, L.F. (2009). Functions and mechanisms of action of CCN matricellular proteins. *Int J Biochem Cell Biol* 41, 771-783.

Chen, Y., Abraham, D.J., Shi-Wen, X., Pearson, J.D., Black, C.M., Lyons, K.M., and Leask, A. (2004). CCN2 (connective tissue growth factor) promotes fibroblast adhesion to fibronectin. *Mol Biol Cell* 15, 5635-5646.

Chung, U.I., Schipani, E., McMahon, A.P., and Kronenberg, H.M. (2001). Indian hedgehog couples chondrogenesis to osteogenesis in endochondral bone development. *J Clin Invest* 107, 295-304.

Cicha, I., and Goppelt-Struebe, M. (2009). Connective tissue growth factor: context-dependent functions and mechanisms of regulation. *Biofactors* 35, 200-208.

Cole, T.I. (2002). *WinEDMA Version 1.0.1 beta*. Windows-Based Software for Euclidean Distance Matrix Analysis.

Confavreux, C.B. (2011). Bone: from a reservoir of minerals to a regulator of energy metabolism. *Kidney Int Suppl*, S14-19.

Crawford, L.A., Guney, M.A., Oh, Y.A., Deyoung, R.A., Valenzuela, D.M., Murphy, A.J., Yancopoulos, G.D., Lyons, K.M., Brigstock, D.R., Economides, A., *et al.* (2009). Connective tissue growth factor (CTGF) inactivation leads to defects in islet cell lineage allocation and beta-cell proliferation during embryogenesis. *Mol Endocrinol* 23, 324-336.

Dallas, S.L., and Bonewald, L.F. (2010). Dynamics of the transition from osteoblast to osteocyte. *Ann N Y Acad Sci* 1192, 437-443.

de Winter, P., Leoni, P., and Abraham, D. (2008). Connective tissue growth factor: structure-function relationships of a mosaic, multifunctional protein. *Growth Factors* 26, 80-91.

Dendooven, A., Nguyen, T.Q., Brosens, L., Li, D., Tarnow, L., Parving, H.H., Rossing, P., and Goldschmeding, R. (2011). The CTGF -945GC polymorphism is not associated with plasma CTGF and does not predict nephropathy or outcome in type 1 diabetes. *J Negat Results Biomed* 10, 4.

Denton, C.P., Black, C.M., and Abraham, D.J. (2006). Mechanisms and consequences of fibrosis in systemic sclerosis. *Nat Clin Pract Rheumatol* 2, 134-144.

Dhar, A., and Ray, A. (2010). The CCN family proteins in carcinogenesis. *Exp Oncol* 32, 2-9.

Dornhofer, N., Spong, S., Bennewith, K., Salim, A., Klaus, S., Kambham, N., Wong, C., Kaper, F., Sutphin, P., Nacamuli, R., *et al.* (2006). Connective tissue growth factor-specific monoclonal antibody therapy inhibits pancreatic tumor growth and metastasis. *Cancer Res* 66, 5816-5827.

Drake, A.G., and Klingenberg, C.P. (2008). The pace of morphological change: historical transformation of skull shape in St Bernard dogs. *Proc Biol Sci* 275, 71-76.

Dryden, I., and Mardia, K.V. (1998). Statistical shape analysis (Chichester: John Wiley and Sons).

Duan, Y., Beck, T.J., Wang, X.F., and Seeman, E. (2003). Structural and biomechanical basis of sexual dimorphism in femoral neck fragility has its origins in growth and aging. *J Bone Miner Res* 18, 1766-1774.

Einhorn, T.A. (1998). The cell and molecular biology of fracture healing. *Clin Orthop Relat Res*, S7-21.

Farnum, C.E., and Wilsman, N.J. (1987). Morphologic stages of the terminal hypertrophic chondrocyte of growth plate cartilage. *Anat Rec* 219, 221-232.

FibroGen (2012). Anti-CTGF Therapy: Development of Anti-CTGF Monoclonal Antibodies (San Francisco, CA).

Fonseca, C., Lindahl, G.E., Ponticos, M., Sestini, P., Renzoni, E.A., Holmes, A.M., Spagnolo, P., Pantelidis, P., Leoni, P., McHugh, N., *et al.* (2007). A polymorphism in the CTGF promoter region associated with systemic sclerosis. *N Engl J Med* 357, 1210-1220.

Frediani, B., Baldi, F., Falsetti, P., Acciai, C., Filippou, G., Spreafico, A., Chellini, F., Capperucci, C., Filipponi, P., Galeazzi, M., *et al.* (2004a). Bone mineral density in patients with systemic sclerosis. *Ann Rheum Dis* 63, 326-327.

Frediani, B., Baldi, F., Falsetti, P., Acciai, C., Filippou, G., Spreafico, A., Siagri, C., Chellini, F., Capperucci, C., Filipponi, P., *et al.* (2004b). Clinical determinants of bone mass and bone ultrasonometry in patients with systemic sclerosis. *Clin Exp Rheumatol* 22, 313-318.

Friedrichsen, S., Heuer, H., Christ, S., Winckler, M., Brauer, D., Bauer, K., and Raivich, G. (2003). CTGF expression during mouse embryonic development. *Cell Tissue Res* 312, 175-188.

Gao, R., and Brigstock, D.R. (2004). Connective tissue growth factor (CCN2) induces adhesion of rat activated hepatic stellate cells by binding of its C-terminal domain to integrin alpha(v)beta(3) and heparan sulfate proteoglycan. *J Biol Chem* 279, 8848-8855.

Gao, R., and Brigstock, D.R. (2006). A novel integrin alpha5beta1 binding domain in module 4 of connective tissue growth factor (CCN2/CTGF) promotes adhesion and migration of activated pancreatic stellate cells. *Gut* 55, 856-862.

Garciadiego-Cazares, D., Rosales, C., Katoh, M., and Chimal-Monroy, J. (2004). Coordination of chondrocyte differentiation and joint formation by alpha5beta1 integrin in the developing appendicular skeleton. *Development* 131, 4735-4742.

Garn, S.M. (1972). The course of bone gain and the phases of bone loss. *Orthop Clin North Am* 3, 503-520.

Gerber, H.P., Vu, T.H., Ryan, A.M., Kowalski, J., Werb, Z., and Ferrara, N. (1999). VEGF couples hypertrophic cartilage remodeling, ossification and angiogenesis during endochondral bone formation. *Nat Med* 5, 623-628.

Gerstenfeld, L.C., Cullinane, D.M., Barnes, G.L., Graves, D.T., and Einhorn, T.A. (2003). Fracture healing as a post-natal developmental process: molecular, spatial, and temporal aspects of its regulation. *J Cell Biochem* 88, 873-884.

Goldring, M.B., Tsuchimochi, K., and Ijiri, K. (2006). The control of chondrogenesis. *J Cell Biochem* 97, 33-44.

Grotendorst, G.R., and Duncan, M.R. (2005). Individual domains of connective tissue growth factor regulate fibroblast proliferation and myofibroblast differentiation. *FASEB J* 19, 729-738.

Grotendorst, G.R., Rahamanie, H., and Duncan, M.R. (2004). Combinatorial signaling pathways determine fibroblast proliferation and myofibroblast differentiation. *FASEB J* 18, 469-479.

Haigh, J.J., Gerber, H.P., Ferrara, N., and Wagner, E.F. (2000). Conditional inactivation of VEGF-A in areas of collagen2a1 expression results in embryonic lethality in the heterozygous state. *Development* 127, 1445-1453.

Hall, B.K., and Miyake, T. (2000). All for one and one for all: condensations and the initiation of skeletal development. *Bioessays* 22, 138-147.

Hanifi, A., Richardson, J.B., Kuiper, J.H., Roberts, S., and Pleshko, N. (2012). Clinical outcome of autologous chondrocyte implantation is correlated with infrared spectroscopic imaging-derived parameters. *Osteoarthritis Cartilage* 20, 988-996.

Harris, C.P., Townsend, J.J., and Carey, J.C. (1993). Acalvaria: a unique congenital anomaly. *Am J Med Genet* 46, 694-699.

Hendy, G.N., Kaji, H., Sowa, H., Lebrun, J.J., and Canaff, L. (2005). Menin and TGF-beta superfamily member signaling via the Smad pathway in pituitary, parathyroid and osteoblast. *Horm Metab Res* 37, 375-379.

Hoshijima, M., Hattori, T., Inoue, M., Araki, D., Hanagata, H., Miyauchi, A., and Takigawa, M. (2006). CT domain of CCN2/CTGF directly interacts with fibronectin and enhances cell adhesion of chondrocytes through integrin alpha5beta1. *FEBS Lett* *580*, 1376-1382.

Hunziker, E.B., and Schenk, R.K. (1989). Physiological mechanisms adopted by chondrocytes in regulating longitudinal bone growth in rats. *J Physiol* *414*, 55-71.

Hunziker, E.B., Schenk, R.K., and Cruz-Orive, L.M. (1987). Quantitation of chondrocyte performance in growth-plate cartilage during longitudinal bone growth. *J Bone Joint Surg Am* *69*, 162-173.

Hurvitz, J.R., Suwairi, W.M., Van Hul, W., El-Shanti, H., Superti-Furga, A., Roudier, J., Holderbaum, D., Pauli, R.M., Herd, J.K., Van Hul, E.V., et al. (1999). Mutations in the CCN gene family member WISP3 cause progressive pseudorheumatoid dysplasia. *Nat Genet* *23*, 94-98.

Igarashi, A., Nashiro, K., Kikuchi, K., Sato, S., Ihn, H., Fujimoto, M., Grotendorst, G.R., and Takehara, K. (1996). Connective tissue growth factor gene expression in tissue sections from localized scleroderma, keloid, and other fibrotic skin disorders. *J Invest Dermatol* *106*, 729-733.

Igarashi, A., Nashiro, K., Kikuchi, K., Sato, S., Ihn, H., Grotendorst, G.R., and Takehara, K. (1995). Significant correlation between connective tissue growth factor gene expression and skin sclerosis in tissue sections from patients with systemic sclerosis. *J Invest Dermatol* *105*, 280-284.

Igarashi, A., Okochi, H., Bradham, D.M., and Grotendorst, G.R. (1993). Regulation of connective tissue growth factor gene expression in human skin fibroblasts and during wound repair. *Mol Biol Cell* *4*, 637-645.

Ito, Y., Aten, J., Bende, R.J., Oemar, B.S., Rabelink, T.J., Weening, J.J., and Goldschmeding, R. (1998). Expression of connective tissue growth factor in human renal fibrosis. *Kidney Int* *53*, 853-861.

Ito, Y., Yeo, J.Y., Chytil, A., Han, J., Bringas, P., Jr., Nakajima, A., Shuler, C.F., Moses, H.L., and Chai, Y. (2003). Conditional inactivation of Tgfbr2 in cranial neural crest causes cleft palate and calvaria defects. *Development* *130*, 5269-5280.

Ivkovic, S., Yoon, B.S., Popoff, S.N., Safadi, F.F., Libuda, D.E., Stephenson, R.C., Daluiski, A., and Lyons, K.M. (2003). Connective tissue growth factor coordinates chondrogenesis and angiogenesis during skeletal development. *Development* 130, 2779-2791.

Iwata, J., Hosokawa, R., Sanchez-Lara, P.A., Urata, M., Slavkin, H., and Chai, Y. (2010). Transforming growth factor-beta regulates basal transcriptional regulatory machinery to control cell proliferation and differentiation in cranial neural crest-derived osteoprogenitor cells. *J Biol Chem* 285, 4975-4982.

Jiang, X., Iseki, S., Maxson, R.E., Sucov, H.M., and Morriss-Kay, G.M. (2002a). Tissue origins and interactions in the mammalian skull vault. *Dev Biol* 241, 106-116.

Jiang, Y., Jahagirdar, B.N., Reinhardt, R.L., Schwartz, R.E., Keene, C.D., Ortiz-Gonzalez, X.R., Reyes, M., Lenvik, T., Lund, T., Blackstad, M., et al. (2002b). Pluripotency of mesenchymal stem cells derived from adult marrow. *Nature* 418, 41-49.

Junqueira, L.C., and Carneiro, J. (2005). *Basic Histology: Text and Atlas*, 11 edn (McGraw-Hill Companies, The).

Kadota, H., Nakanishi, T., Asaumi, K., Yamaai, T., Nakata, E., Mitani, S., Aoki, K., Aiga, A., Inoue, H., and Takigawa, M. (2004). Expression of connective tissue growth factor/hypertrophic chondrocyte-specific gene product 24 (CTGF/Hcs24/CCN2) during distraction osteogenesis. *J Bone Miner Metab* 22, 293-302.

Karaplis, A.C., Luz, A., Glowacki, J., Bronson, R.T., Tybulewicz, V.L., Kronenberg, H.M., and Mulligan, R.C. (1994). Lethal skeletal dysplasia from targeted disruption of the parathyroid hormone-related peptide gene. *Genes Dev* 8, 277-289.

Karsenty, G. (1998). Genetics of skeletogenesis. *Dev Genet* 22, 301-313.

Karsenty, G. (2003). The complexities of skeletal biology. *Nature* 423, 316-318.

Karsenty, G., Kronenberg, H.M., and Settembre, C. (2009). Genetic control of bone formation. *Annu Rev Cell Dev Biol* 25, 629-648.

Karsenty, G., and Wagner, E.F. (2002). Reaching a genetic and molecular understanding of skeletal development. *Dev Cell* 2, 389-406.

Katsube, K., Sakamoto, K., Tamamura, Y., and Yamaguchi, A. (2009). Role of CCN, a vertebrate specific gene family, in development. *Dev Growth Differ* 51, 55-67.

Kawaki, H., Kubota, S., Suzuki, A., Lazar, N., Yamada, T., Matsumura, T., Ohgawara, T., Maeda, T., Perbal, B., Lyons, K.M., *et al.* (2008a). Cooperative regulation of chondrocyte differentiation by CCN2 and CCN3 shown by a comprehensive analysis of the CCN family proteins in cartilage. *J Bone Miner Res* 23, 1751-1764.

Kawaki, H., Kubota, S., Suzuki, A., Suzuki, M., Kohsaka, K., Hoshi, K., Fujii, T., Lazar, N., Ohgawara, T., Maeda, T., *et al.* (2011). Differential roles of CCN family proteins during osteoblast differentiation: Involvement of Smad and MAPK signaling pathways. *Bone* 49, 975-989.

Kawaki, H., Kubota, S., Suzuki, A., Yamada, T., Matsumura, T., Mandai, T., Yao, M., Maeda, T., Lyons, K.M., and Takigawa, M. (2008b). Functional requirement of CCN2 for intramembranous bone formation in embryonic mice. *Biochem Biophys Res Commun* 366, 450-456.

Kerkhofs, J., Roberts, S.J., Luyten, F.P., Van Oosterwyck, H., and Geris, L. (2012). Relating the chondrocyte gene network to growth plate morphology: from genes to phenotype. *PLoS One* 7, e34729.

Kikuchi, T., Kubota, S., Asaumi, K., Kawaki, H., Nishida, T., Kawata, K., Mitani, S., Tabata, Y., Ozaki, T., and Takigawa, M. (2008). Promotion of bone regeneration by CCN2 incorporated into gelatin hydrogel. *Tissue Eng Part A* 14, 1089-1098.

Klingenberg, C. (2008). MorphoJ. In Faculty of Life Sciences, University of Manchester, UK (http://www.flywings.org.uk/MorphoJ_page.htm).

Koyama, E., Yasuda, T., Minugh-Purvis, N., Kinumatsu, T., Yallowitz, A.R., Wellik, D.M., and Pacifici, M. (2010). Hox11 genes establish synovial joint organization and phylogenetic characteristics in developing mouse zeugopod skeletal elements. *Development* 137, 3795-3800.

Kronenberg, H.M. (2003). Developmental regulation of the growth plate. *Nature* 423, 332-336.

Kubota, S., Eguchi, T., Shimo, T., Nishida, T., Hattori, T., Kondo, S., Nakanishi, T., and Takigawa, M. (2001). Novel mode of processing and secretion of connective tissue growth factor/ecogenin (CTGF/Hcs24) in chondrocytic HCS-2/8 cells. *Bone* 29, 155-161.

Kubota, S., and Takigawa, M. (2007). Role of CCN2/CTGF/Hcs24 in bone growth. *Int Rev Cytol* 257, 1-41.

Kuiper, E.J., Roestenberg, P., Ehlken, C., Lambert, V., van Treslong-de Groot, H.B., Lyons, K.M., Agostini, H.J., Rakic, J.M., Klaassen, I., Van Noorden, C.J., *et al.* (2007). Angiogenesis is not impaired in connective tissue growth factor (CTGF) knock-out mice. *J Histochem Cytochem* 55, 1139-1147.

Kutz, W.E., Gong, Y., and Warman, M.L. (2005). WISP3, the gene responsible for the human skeletal disease progressive pseudorheumatoid dysplasia, is not essential for skeletal function in mice. *Mol Cell Biol* 25, 414-421.

Lambi, A.G., Pankratz, T.L., Mundy, C., Gannon, M., Barbe, M.F., Richtsmeier, J.T., and Popoff, S.N. (2012). The skeletal site-specific role of connective tissue growth factor in prenatal osteogenesis. *Dev Dyn* 241, 1944-1959.

Lanske, B., Karaplis, A.C., Lee, K., Luz, A., Vortkamp, A., Pirro, A., Karperien, M., Defize, L.H., Ho, C., Mulligan, R.C., *et al.* (1996). PTH/PTHrP receptor in early development and Indian hedgehog-regulated bone growth. *Science* 273, 663-666.

Lasky, J.A., Ortiz, L.A., Tonthat, B., Hoyle, G.W., Corti, M., Athas, G., Lungarella, G., Brody, A., and Friedman, M. (1998). Connective tissue growth factor mRNA expression is upregulated in bleomycin-induced lung fibrosis. *Am J Physiol* 275, L365-371.

Lau, L.F., and Lam, S.C. (1999). The CCN family of angiogenic regulators: the integrin connection. *Exp Cell Res* 248, 44-57.

Le, A.X., Miclau, T., Hu, D., and Helms, J.A. (2001). Molecular aspects of healing in stabilized and non-stabilized fractures. *J Orthop Res* 19, 78-84.

Lee, S.K., Kim, Y.S., Oh, H.S., Yang, K.H., Kim, E.C., and Chi, J.G. (2001). Prenatal development of the human mandible. *Anat Rec* 263, 314-325.

Lele, S., and Richtsmeier, J. (1995a). Euclidean distance matrix analysis: confidence intervals for form and growth differences. *Am J Phys Anthropol* 98, 73-86.

Lele, S., and Richtsmeier, J.T. (1995b). Euclidean distance matrix analysis: confidence intervals for form and growth differences. *Am J Phys Anthropol* 98, 73-86.

Lele, S., and Richtsmeier, J.T. (2001). An invariant approach to statistical analysis of shapes (Boca Raton: Chapman and Hall/CRC).

Lenton, K.A., Nacamuli, R.P., Wan, D.C., Helms, J.A., and Longaker, M.T. (2005). Cranial suture biology. *Curr Top Dev Biol* 66, 287-328.

Logan, M., Martin, J.F., Nagy, A., Lobe, C., Olson, E.N., and Tabin, C.J. (2002). Expression of Cre Recombinase in the developing mouse limb bud driven by a Prx1 enhancer. *Genesis* 33, 77-80.

Luo, Q., Kang, Q., Si, W., Jiang, W., Park, J.K., Peng, Y., Li, X., Luu, H.H., Luo, J., Montag, A.G., et al. (2004). Connective tissue growth factor (CTGF) is regulated by Wnt and bone morphogenetic proteins signaling in osteoblast differentiation of mesenchymal stem cells. *J Biol Chem* 279, 55958-55968.

Maeda, A., Nishida, T., Aoyama, E., Kubota, S., Lyons, K.M., Kuboki, T., and Takigawa, M. (2009). CCN family 2/connective tissue growth factor modulates BMP signalling as a signal conductor, which action regulates the proliferation and differentiation of chondrocytes. *J Biochem* 145, 207-216.

Mandarim-de-Lacerda, C.A., and Alves, M.U. (1992). Growth of the cranial bones in human fetuses (2nd and 3rd trimesters). *Surg Radiol Anat* 14, 125-129.

Manolagas, S.C. (2000). Birth and death of bone cells: basic regulatory mechanisms and implications for the pathogenesis and treatment of osteoporosis. *Endocr Rev* 21, 115-137.

Marks, S.C., Jr., and Popoff, S.N. (1990). Chapter 13: Ultrastructural biology and pathology of the osteoclast. In (Norwell: Kluwer Academic Publishers), pp. 239-252.

Martin, J.F., and Olson, E.N. (2000). Identification of a prx1 limb enhancer. *Genesis* 26, 225-229.

Martinez-Abadias, N., Percival, C., Aldridge, K., Hill, C.A., Ryan, T., Sirivunnabood, S., Wang, Y., Jabs, E.W., and Richtsmeier, J.T. (2010). Beyond the closed suture in apert syndrome mouse models: evidence of primary effects of FGFR2 signaling on facial shape at birth. *Dev Dyn* 239, 3058-3071.

McBratney-Owen, B., Iseki, S., Bamforth, S.D., Olsen, B.R., and Morriss-Kay, G.M. (2008). Development and tissue origins of the mammalian cranial base. *Dev Biol* 322, 121-132.

Morales, M.G., Cabello-Verrugio, C., Santander, C., Cabrera, D., Goldschmeding, R., and Brandan, E. (2011). CTGF/CCN-2 over-expression can directly induce features of skeletal muscle dystrophy. *J Pathol* 225, 490-501.

Morgelin, M., Heinegard, D., Engel, J., and Paulsson, M. (1994). The cartilage proteoglycan aggregate: assembly through combined protein-carbohydrate and protein-protein interactions. *Biophys Chem* 50, 113-128.

Mori, Y., Hinchcliff, M., Wu, M., Warner-Blankenship, M., K, M.L., and Varga, J. (2008). Connective tissue growth factor/CCN2-null mouse embryonic fibroblasts retain intact transforming growth factor-beta responsiveness. *Exp Cell Res* 314, 1094-1104.

Nakanishi, T., Kimura, Y., Tamura, T., Ichikawa, H., Yamaai, Y., Sugimoto, T., and Takigawa, M. (1997). Cloning of a mRNA preferentially expressed in chondrocytes by differential display-PCR from a human chondrocytic cell line that is identical with connective tissue growth factor (CTGF) mRNA. *Biochem Biophys Res Commun* 234, 206-210.

Nakanishi, T., Nishida, T., Shimo, T., Kobayashi, K., Kubo, T., Tamatani, T., Tezuka, K., and Takigawa, M. (2000). Effects of CTGF/Hcs24, a product of a hypertrophic chondrocyte-specific gene, on the proliferation and differentiation of chondrocytes in culture. *Endocrinology* 141, 264-273.

Nakanishi, T., Yamaai, T., Asano, M., Nawachi, K., Suzuki, M., Sugimoto, T., and Takigawa, M. (2001). Overexpression of connective tissue growth factor/hypertrophic chondrocyte-specific gene product 24 decreases bone density in adult mice and induces dwarfism. *Biochem Biophys Res Commun* 281, 678-681.

Nakata, E., Nakanishi, T., Kawai, A., Asaumi, K., Yamaai, T., Asano, M., Nishida, T., Mitani, S., Inoue, H., and Takigawa, M. (2002). Expression of connective tissue growth factor/hypertrophic chondrocyte-specific gene product 24 (CTGF/Hcs24) during fracture healing. *Bone* 31, 441-447.

Nishida, T., Emura, K., Kubota, S., Lyons, K.M., and Takigawa, M. (2011). CCN family 2/connective tissue growth factor (CCN2/CTGF) promotes osteoclastogenesis via induction of and interaction with dendritic cell-specific transmembrane protein (DC-STAMP). *J Bone Miner Res* 26, 351-363.

Nishida, T., Kawaki, H., Baxter, R.M., Deyoung, R.A., Takigawa, M., and Lyons, K.M. (2007). CCN2 (Connective Tissue Growth Factor) is essential for extracellular matrix production and integrin signaling in chondrocytes. *J Cell Commun Signal* *1*, 45-58.

Nishida, T., Nakanishi, T., Asano, M., Shimo, T., and Takigawa, M. (2000). Effects of CTGF/Hcs24, a hypertrophic chondrocyte-specific gene product, on the proliferation and differentiation of osteoblastic cells in vitro. *J Cell Physiol* *184*, 197-206.

Noden, D.M., and Trainor, P.A. (2005). Relations and interactions between cranial mesoderm and neural crest populations. *J Anat* *207*, 575-601.

Noonan, K.J., Hunziker, E.B., Nessler, J., and Buckwalter, J.A. (1998). Changes in cell, matrix compartment, and fibrillar collagen volumes between growth-plate zones. *J Orthop Res* *16*, 500-508.

Novack, D.V., and Teitelbaum, S.L. (2008). The osteoclast: friend or foe? *Annu Rev Pathol* *3*, 457-484.

Nowlan, N.C., Dumas, G., Tajbakhsh, S., Prendergast, P.J., and Murphy, P. (2012). Biophysical stimuli induced by passive movements compensate for lack of skeletal muscle during embryonic skeletogenesis. *Biomech Model Mechanobiol* *11*, 207-219.

Nowlan, N.C., Murphy, P., and Prendergast, P.J. (2007). Mechanobiology of embryonic limb development. *Ann N Y Acad Sci* *1101*, 389-411.

Nowlan, N.C., Murphy, P., and Prendergast, P.J. (2008). A dynamic pattern of mechanical stimulation promotes ossification in avian embryonic long bones. *J Biomech* *41*, 249-258.

Nowlan, N.C., Sharpe, J., Roddy, K.A., Prendergast, P.J., and Murphy, P. (2010). Mechanobiology of embryonic skeletal development: Insights from animal models. *Birth Defects Res C Embryo Today* *90*, 203-213.

Oka, K., Oka, S., Sasaki, T., Ito, Y., Bringas, P., Jr., Nonaka, K., and Chai, Y. (2007). The role of TGF-beta signaling in regulating chondrogenesis and osteogenesis during mandibular development. *Dev Biol* *303*, 391-404.

Okada, S., Yoshida, S., Ashrafi, S.H., and Schraufnagel, D.E. (2002). The canalicular structure of compact bone in the rat at different ages. *Microsc Microanal* *8*, 104-115.

Ono, M., Kubota, S., Fujisawa, T., Sonoyama, W., Kawaki, H., Akiyama, K., Oshima, M., Nishida, T., Yoshida, Y., Suzuki, K., *et al.* (2007). Promotion of attachment of human bone marrow stromal cells by CCN2. *Biochem Biophys Res Commun* 357, 20-25.

Ono, M., Kubota, S., Fujisawa, T., Sonoyama, W., Kawaki, H., Akiyama, K., Shimono, K., Oshima, M., Nishida, T., Yoshida, Y., *et al.* (2008). Promotion of hydroxyapatite-associated, stem cell-based bone regeneration by CCN2. *Cell Transplant* 17, 231-240.

Orwoll, E.S. (2003). Toward an expanded understanding of the role of the periosteum in skeletal health. *J Bone Miner Res* 18, 949-954.

Otto, F., Thornell, A.P., Crompton, T., Denzel, A., Gilmour, K.C., Rosewell, I.R., Stamp, G.W., Beddington, R.S., Mundlos, S., Olsen, B.R., *et al.* (1997). Cbfa1, a candidate gene for cleidocranial dysplasia syndrome, is essential for osteoblast differentiation and bone development. *Cell* 89, 765-771.

Pacheco, M.S., Reis, A.H., Aguiar, D.P., Lyons, K.M., and Abreu, J.G. (2008). Dynamic analysis of the expression of the TGFbeta/SMAD2 pathway and CCN2/CTGF during early steps of tooth development. *Cells Tissues Organs* 187, 199-210.

Pala, D., Kapoor, M., Woods, A., Kennedy, L., Liu, S., Chen, S., Bursell, L., Lyons, K.M., Carter, D.E., Beier, F., *et al.* (2008). Focal adhesion kinase/Src suppresses early chondrogenesis: central role of CCN2. *J Biol Chem* 283, 9239-9247.

Paradis, V., Dargere, D., Bonvoust, F., Vidaud, M., Segarini, P., and Bedossa, P. (2002). Effects and regulation of connective tissue growth factor on hepatic stellate cells. *Lab Invest* 82, 767-774.

Parisi, M.S., Gazzero, E., Rydziel, S., and Canalis, E. (2006). Expression and regulation of CCN genes in murine osteoblasts. *Bone* 38, 671-677.

Perbal, B. (2001). NOV (nephroblastoma overexpressed) and the CCN family of genes: structural and functional issues. *Mol Pathol* 54, 57-79.

Perbal, B. (2004). CCN proteins: multifunctional signalling regulators. *Lancet* 363, 62-64.

Provost, S., and Schipani, E. (2005). Molecular mechanisms of endochondral bone development. *Biochem Biophys Res Commun* 328, 658-665.

Rachfal, A.W., and Brigstock, D.R. (2005). Structural and functional properties of CCN proteins. *Vitam Horm* 70, 69-103.

Rauch, F., and Schoenau, E. (2001a). Changes in bone density during childhood and adolescence: an approach based on bone's biological organization. *J Bone Miner Res* 16, 597-604.

Rauch, F., and Schoenau, E. (2001b). The developing bone: slave or master of its cells and molecules? *Pediatr Res* 50, 309-314.

Reyment, R., Blackith, R., and Campbell, N. (1984). Multivariate morphometrics, 2 edn (London: Academic Press).

Rice, D.P. (2008). Craniofacial Sutures: Development, Disease and Treatment, Vol 12 (Basel: S Karger AG).

Richtsmeier, J., Paik, C., Elfert, P., Cole, T.I., and Dahlman, H. (1995). Precision, repeatability, and validation of the localization of cranial landmarks using computed tomography scans. *Cleft Palate Craniofac J* 32, 217-227.

Richtsmeier, J.T., and Lele, S. (1993). A coordinate-free approach to the analysis of growth patterns: models and theoretical considerations. *Biol Rev Camb Philos Soc* 68, 381-411.

Rohlf, F.J., and Slice, D.E. (1990). Extensions of the Procrustes method for the optimal superimposition of landmarks. *Systematic Zoology* 39, 40-59.

Sadler, T.W., and Langman, J. (2009). Langman's Medical Embryology, 11th edn (Baltimore: Lippincott William & Wilkins).

Safadi, F.F., Xu, J., Smock, S.L., Kanaan, R.A., Selim, A.H., Odgren, P.R., Marks, S.C., Jr., Owen, T.A., and Popoff, S.N. (2003). Expression of connective tissue growth factor in bone: its role in osteoblast proliferation and differentiation in vitro and bone formation in vivo. *J Cell Physiol* 196, 51-62.

Sage, E.H., and Bornstein, P. (1991). Extracellular proteins that modulate cell-matrix interactions: SPARC, tenascin, and thrombospondin. *J Biol Chem* 266, 14831-14834.

Salter, R.B. (1999). Textbook of Disorders and Injuries of the Musculoskeletal System, Third Edition edn (Baltimore: Lippincott Williams & Wilkins).

Scherft, J.P., and Groot, C.G. (1990). Chapter 11: The electron microscopic structure of the osteoblast. In (Norwell: Kluwer Academic Publishers), pp. 209-222.

Schipani, E. (2005). Hypoxia and HIF-1 alpha in chondrogenesis. *Semin Cell Dev Biol* 16, 539-546.

Sharir, A., Stern, T., Rot, C., Shahar, R., and Zelzer, E. (2011). Muscle force regulates bone shaping for optimal load-bearing capacity during embryogenesis. *Development* 138, 3247-3259.

Shimo, T., Kanyama, M., Wu, C., Sugito, H., Billings, P.C., Abrams, W.R., Rosenbloom, J., Iwamoto, M., Pacifici, M., and Koyama, E. (2004). Expression and roles of connective tissue growth factor in Meckel's cartilage development. *Dev Dyn* 231, 136-147.

Shimo, T., Kubota, S., Yoshioka, N., Ibaragi, S., Isowa, S., Eguchi, T., Sasaki, A., and Takigawa, M. (2006). Pathogenic role of connective tissue growth factor (CTGF/CCN2) in osteolytic metastasis of breast cancer. *J Bone Miner Res* 21, 1045-1059.

Shimo, T., Wu, C., Billings, P.C., Piddington, R., Rosenbloom, J., Pacifici, M., and Koyama, E. (2002). Expression, gene regulation, and roles of Fisp12/CTGF in developing tooth germs. *Dev Dyn* 224, 267-278.

Smerdel-Ramoya, A., Zanotti, S., Stadmeyer, L., Durant, D., and Canalis, E. (2008). Skeletal overexpression of connective tissue growth factor impairs bone formation and causes osteopenia. *Endocrinology* 149, 4374-4381.

Song, J.J., Aswad, R., Kanaan, R.A., Rico, M.C., Owen, T.A., Barbe, M.F., Safadi, F.F., and Popoff, S.N. (2007). Connective tissue growth factor (CTGF) acts as a downstream mediator of TGF-beta1 to induce mesenchymal cell condensation. *J Cell Physiol* 210, 398-410.

Souza, R.B., Borges, C.T., Takayama, L., Aldrighi, J.M., and Pereira, R.M. (2006). Systemic sclerosis and bone loss: the role of the disease and body composition. *Scand J Rheumatol* 35, 384-387.

Sperber, G.H., Sperber, S.M., and Guttmann, G.D. (2010). Craniofacial Embryogenetics and Development, 2 edn (Shelton: People's Medical Publishing House).

St-Jacques, B., Hammerschmidt, M., and McMahon, A.P. (1999). Indian hedgehog signaling regulates proliferation and differentiation of chondrocytes and is essential for bone formation. *Genes Dev* 13, 2072-2086.

Stein, G.S., and Lian, J.B. (1993). Molecular mechanisms mediating proliferation/differentiation interrelationships during progressive development of the osteoblast phenotype. *Endocr Rev* 14, 424-442.

Stein, G.S., Lian, J.B., van Wijnen, A.J., Stein, J.L., Montecino, M., Javed, A., Zaidi, S.K., Young, D.W., Choi, J.Y., and Pockwinse, S.M. (2004). Runx2 control of organization, assembly and activity of the regulatory machinery for skeletal gene expression. *Oncogene* 23, 4315-4329.

Su, J.L., Chiou, J., Tang, C.H., Zhao, M., Tsai, C.H., Chen, P.S., Chang, Y.W., Chien, M.H., Peng, C.Y., Hsiao, M., *et al.* (2010). CYR61 regulates BMP-2-dependent osteoblast differentiation through the α v β 3 integrin/integrin-linked kinase/ERK pathway. *J Biol Chem* 285, 31325-31336.

Suda, T., Takahashi, N., Udagawa, N., Jimi, E., Gillespie, M.T., and Martin, T.J. (1999). Modulation of osteoclast differentiation and function by the new members of the tumor necrosis factor receptor and ligand families. *Endocr Rev* 20, 345-357.

Taher, L., Collette, N.M., Murugesh, D., Maxwell, E., Ovcharenko, I., and Loots, G.G. (2011). Global gene expression analysis of murine limb development. *PLoS One* 6, e28358.

Takahashi, N., Yamana, H., Yoshiki, S., Roodman, G.D., Mundy, G.R., Jones, S.J., Boyde, A., and Suda, T. (1988). Osteoclast-like cell formation and its regulation by osteotropic hormones in mouse bone marrow cultures. *Endocrinology* 122, 1373-1382.

Takigawa, M., Nakanishi, T., Kubota, S., and Nishida, T. (2003). Role of CTGF/HCS24/ecogenin in skeletal growth control. *J Cell Physiol* 194, 256-266.

Tan, T.W., Lai, C.H., Huang, C.Y., Yang, W.H., Chen, H.T., Hsu, H.C., Fong, Y.C., and Tang, C.H. (2009). CTGF enhances migration and MMP-13 up-regulation via alphavbeta3 integrin, FAK, ERK, and NF-kappaB-dependent pathway in human chondrosarcoma cells. *J Cell Biochem* 107, 345-356.

Teitelbaum, S.L. (2000). Bone resorption by osteoclasts. *Science* 289, 1504-1508.

Theiler, K. (1989). *The House Mouse: Atlas of Embryonic Development* (New York: Springer-Verlag).

Thompson, Z., Miclau, T., Hu, D., and Helms, J.A. (2002). A model for intramembranous ossification during fracture healing. *J Orthop Res* 20, 1091-1098.

Toma, C.D., Schaffer, J.L., Meazzini, M.C., Zurakowski, D., Nah, H.D., and Gerstenfeld, L.C. (1997). Developmental restriction of embryonic calvarial cell populations as characterized by their in vitro potential for chondrogenic differentiation. *J Bone Miner Res* 12, 2024-2039.

van den Bergh, J.P., van Geel, T.A., and Geusens, P.P. (2012). Osteoporosis, frailty and fracture: implications for case finding and therapy. *Nat Rev Rheumatol* 8, 163-172.

Vortkamp, A., Lee, K., Lanske, B., Segre, G.V., Kronenberg, H.M., and Tabin, C.J. (1996). Regulation of rate of cartilage differentiation by Indian hedgehog and PTH-related protein. *Science* 273, 613-622.

Vu, T.H., Shipley, J.M., Bergers, G., Berger, J.E., Helms, J.A., Hanahan, D., Shapiro, S.D., Senior, R.M., and Werb, Z. (1998). MMP-9/gelatinase B is a key regulator of growth plate angiogenesis and apoptosis of hypertrophic chondrocytes. *Cell* 93, 411-422.

Wan, M., and Cao, X. (2005). BMP signaling in skeletal development. *Biochem Biophys Res Commun* 328, 651-657.

Wang, Y., Sun, M., Uhlhorn, V.L., Zhou, X., Peter, I., Martinez-Abadias, N., Hill, C.A., Percival, C.J., Richtsmeier, J.T., Huso, D.L., *et al.* (2010). Activation of p38 MAPK pathway in the skull abnormalities of Apert syndrome Fgfr2(+P253R) mice. *BMC Dev Biol* 10, 22.

Watanabe, H., and Yamada, Y. (1999). Mice lacking link protein develop dwarfism and craniofacial abnormalities. *Nat Genet* 21, 225-229.

Wellik, D.M., and Capecchi, M.R. (2003). Hox10 and Hox11 genes are required to globally pattern the mammalian skeleton. *Science* (New York, NY) 301, 363-367.

Xu, J., Smock, S.L., Safadi, F.F., Rosenzweig, A.B., Odgren, P.R., Marks, S.C., Jr., Owen, T.A., and Popoff, S.N. (2000). Cloning the full-length cDNA for rat connective tissue growth factor: implications for skeletal development. *J Cell Biochem* 77, 103-115.

Yamashiro, T., Fukunaga, T., Kobashi, N., Kamioka, H., Nakanishi, T., Takigawa, M., and Takano-Yamamoto, T. (2001). Mechanical stimulation induces CTGF expression in rat osteocytes. *J Dent Res* 80, 461-465.

Yoshioka, H., Iyama, K., Inoguchi, K., Khaleduzzaman, M., Ninomiya, Y., and Ramirez, F. (1995). Developmental pattern of expression of the mouse alpha 1 (XI) collagen gene (Col11a1). *Dev Dyn* 204, 41-47.

Yosimichi, G., Kubota, S., Nishida, T., Kondo, S., Yanagita, T., Nakao, K., Takano-Yamamoto, T., and Takigawa, M. (2006). Roles of PKC, PI3K and JNK in multiple transduction of CCN2/CTGF signals in chondrocytes. *Bone* 38, 853-863.

Yosimichi, G., Nakanishi, T., Nishida, T., Hattori, T., Takano-Yamamoto, T., and Takigawa, M. (2001). CTGF/Hcs24 induces chondrocyte differentiation through a p38 mitogen-activated protein kinase (p38MAPK), and proliferation through a p44/42 MAPK/extracellular-signal regulated kinase (ERK). *Eur J Biochem* 268, 6058-6065.

Zaidi, M. (2007). Skeletal remodeling in health and disease. *Nat Med* 13, 791-801.

Zakany, J., and Duboule, D. (2007). The role of Hox genes during vertebrate limb development. *Curr Opin Genet Dev* 17, 359-366.

Zhang, M., Xuan, S., Bouxsein, M.L., von Stechow, D., Akeno, N., Faugere, M.C., Malluche, H., Zhao, G., Rosen, C.J., Efstratiadis, A., *et al.* (2002). Osteoblast-specific knockout of the insulin-like growth factor (IGF) receptor gene reveals an essential role of IGF signaling in bone matrix mineralization. *J Biol Chem* 277, 44005-44012.

Zhou, X., Zhang, Z., Feng, J.Q., Dusevich, V.M., Sinha, K., Zhang, H., Darnay, B.G., and de Crombrugghe, B. (2010). Multiple functions of Osterix are required for bone growth and homeostasis in postnatal mice. *Proc Natl Acad Sci U S A* 107, 12919-12924.